Technische Universität München

Institut für Organische Chemie und Biochemie

Max-Planck-Institut für Biochemie

Abteilung NMR

NMR high resolution spectroscopy
and X-ray crystallography for development of
MDM2/X-p53 interaction antagonists

Michał Biśta

Vollständiger Abdruck der von der Fakultät für Chemie der Technischen Universität München zur Erlangung des akademischen Grades eines

Doktors der Naturwissenschaften

genehmigten Dissertation.

Vorsitzender: Univ.-Prof. Dr. Michael Groll

Prüfer der Dissertation: 1. Univ.-Prof. Dr. Michael Sattler
                           2. Univ.-Prof. Dr. Dieter Langosch

Die Dissertation wurde am 07.07.2011 bei der Technischen Universität München eingereicht und durch die Fakultät für Chemie am 01.08.2011 angenommen.

I dedicate this work to the memory of recently deceased Stanislawa Zajchowska.

Acknowledgements

I would like to thank all the people who have contributed to this work.

I am especially indebted to my supervisor Prof. Tad A. Holak for his scientific and personal support and corrections to the thesis.

I have to greatly acknowledge all my former and current groupmates (particularly Ania Czarny, Ania Ducka, Weronika Janczyk, Kaja Kowalska, Linda Wolf, Marcelino Arciniega Castro, Marcin Krajewski, Grzegorz Maria Popowicz, Arkadiusz Sikora, Tomasz Sitar) for creating a friendly atmosphere, cooperating and providing support in research.

I would like to thank Prof. Dr. Alexander Siegfried Dömling and his co-workers for fruitful cooperation on development of MDM2-p53 interaction antagonists.

I am also very grateful to Prof. Dr. Michael Sattler, for being my thesis advisor.

The results presented in the Thesis would be impossible to achieve without excellent support of the workers of Microchemistry and Crystallization Core Facilities in the Institute.

My apologies to all others who I have not mention by name I am indebted to them for their help.

Publications

Publications describing the work discussed in the Dissertation:

Bista M, Kowalska K, Janczyk W, Dömling A, Holak TA. *Robust NMR screening for lead compounds using tryptophan-containing proteins.* **J Am Chem Soc.** 2009 Jun 10;131(22):7500-1.

Bista M, Wolf S, Kowalska K, Janczyk W, Dömling A, Holak TA, Popowicz GM *Extending the pharmacophore of MDM2-p53 interaction with new classes of acyclic inhibitors.* **In preparation**

Czarna A, Beck B, Srivastava S, Popowicz GM, Wolf S, Huang Y, **Bista M**, Holak TA, Dömling A. *Robust generation of lead compounds for protein-protein interactions by computational and MCR chemistry: p53/Hdm2 antagonists.* **Angew Chem Int Ed Engl.** 2010 Jul 19;49(31):5352-6

Koes D, Khoury K, Huang Y, Wang W, **Bista M**, Popowicz GM, Wolf S, Holak TA, Dömling A, Camacho C *Enabling large-scale design, synthesis and validation of small molecule protein-protein antagonists.* **PLoS Comput Biol**, submitted

Huang Y, Wolf S, **Bista M**, Meireles L, Camacho C, Holak TA, Dömling A. *1,4-Thienodiazepine-2,5-diones via MCR (I): synthesis, virtual space and p53-Mdm2 activity.* **Chem Biol Drug Des.** 2010 Aug;76(2):116-29

Publications on other works not discussed in the thesis (but prepared or partially prepared during period of my PhD study):

Riedl J, Crevenna AH, Kessenbrock K, Yu JH, Neukirchen D, **Bista M**, Bradke F, Jenne D, Holak TA, Werb Z, Sixt M, Wedlich-Soldner R. *Lifeact: a versatile marker to visualize F-actin.* **Nature Methods**. 2008 Jul;5(7):605-7

Stec-Niemczyk J, Pustelny K, Kisielewska M, **Bista M**, Boulware KT, Stennicke HR, Thogersen IB, Daugherty PS, Enghild JJ, Baczynski K, Popowicz GM, Dubin A, Potempa J, Dubin G. *Structural and functional characterization of SplA, an exclusively specific protease of Staphylococcus aureus.* **Biochem J.** 2009 May 1;419(3):555-64.

Dubin G, Stec-Niemczyk J, Kisielewska M, Pustelny K, Popowicz GM, **Bista M**, Kantyka T, Boulware KT, Stennicke HR, Czarna A, Phopaisarn M, Daugherty PS, Thøgersen IB, Enghild JJ, Thornberry N, Dubin A, Potempa J. *Enzymatic activity of the Staphylococcus aureus SplB serine protease is induced by substrates containing the sequence Trp-Glu-Leu-Gln.* **J Mol Biol. 2008** May 30;379(2):343-56.

Contents

1. Biological background of the study

The p53 protein is the most important tumour suppressor, that is mutated in 50% of all human cancers. In the remaining 50% of the tumours, p53 retains its wild-type sequence, but is downregulated or misregulated mostly by the interaction with its main negative regulators – MDM2 and MDMX. A low-molecular-weight antagonist capable to disrupt the p53-MDM2/X interaction should reactivate p53 and inhibit or reverse tumour formation.

p53 is functionally situated at the crossroads of variety of pathways, that regulate cell proliferation and survival. In over three decades, that passed from discovery of p53 to today many fascinating facts about the protein were uncovered and TP53 has become one of the most frequently researched genes (with over 58000 research articles mentioning p53, according to the PubMed database). The complexity of p53 regulation and the variety of roles, that may be played by this protein make it probably one of the best known and, at the same time, one of the most challenging medically relevant proteins.

The three best known outcomes of p53 activation are: apoptosis, senescence or cell cycle arrest (Vousden et al., 2007). The classical, most widely researched functionality of p53 is its involvement in transcription regulation, it is however becoming increasingly clear, that the transcriptional activity of p53 is not the only function and the protein was recently shown to be directly involved in triggering apoptosis in the absence of transcription (Chipuk et al., 2003; Sayan et al., 2006) or to regulate mRNA stability by miRNAs (Suzuki et al., 2009; Toledo et al., 2009).

1.1 p53

1.1.1 Primary sequence

The human protein is 393 amino acid long and consists of five domains: the N-terminal transactivation domain responsible for interaction with transcription machinery and its negative regulators of p53: MDM2/X, the proline-rich domain, that has structural and regulatory functions, the DNA binding part, the tetramerization domain and the C-terminal domain, that is a subject of numerous posttranscriptional modifications modulating the stability and affinity of DNA binding by the protein. An overview of primary structure of p53 is shown in Figure 1.
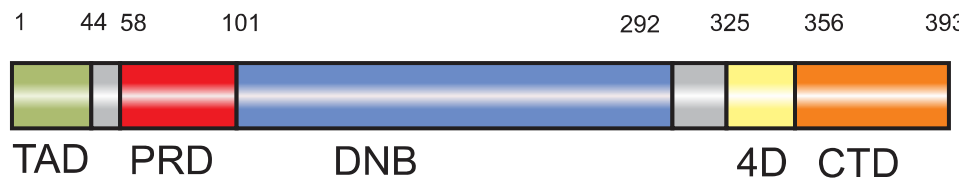
Figure 1 Overview of the p53 primary structure; TAD - transactivation domain, PRD - proline rich domain, DNB - DNA binding core domain, 4D - tetramerization domain and CTD - C-terminal domain.

1.1.2 Transactivation domain

The transactivation domain of p53 is natively unstructured with short patches of nascent fold; particularly amino acids 18-25 were shown to have a nascent helix structure populated at level ca. 30% (Wells et al., 2008). The domain is a binding site for many interacting proteins, such as components of the transcription machinery (Thut et al., 1995), transcription enhancer p300 (Gu et al., 1997), the negative regulators MDM2 and MDMX (Kussie et al., 1996; Marine et al., 2005), or anti-apoptotic proteins from the Bcl-2 family (Ha et al., 2011). The interactions of this domain are based on typical macromolecular recognition mechanisms in which intrinsically unstructured amino-acid patches adopt α-helical structures upon interaction with binding partners. The ability of TAD to bind the protein partners is a subject of post-translational regulation, e.g. phosphorylation of Thr18^{p53} by VRK-1 kinase (Lopez-Borges et al., 2000). The casein

kinase 1-δ (Sakaguchi et al., 2000) was shown to impair the ability of MDM2 to bind p53 and strengthen the binding of transcription enhancer p300 (Dornan et al., 2001; Schon et al., 2002).

1.1.3 Proline-rich domain

The proline rich domain is also unstructured, however, NMR and SAXS data suggest, that the domain may possess some stiffness and be able to modulate the relative position of transactivation domain and the DNA-binding core domain (Wells et al., 2008). The domain contains five PXXP motifs, that are generally known to be recognized by signaling proteins containing the SH3 domains (Walker et al., 1996). Additionally, the structure of the proline-rich domain can be modulated by proline isomerase 1 (Pin1), that was shown to bind to phosphorylated amino acid residues (particularly Ser33^{p53}, Thr81^{p53}) adjacent to prolines and enhance the transactivation activity of p53 (Takahashi et al., 2008). This elegant mechanism explains how local posttranslational modifications may result in large conformational rearrangements modulating the activity of the whole cell.

1.1.4 DNA-binding core domain

The central domain consists of an immunoglobulin-like β-sandwich, that provides the basic scaffold for the DNA-binding surface (see Figure 2A-B, D) (Cho et al., 1994). This domain is the target of the largest number of pro-oncogenic mutations (Olivier et al., 2002), that may be mapped mainly to area at the DNA-binding interface (resulting in decreasing the ability of the protein to bind DNA) or to the amino acids stabilizing the β-sandwich motif (thus, reducing the stability of the domain) (Joerger et al., 2008).

Reversing effect of mutations of the p53 DNA-binding core domain with small molecules is a Holy Grail of the p53 research, fortunately preliminary results suggest,, that such strategy might be possible and effective, i.e. an X-ray structure of a

thermodynamically unstable p53 Y330C mutant stabilized by a small molecule has been reported recently (see Figure 2B) (Boeckler et al., 2008).

p53 binds as a tetramer to consensus DNA sites containing two copies of the sequence RRRC(A/T)|(T/A)GYYY (R, purine; Y, pyrimidine) separated by up to 13 bp (el-Deiry et al., 1992). The protein acts by enhancing expression of cell cycle regulators (i.e. cyclin inhibitor p21) (el-Deiry et al., 1993), genes involved in apoptosis (i.e. BAX) (Miyashita et al., 1995), DNA-repair factors (i.e. PCNA) (Xu et al., 1999; Helton et al., 2007) and also its own down-regulators (i.e. MDM2) (Barak et al., 1993). The DNA-binding domain was also shown to interact with multiple protein partners, i.e. interferon-inducible protein 16 (Liao et al., 2011) or Bcl-2 family members (Sot et al., 2007).

1.1.5 Tetramerization domain

There is strong evidence, that this short domain is essential for p53's oligomerization, that is vital for transcription activation (Veprintsev et al., 2006). The structure of the domain was determined by X-ray crystallography (Jeffrey et al., 1995) and NMR (Clore et al., 1995) and shows, that a single oligomerization domain comprises a β-strand and an α-helix linked by a sharp turn (see Figure 2C). Two monomers associate in a primary dimer, that is stabilized via an antiparallel β-sheet motif formed by β-strands of the monomers. The nuclear export signals of p53 are concealed within the tetramerization domain, therefore export of p53 to cytoplasm requires its dissociation into dimers (Stommel et al., 1999).

1.1.6 The C-terminal domain

The extreme C-terminus of p53, similarly to the N-terminus, is intrinsically disordered. The domain is a subject of numerous posttranslational modifications, that include: acetylation, ubiquitination, phosphorylation, sumoylation, methylation, and neddylation (Joerger et al., 2008). The modifications significantly modulate the activity and stability of p53, i.e. ubiquitination by MDM2 targets p53 for degradation whereas

acetylation of C-terminal lysines enhances affinity of p53 to DNA both in vitro and in vivo. The p53 C-terminal peptide (residues 367-388) was shown to bind the calcium-binding protein S100B (Rustandi et al., 2000) and was also suggested to be able to interact with the N-terminal domain of MDM2 (Prives et al., 2010), however neither in vitro NMR ((Prives et al., 2010), own research) nor in-cell NMR analysis (Phil Selenko, personal communication) show any physical interaction between those domains.

1.1.7 Quaternary structure of p53

Even though the individual domains of p53 were thoroughly characterized by structural biochemistry methods, the arrangement of the domains in the full-length protein is an elusive issue, that has only recently started to be resolved by combination of NMR spectroscopy, small-angle X-scattering and electron microscopy. Free full-length p53 is very unstable in solution (Bullock et al., 1997) and different models of quaternary structure were obtained by different groups (Okorokov et al., 2006; Tidow et al., 2007). In all the models, however, the N-terminal and C-terminal domains of p53 are invisible and thus thought to be exposed to interaction with their numerous protein binding partners. Models of quaternary structure of p53 bound to DNA are more consistent and generally show,, that p53 upon binding to DNA gets rigidified, wraps around the DNA helix with tetramerization domains placed 40-120 Å away from the DNA and core domains (see Figure 2E) (Tidow et al., 2007).
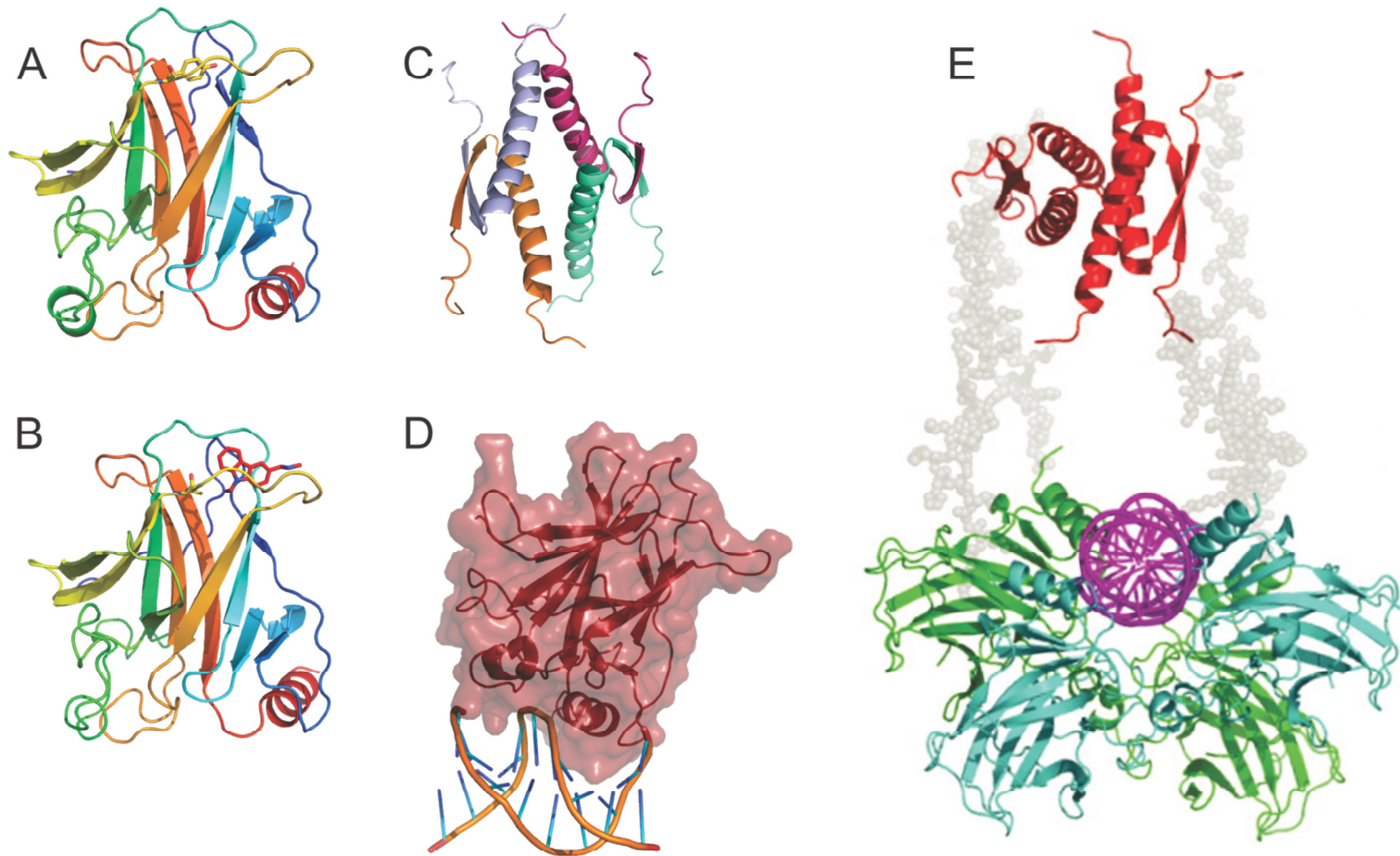
Figure 2 Available structures of p53 protein: (A) wild-type free DNA-binding core domain with an immunoglobulin-like fold; the Y220 residue is marked (PDB ID: 2OCJ (Wang et al., 2007)), (B) Y220C mutant stabilized by a small-molecule binding in proximity of the mutation site (PDB ID: 2VUK (Boeckler et al., 2008)), (C) tetramerization domain comprising of 4 monomers arranged in an orthogonal mode (PDB ID: 1C26 (Jeffrey et al., 1995)), (D) DNA-binding domain recognizing the major and minor grooves with α-helices (adapted from PDB ID: 2AHI (Kitayner et al., 2006)), (E) model of quaternary structure of the p53-DNA complex; the EM images show only two areas of density separated by 4-12 nm, that may be filled with tetramerization domains and DNA-DNB complex (E) adapted from (Joerger et al., 2008).

1.2 MDM2 and MDMX

MDM2 and MDMX are proteins with a high degree of sequence similarity, that was probably retained following duplication from a single ancestral gene.

p53 is the main, but not the only, protein partner of MDM2 and MDMX. MDM2 was shown to interact through its central unstructured region also with Arf tumor suppressor (Sherr 2006), that is able to sequester MDM2 in the nucleolus (Weber et al., 1999; Sivakolundu et al., 2008) and ribosomal proteins,, that may prevent it from binding p53 in case of ribosomal stress (Lohrum et al., 2003; Miliani de Marval et al., 2011).

1.2.1 Primary sequences

Human MDM2 and MDMX are proteins of 491 and 490 amino acids, respectively. The greatest sequential similarity is observed between their N-terminal p53-interacting domains. The sequential alignment of the proteins is shown in Chapter 8.2; the domain organization of the proteins is shown in Figure 3. Both proteins consist of ca. 60% of unstructured regions and only ca. 40% of structured parts.
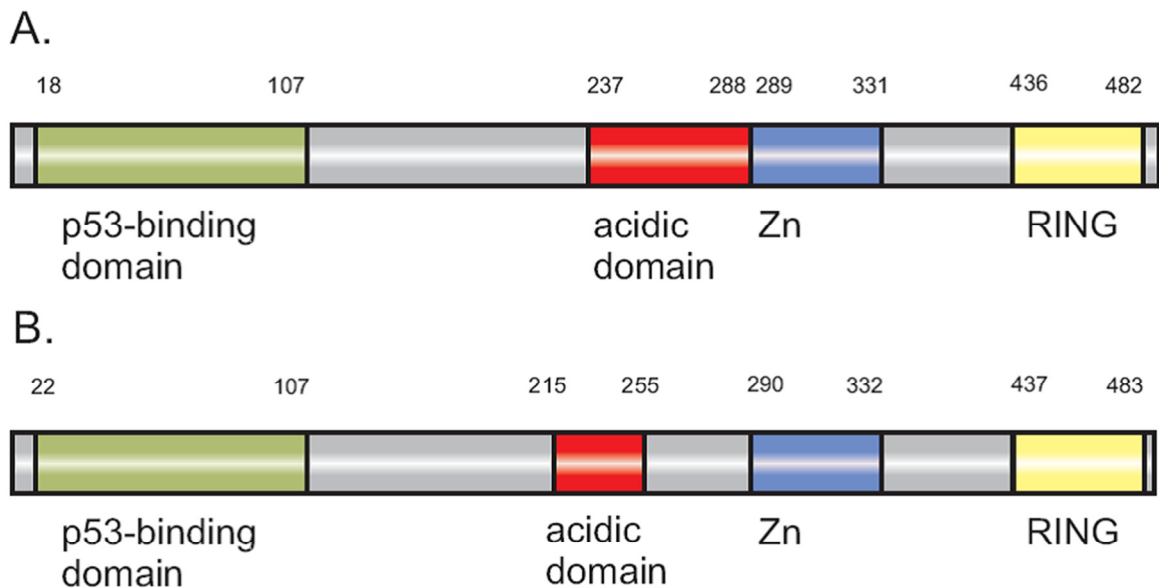
Figure 3 Domain organization of MDM2 (A) and MDMX (B).

1.2.2 The p53-binding domain

The N-terminal domain is probably the most thoroughly studied element of both proteins, as it provides the strongest contacts with p53 and is a target of small molecules antagonizing the MDM2-p53 and MDMX-p53 interactions.

Residues from ca. 27 to 110 fold into a globular assembly of helices, that is classified as SWIB/MDM2 domain fold (Bennett-Lovsey et al., 2002). Surprisingly, structural analysis shows, that the domain shares fold with the ATP-dependent chromatin-remodelling proteins, which facilitate transcription activation by destabilizing histone-DNA interactions (Tang et al., 2010).

The p53-binding domains of both MDM2 and MDMX in their apo states are to large degree flexible and therefore the only high-resolution structures of MDM2 and MDMX available are co-crystal structures of the proteins bound to various ligands (including the p53-derived peptide; see Figure 4).

Human MDM2 and MDMX in complex with the transactivation domain of p53 (17-29) have 4 α-helices and 2 short β-strands forming an antiparallel β-sheet element. MDM2 consists of helix I spanning from P32 to V41, helix II from M50 to K64, helix III from L81 to F86, helix IV from H96 to N106, strand 1 from I74 to Y76 and strand II from S90 to S92. Two longer helices (II and IV) and two shorter helices (I and III) form a p53 binding site (Kussie et al., 1996). MDMX has identical structural organization and the boundaries of secondary structure elements are analogous (see sequential alignment in Chapter 8.2 and Figure 4B). The overall fold of N-terminal domains of both proteins is almost identical, with only minor differences in location of helix IV, that is displaced by 1.5Å-3Å when MDM2 and MDMX are compared.

The p53 binding pockets of both proteins have hydrophobic surfaces and in both cases, residues 19-26 of the TAD domain of p53 form an amphipathic helix interacting by its hydrophobic side with MDM2 or MDMX. Besides van der Waals contacts, the interaction between MDM2/MDMX and p53 is stabilized by a hydrogen bond between the carbonyl oxygen of Leu54^{MDM2}/Met53^{MDMX} and the indole $^{N}H^{\varepsilon}$ proton of Trp23^{p53}.

Even though the secondary and tertiary structures of N-terminal domains of both proteins are almost identical, there are some differences in recognition of p53 by MDM2 and MDMX, that originate from different arrangement of amino acid side chains forming the p53 binding sites (see Figure 4A, C). Particularly the configuration of Tyr99^{MDMX}/Tyr100^{MDM2} in p53-bound complexes of both proteins is different; in MDM2, the χ_1=-162°, whereas in MDMX is χ_1=-72°. As a consequence, the Tyr99^{MDMX} side chain points toward the p53 peptide and thus, limits the size of the hydrophobic p53-binding pocket. Interestingly, X-ray structures of other MDM2 and MDMX complexes show some degree of flexibility of Tyr side chains in both proteins, that may exists either in "open" or "closed" states, however the structures with the "closed" conformations are definitely more abundant.

Low-resolution solution-state NMR structure of the N-terminal domain of apo-MDM2 shows identical arrangement of secondary structure elements and backbone fold very similar to its p53-complex, although the p53-biding cleft in the ensemble of NMR structures is generally narrower than in the p53-bound form and Tyr100^{MDM2} is encountered mostly in the "closed" conformation (Uhrinova et al., 2005).

There is also, based on co-immunoprecipitation, evidence showing the interaction of the N-terminal domain of MDM2 with the PTB domain of Numb (Juven-Gershon et al., 1998; Colaluca et al., 2008). NMR studies, however, do not show any interaction - neither between the full-length domains, nor NUMB and MDM2-derived peptides (^{100}YTMIY^{104} and ^{100}YTMI(p)Y^{104}), that have sequence most similar to the Numb consensus sequence (that is YIGPpYΦ (Li et al., 1997)) (own research).
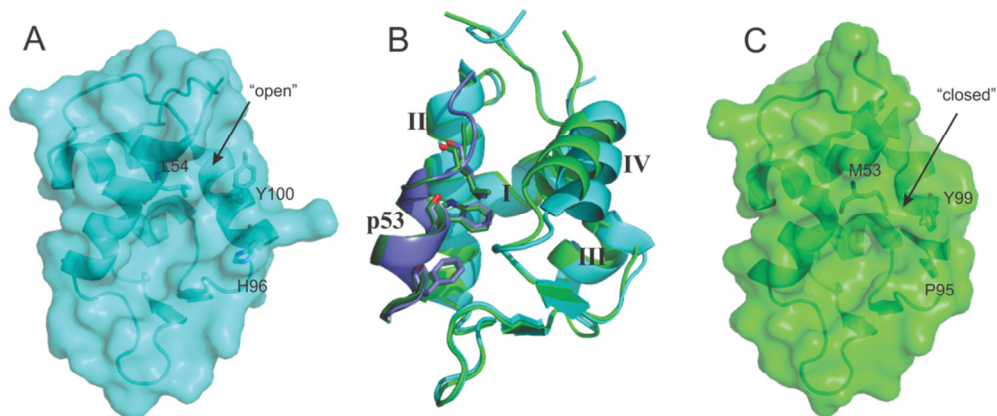
Figure 4 Structures of the N-terminal domains of MDM2 MDM2 (PDB ID: 1YCR (Kussie et al., 1996) and MDMX (PDB ID: 3DAB (Popowicz et al., 2008)). (B) structural alignment of the N-terminal domains of MDM2 (green) and MDMX (cyan); p53 peptide with the most important residues rendered in darker tones. (A) and (C): surface representations of MDM2 and MDMX devoid of p53 peptides. Residues forming the Leu26p53 pocket are marked; in MDMX, the Tyr99[MDMX] side chain points toward the p53-binding pocket, thus limiting its size (the arrangement defined as "closed"), whereas in MDM2, Ty100[MDM2] side chain points in other direction, enlarging the p53-binding site (arrangement defined as "open").

1.2.2.1   The N-terminal "lid"

The very N-terminus of MDM2 is thought to adapt a transient α-helical structure and occupy the p53-binding cleft in the apo state of MDM2. This hypothesis is based on NMR data showing high heteronuclear NOE values for residues 17-26, chemical shifts of C^α and CO carbons, that are positively deviating from their reference random-coil values, and additionally, protection from paramagnetic relaxation enhancement of the p53-binding cleft is similar in case of the apo-protein and its p53-bound form (McCoy et al., 2003; Showalter et al., 2008). The helical "lid" is therefore thought to being able to weakly compete with p53 and phosphorylation of Ser17[MDM2] is expected to suppress the "lid" binding and thus, decrease the stability of p53-binding domain (Worrall et al., 2010). Interestingly, molecular dynamics simulations show, that interaction with "lid" may facilitate Tyr100[MDM2] opening and paradoxically enhance the p53 binding (Dastidar et al., 2011).

In the MDMX primary sequence, the "lid" seems to be broken by Pro and Gly, additionally NMR studies show, that the residues equivalent to the "lid" motif have chemical shifts close to the random coil values (Sanchez et al., 2010).

1.2.3 Acidic domain

Bioinformatics shows, that this part of the proteins is unstructured (Yu et al., 2006); however, functional analysis confirms, that this region contributes to degradation of p53 in a manner independent of E3-ligase activity (Argentini et al., 2001) and forms also a second, weak affinity interaction site between MDM2 and p53 (Yu et al., 2006).

1.2.4 Zinc-finger domain

Central parts of both MDM2 and MDMX contain a short fragment, that forms a zinc finger type RanBP2/NZF C4. The Zn2+ ion is coordinated by four Cys side chains and the loose structure consists of a 3_{10} helix element followed by four short β-strand patches forming two orthogonal hairpins (see Figure 5C) (Yu et al., 2006).

The structure resembles motifs, that are encountered in mRNA binding proteins, however, there is no evidence of interaction of neither MDM2 nor MDMX with mRNA and the exact function of the domain remains unknown (Yu et al., 2006).

1.2.5 RING domain

The RING domains are ca. 50 amino acid long polypeptides coordinating two zinc ions, with one zinc atom coordinated by four cysteines and the other by two cysteines and two histidines (Kostic et al., 2006). The RING domain of MDM2 has activity of the E3 ubiquitin ligase (that transfers the activated ubiquitin from E2 ligases to its final destination), whereas MDMX has no detectable E3 activity (Linares et al., 2003). Dimerization of RING domains of MDM2 and MDMX seems to be their intrinsic property and structural data available for them shows, that the MDM2 RING-domains form homodimers or heterodimers with MDMX (Kostic et al., 2006; Linke et al., 2008). Structural investigation of isolated MDMX RING domains has not been carried out, however, both the MDM2 RING homodimer and the MDM2-MDMX RING heterodimer
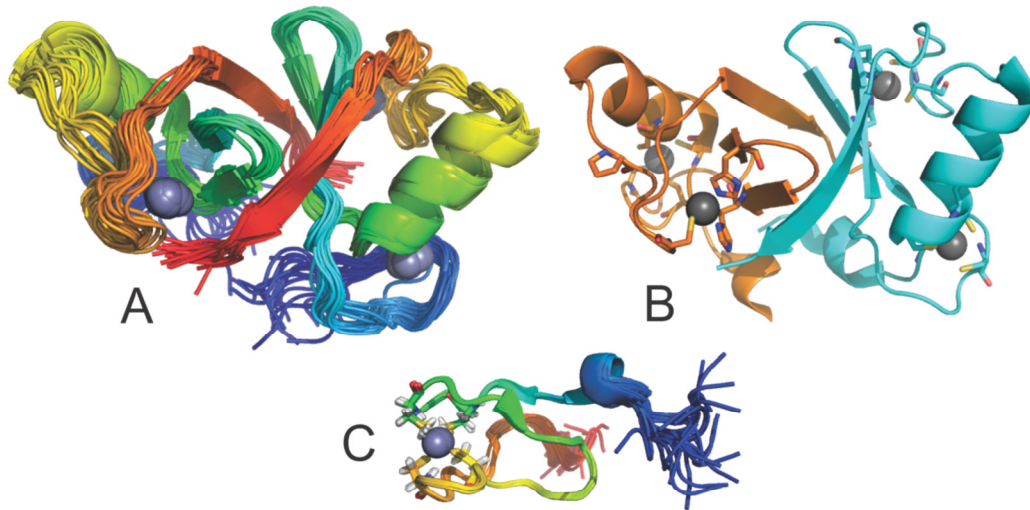
Figure 5 Structures of RING domains: (A) MDM2 homodimer (PDB ID: 2HDP (Kostic et al., 2006)) and (B) MDM2-MDMX heterodimer (MDM2 rendered in orange, MDMX in cyan) (PDB ID: 2VJE (Linke et al., 2008)); (C) structure of a putative zinc finger from the central region of MDM2 (PDB ID: 2C6A (Yu et al., 2006)).

share very similar tertiary structures, which may suggests lack of large structural differences between the RING domains of both proteins. Some reports, however, show, that MDMX alone is monomeric (Linares et al., 2003) .

In both homo- and heterodimers, the very C-terminal residues of RINGs (and MDMs) are engaged in formation of parallel β-sheet by pairing with one of the β-strands of the other RING domain (Kostic et al., 2006; Linke et al., 2008).

The lack of the E3 activity in MDMX was recently associated with mutations affecting the dimer stability and interaction with the E2 partner (Iyappan et al., 2010). Functional assays show, however,, that MDM2-MDMX heterodimers are most effective in transferring ubiquitin to p53, additionally MDM2 is able to transfer ubiquitin to the RING domain of MDMX as well as ubiquitinate itself in the trans-mode (Wade et al., 2010). Disruption of the MDMX-MDM2 heterodimer, leading to decrease of ubiquitination activity, is thus considered another potential therapeutic strategy (Wade et

al., 2009). However, flatness of the interdomain interface makes the task of developing small molecules inhibiting this interaction challenging.

1.2.6 p53 recognition

MDM2 and MDMX bind p53 primarily through their N-terminal domains. Additionally, a weak secondary interaction interface was identified between the DNA-binding core domain of p53 and central, acidic part of human MDM2 (residues ca. 259-275) (Yu et al., 2006). Human MDMX sequence in the analogous area is similar (see Chapter 8.2) therefore similar interaction for MDMX and p53 is likely, though not confirmed experimentally yet.

Thermodynamics of recognition of p53 by MDM2 and MDMX, as well as transitions encountered in MDM2 upon binding of p53, have been thoroughly studied. Both MDM2/MDMX and p53 experience large degree of conformational stabilization upon interaction. The transient helical part of p53 TAD is stabilized to fold into a proper α-helix and forms almost identical structures in both MDM2 and MDMX complexes (see Figure 4B). Also MDM2 and MDMX experience structural stabilization, that is demonstrated, for example, by narrowing of NMR resonances and increasing the spectral dispersion (Stoll et al., 2001; Schon et al., 2002; Sanchez et al., 2010). Binding of p53 is also associated with replacement of the "lid" element followed by its unfolding (Showalter et al., 2008).

The majority of methods used to determine K_Ds of intermolecular interactions show, that MDM2 and MDMX bind p53 with closely similar affinities and the K_D of their interactions oscillates around 0.6 μM (and this averaged value is used in all the calculations in this dissertation). This corresponds to ΔG = -7.4 kcal/mol at room temperature (Schon et al., 2002; Popowicz et al., 2007; Zdzalik et al., 2010). The only report showing, that binding of p53 to MDMX is significantly weaker, with K_D ca. 20 μM, is based on results of cellular biochemistry assays (Bottger et al., 1999) and therefore it may be hypothesized, that some additional factors influenced this, most likely, overestimated K_D value.

The phenomenon for Tyr100^{MDM2} "opening" in the MDM2-p53 complex is elusive and the question why the Tyr100^{MDM2} is in an "open" conformation and Tyr99^{MDMX} is in the "closed" state still needs answering. Molecular dynamics simulations show, that the Tyr100^{MDM2} "opening" may be a step necessary before accommodating the Trp23^{p53} side chain (Dastidar et al., 2009), however, at the same time MDMX is able to bind the Trp23^{p53} side chain with Tyr99^{MDMX} "closed". Comparative computational studies of p53 recognition by MDM2 and MDMX were carried out (Joseph et al., 2010). The results are, however, questionable because the free energies of recognition derived from the MD runs differ significantly from the experimentally determined values.

1.3 The MDM2-MDMX-p53 network

MDM2 and MDMX - due to their high sequential similarity - were at the beginning considered partially redundant factors (Gu et al., 2002). However, a more recent picture of p53 regulation by MDM2 and MDMX shows, that MDM2 and MDMX should be rather considered as independent and equally important players capable of interplay with each other and p53 simultaneously (Marine et al., 2004).

The MDM2 and MDMX p53-binding domains bind a fragment of transactivation domain of p53, thus preventing it from binding transcription co-activators. Additionally, MDM2 has ubiquitin ligase E3 activity and is able to polyubiquitinate the C-terminal parts of p53 itself as well as MDMX. As a consequence, depending on other regulatory factors, p53, MDM2 or MDMX are targeted by MDM2 for degradation in proteasome (Wade et al., 2010).

The most active form of MDM2 is a heterodimer with MDMX and both proteins are at the same time able to bind p53 in very similar ways. In healthy cells, such network controls the p53 level and prevents unnecessary apoptosis by ubiquitylating the p53 and targeting it for degradation in proteasome. Under conditions of cellular stress or DNA damage, several residues around the RING domain of MDM2 get phosphorylated, resulting in destabilization of the dimer and in consequence, p53 stabilization (Cheng et

al., 2009). Additionally, phosphorylation of the TAD domain of p53 leads to decrease of its affinity to MDM2 (and probably also MDMX) and releases the free p53, that may interact in the nucleus with transcription activators like p300, or bind to anti-apoptotic proteins from the Bcl-2 family and thus activate apoptosis by abolition of BAX/BAK inhibition (Toledo et al., 2006).

Last but not least, p53 regulates its level in a negative-feedback loop on transcription level by enhancing the transcription of the mdm2 gene, whereas transcription of mdm4 is not regulated by p53 (Marine et al., 2005).
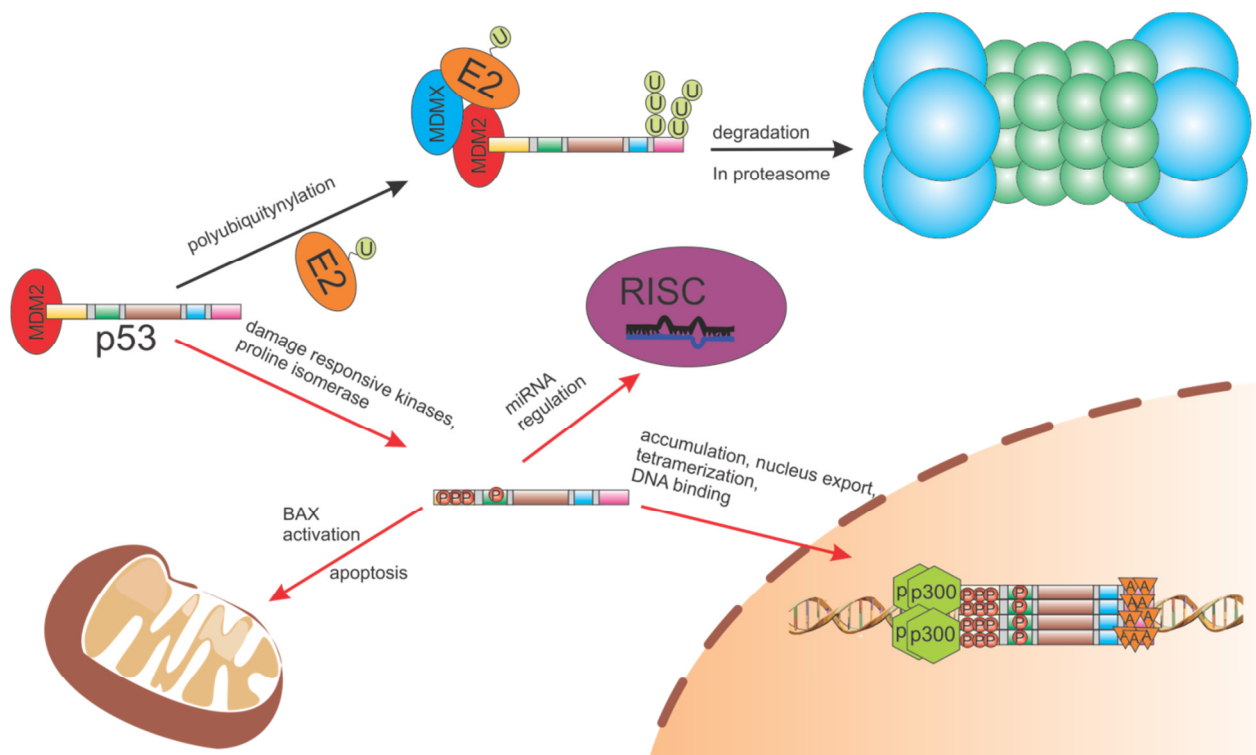
Figure 6 A scheme of p53 regulation: black arrows show negative regulatory pathway (downregulating p53 in healthy or malignant cells), red arrows show p53 response to cellular stress.

1.4 Therapeutic potential of MDM2-MDMX-p53 network regulation

Although ~50% of human cancers retain the wild-type p53 allele, many express increased levels of either MDM2 or MDMX (Vousden et al., 2007). This suggests, that in addition to genetic mutations, p53 may be functionally inactivated by interaction with its

negative regulators. Indeed, transgenic mice models show, that MDM2 overexpression results in formation of tumors (Jones et al., 1998) and additionally, a single nucleotide polymorphism within the MDM2 promoter, that increases the MDM2 expression level was found to be related with poor prognosis and early onset of many human tumors (Bond et al., 2004). Knock-out mice models show, that both MDM2 knock-out as well as MDMX knock-out lead to early embryonic lethality, that may be rescued by concomitant knock-out of p53 (Luna et al., 1995; Finch et al., 2002).

Even though the relationships between the MDM2, MDMX and p53 are relatively complex, the restoration of the impaired function of the p53 protein by disrupting the MDM2-p53 interaction offers a fundamentally new avenue for targeted therapy for broad range of cancers. Cancer cells are extremely sensitive for action of p53 and many current therapeutic strategies, that employ the generally genotoxic agents act through indirect p53 activation (Wade et al., 2009).

Despite of the high sequential and structural homology of N-terminal domains of MDM2 and MDMX, known inhibitors of MDM2-p53 are generally not effective in the MDMX-p53 interaction (Popowicz et al., 2007; Wade et al., 2009). Unfortunately, the effectiveness of MDM2-p53 inhibitors in vivo is significantly decreased due to increase in MDMX expression (Wade et al., 2006). Several studies indicated, that dual inhibition of both the MDM2- and MDMX-p53 interaction has greater therapeutic potential (Hu et al., 2007).

MDM2 and MDMX antagonists may have also important utility in protecting normal proliferating tissues during antimitotic chemotherapy of tumors expressing mutant p53. Normal cells possess wild type functional p53, and pretreatment with MDM2/X antagonists will arrest their proliferation and may protect them from the toxicity of chemotherapy. They may resume proliferation after drug removal. Cancer cells with defective mutant p53 will be insensitive to MDM2/X antagonists and thus be selectively vulnerable to the mitotic poison (Vassilev 2007).

The crystal structure of N-terminal domains of MDM2 and MDMX in complex with the p53 peptide (residues 15-29) show, that the interface of p53/MDMX relies on the

steric complementarity between the MDM2/X and the hydrophobic face of the p53 α-helix and, in particular, on a triad of p53 amino acids Phe19, Trp23, and Leu26, which insert deep into the MDM2/X. Thus the p53 amino acid triad comprises the "hot spot" of the p53-MDM"2/X interaction. Noteworthy is the cross section dimension of the p53 binding site in both MDM2 and MDMX of ca. 17 Å (from Cα-Tyr75 to Cα-Tyr99), which is the size of small organic molecules thus indicating the possibility of small molecule interference.

1.5 Inhibitors of MDM2-p53 and MDMX-p53 interactions

Great therapeutic potential of the disruption of the MDM2/X-p53 interaction resulted in large interest of pharma industry and academic groups in development of small molecules targeting their primary interaction site consisting of their N-terminal regions. Several low-molecular-weight inhibitors of MDM2 have been developed and some of them are probably already in clinical trials on humans. Essentially, all the known potent inhibitors currently available are based on either p-halogenated phenyl groups or a combination of 6-chloro(ox)indole with other hydrophobic groups, that are used to fill the Phe19^{p53} and Leu26^{p53} pockets (Popowicz et al., 2011). Some of the most developed inhibitors of the interaction are described in the following subsections.

1.5.1 Nutlins

Compounds from the Nutlin family were discovered by HTS at Roche and are based on a tetrasubstituted imidazoline scaffold. The most potent in vitro, Nutlin-3a binds MDM2 with K_i of 36 nM – 90 nM (as derived by various assays) and MDMX about 1000-fold weaker (Vassilev et al., 2004; Popowicz et al., 2007; Popowicz et al., 2011). Nutlins occupy the Trp23^{p53} and Leu26^{p53} binding pockets by p-chlorophenyl group and the third phenyl substituent of Nutlin reaches the Phe19^{p53} only indirectly by an ortho-isopropoxy group. The Tyr100^{MDM2} in the MDM2-Nutlin cocrystal structure is in "closed" conformation. Nutlins induce apoptosis in p53 wild-type cells and show *in vivo* efficacy

in mice xenograft models, however, only at high non-physiological concentrations (Vassilev et al., 2004). Next generation of Nutlins is in clinical trials (i.e. (Marx 2007), http://www.wellsphere.com/).
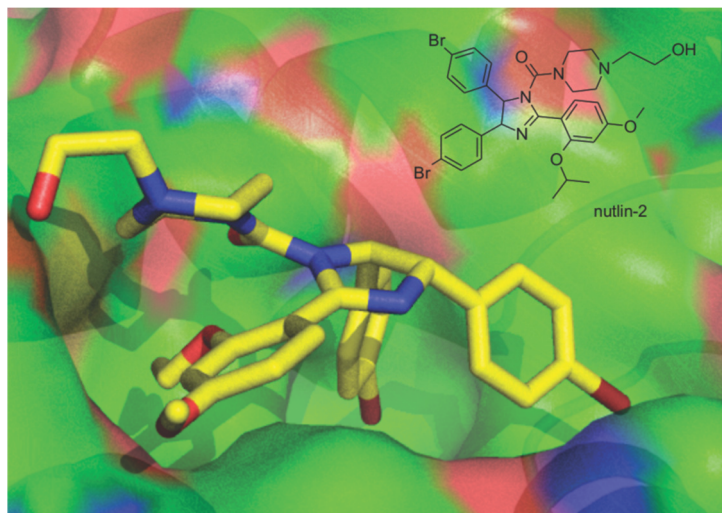
Figure 7 Structure of Nutlin-2 bound to MDM2 (PDB ID: 1RV1 (Vassilev 2007)).

1.5.2 Benzodiazepinediones

These compounds were discovered by HTS employing the ThermoFluor – a temperature-dependent protein unfolding assay. The strongest MDM2-binding compound has a K_i of 80 nM (Grasberger et al., 2005). The inhibitor belongs to a well-known drugs family of benzodiazepines and similarly to Nutlins explores the the Trp23[p53] and Leu26[p53] binding pockets by p-chlorophenyl groups, the Phe19[p53] pocket is filled by a part of benzodiazepine scaffold. The Tyr100[MDM2] in MDM2-inhibitor cocrystal structure is in the "closed" conformation. No data about affinity of the compounds to MDMX is available.
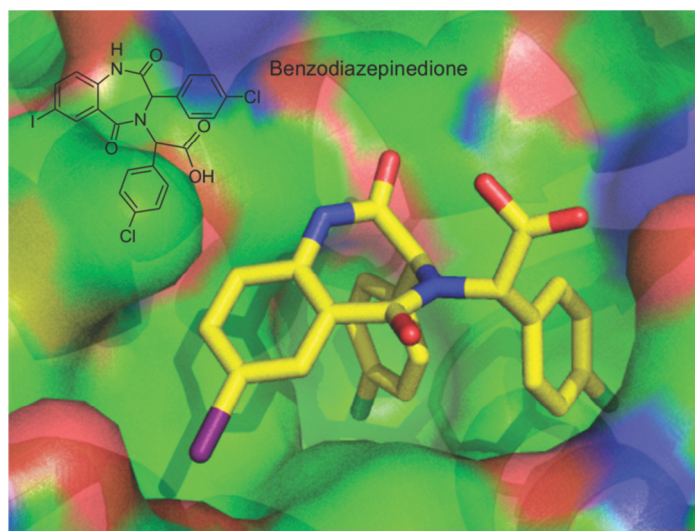
Figure 8 Structure of the benzodiazepinedione inhibitor bound to MDM2 (PDB ID: 1T4E (Grasberger et al., 2005)).

1.5.3 Imidazole-indoles

Compounds from the imidazole-indole family are the first examples of the compounds binding efficiently to both MDM2 and MDMX with the K_is toward MDM2 in range of 0.1 μM and MDMX – ca. 1 μM (Popowicz et al., 2010). The compounds were developed independently by two groups (Boetther 2008; Czarna et al., 2010; Popowicz et al., 2010). The imidazole scaffold provides arrangement of substituents very similar to this encountered in the Nutlins family, however, this class of the compounds explores the Trp23^{p53} binding pocket with 6-chloroindole ring and 26Leu^{p53} pocket with a p-chlorophenyl ring. The Phe19^{p53} pocket is filled with the phenyl ring. Surprisingly, the structure of the MDMX-imidazole-indole complex is very similar to the MDM2-inhibitor complex, proving, that both proteins may adapt the same conformation and be targeted with a single low-molecular-weight inhibitor. In both cases, the Tyr99^{MDMX}/Tyr100^{MDM2} is in the "closed" conformation. No in-vivo data is available for these compounds.
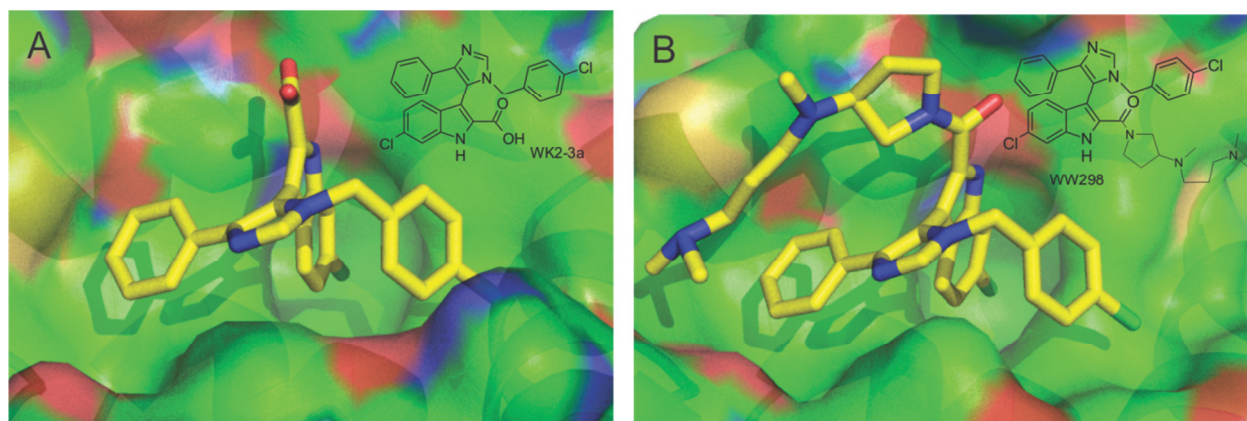
Figure 9 Imidazole-indole inhibitors bound to MDM2 (PDB ID: 3LBK) and MDMX (PDB ID: 3LBL) (Popowicz et al., 2010).

1.5.4 Spiro-oxindoles

The compounds were designed in a rational way by extension of a spiro-oxindole group, that was expected to be a good starting fragment filling the $\text{Trp23}^{\text{p53}}$ cavity (Ding et al., 2005). Surprisingly, the compound was expected to fill the $\text{Phe19}^{\text{MDM2}}$ and $\text{Leu23}^{\text{MDM2}}$ with phenyl-derivative and neopentyl groups, respectively (Shangary et al., 2008), but it actually binds the opposite way and is seemingly "flipped" by 180° (Popowicz et al., 2010). The compounds bind MDM2 with affinities in low nM range and interact only weakly with MDMX (with K_is about 10000 times weaker) (Popowicz et al., 2010). Compounds named MI-219 and MI-63 were shown to be highly potent in cell lines and animal models (Mohammad et al., 2009; Azmi et al., 2011). Again, in the cocrystal structure of MI-63 analogue with MDM2, $\text{Tyr100}^{\text{MDM2}}$ is in the "closed" conformation.
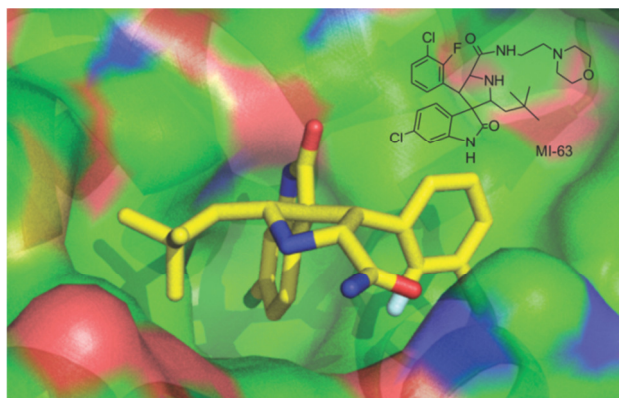
Figure 10 Cocrystal structure of the MI-63 analogue bound to MDM2 (PDB ID: 3LBL (Popowicz et al., 2010)).

1.5.5 High-affinity peptides

Numerous studies show, that the molecular recognition of p53 by both MDMX and MDM2 is not perfect energetically and more potent peptide-based dual antagonists of the interaction may be derived. All the high-affinity peptides share a common feature: Pro27^{p53} is replaced by other amino-acid, thus prolonging the helical-path in TAD domain and facilitating more favorable contacts (Zondlo et al., 2006; Czarna et al., 2009; Pazgier et al., 2009). This results in low nanomolar affinities. The big drawback of peptide-based inhibitors are however their instability and lack of cell-permeability; their therapeutic potential may be however employed in combination with gene therapy.

The other promising peptide-based therapeutic approach uses hydrocarbon stapled-peptides. This recently emerged class of drug candidates is based on a peptide chain, that is "stapled" in a helical configuration with a hydrocarbon chain to make a cyclic form (Bernal et al., 2007; Crunkhorn 2011). This approach is beneficial for three reasons: covalent modification stabilizing the transient α-helix of TAD decreases the entropic cost of binding, the staple protects the peptides from proteolytic degradation and enables them to cross the membrane (Guo et al., 2010). The peptides show low nanomolar affinities to MDMX and MDM2 and surprisingly, bind preferentially MDMX (Bernal et al., 2010). The peptides show high activity in cellular assays and the license

for the "stapling" technology has been recently bought from Aierlon Therapeutics by Roche for an astronomical value of 1.1 billion dollars (http://www.dailyfinance.com/).
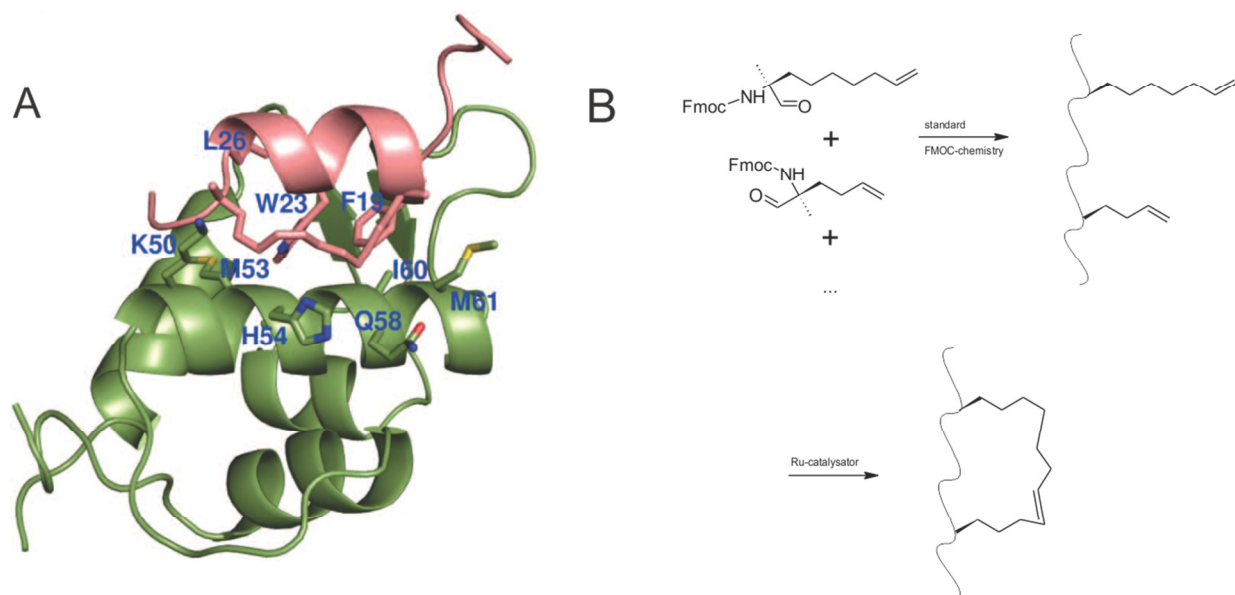
Figure 11 (A) Binding of a stapled peptide to MDMX according to MD simulations exploits the usual interactions of the p53 amino acid triad and additional favorable contacts of the staple (adapted from (Joseph et al., 2010)) (B) synthesis of stapled peptides: modified amino-acids are incorporated to the polypeptide chain using standard FMOC-synthesis and the staple is then closed via the ruthenium-catalyzed ring closing metathesis (Schafmeister et al., 2000).

2. NMR investigations of protein-ligand interactions

2.1 Introduction

2.1.1 Different ways of expressing ligand affinity: K_D, K_i, IC_{50} and EC_{50}

The terminology used in protein-ligand interaction studies is not uniform and in publications on protein-ligand interactions at least four parameters describing the affinity of the ligand to the protein are used. The values of K_D, K_i, IC_{50} and EC_{50} are frequently used interchangeably (i.e. (Kuntz et al., 1999)) and practically the differences arising from different calculation formalisms are often smaller than the differences in affinities that are obtained by different experimental methods. Understanding of the differences is, however, a prerequisite for proper data analysis and for resolving ambiguities and problems associated with structure-affinity relationships.

The definitions and symbols defined here would be also used in further parts of this section.

K_D of the interaction is a parameter determined for binary interactions:
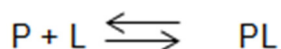
$$P + L \rightleftharpoons PL$$

$$K_D = \frac{[P][L]}{[PL]}$$

In, this case P always denotes the protein and L may be a small molecule or protein partner.

K_i is an analogous parameter that is determined in a two-ligands one-site competitive setup (where P is always a protein, L is a protein partner, peptide or small molecule and I is an inhibitor of the interaction, usually small molecule):

$$PI \underset{+I}{\rightleftarrows} P \underset{+L}{\rightleftarrows} PL$$
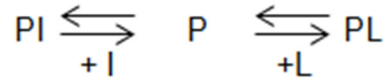
$$K_D = \frac{[P][L]}{[PL]}$$

$$K_i = \frac{[P][I]}{[PI]}$$

The values of K_D and K_i are the same if the ligand and inhibitor bind to the same site and a ternary complex PLI is impossible. Since this is the case for most of the protein-protein and protein-ligand interactions, the values are very often used interchangeably.

The parameters defined as IC_{50} and EC_{50} are the half maximal inhibitory concentration and half maximal effective concentration, respectively. Those quantities are determined from a dose-response curves for protein-agonist (EC_{50}) and protein-antagonist (IC_{50}) interactions. Since distinction between the agonist and antagonist is not always straightforward, the values are often used interchangeably. The relationship between the K_i and IC_{50}/EC_{50} is expressed by the equation:

$$IC_{50} = \left(\frac{f_0 \cdot K_D}{(1-f_0)(2-f_0)} + \frac{f_0 \cdot L_T}{2} \right) \left(\frac{K_i \cdot (2-f_0)}{f_0 \cdot K_D} + 1 \right)$$

<div align="right">Equation 1</div>

where f_0 is defined as dilution-related dissociation fraction of protein-ligand complex in the absence of inhibitor and for equimolar protein-ligand complexes (Huang 2003):

$$f_0 = \frac{[P]}{P_T} = \frac{[L]}{L_T}$$

The IC_{50} and EC_{50} are values thus concentration dependent and special care must be taken when comparing the EC_{50}/IC_{50} and K_D/K_i values.

2.1.2 Ligand- and protein-oriented approaches

Nuclear magnetic resonance spectroscopy is one of the most powerful methods used to probe protein-ligand interactions and numerous techniques employing various NMR observables may be employed to thoroughly characterize interaction of small molecules with the protein. The unquestionable advantage of NMR in studies of protein-ligand interactions is that it relies on direct measurement of the chemical environment of the nuclei. Thus, compared to fluorescence and calorimetry-based methods, NMR is much less prone to give experimental artifacts (Pellecchia et al., 2008).

NMR-based detection of small molecules interacting with the proteins may be carried out by both, the observation of signals originating from the ligands or from the protein. Unfortunately it is impossible to observe both protein and ligand in a single experiment. Methods relying on ligand signals are rather fast and require good solubility of the small molecule and low (μM) protein concentration. On the contrary, the protein-oriented NMR screening, due to low inherent sensitivity of protein signals, is generally material- and time-consuming, however the issue of low solubility of the ligands may be often at least partially overcome (as discussed in the following pages) (Pellecchia et al., 2002).

Because of highly hydrophobic character of the MDM2-p53 interaction, the antagonists of the interaction are also usually also highly hydrophobic and their low solubility is a common problem. Therefore, the usage of ligand-oriented approach is highly limited for this particular system and, to my knowledge, there has been not a single example of successful usage of ligand-observed methods for development of MDM2/X-p53 antagonists (for an overview of current effort in this subject, see i.e. (Popowicz et al., 2011). The next chapters will thus describe two powerful protein-oriented approaches in NMR screening – the SAR by NMR employing characterization of the interaction by performing HSQC titrations of the protein with ligands (Shuker et al., 1996) and competition experiments, particularly AIDA-NMR, that allow for monitoring the dissociation of a protein-protein complex in an NMR tube (D'Silva et al., 2005; Krajewski et al., 2007).

2.1.3 SAR by NMR

The two-dimensional heteronuclear single quantum coherence spectroscopy (HSQC) is performed by excitation of sensitive nuclei (i.e. hydrogen), transfer of the magnetization through scalar coupling to insensitive heteronuclei (e.g. ^{15}N or ^{13}C), creation of a single-quantum coherence on the insensitive nuclei and evolution under chemical shift of the heteronuclei followed by a back-transfer of magnetization through J-coupling to hydrogen and signal detection. This type of spectrum gives a crosspeak at the intersection of frequencies of both J-coupled nuclei; i.e. a single crosspeak in ^{1}H-^{15}N-HSQC spectrum corresponds to a single H-N group (which usually originates from the peptide bond).
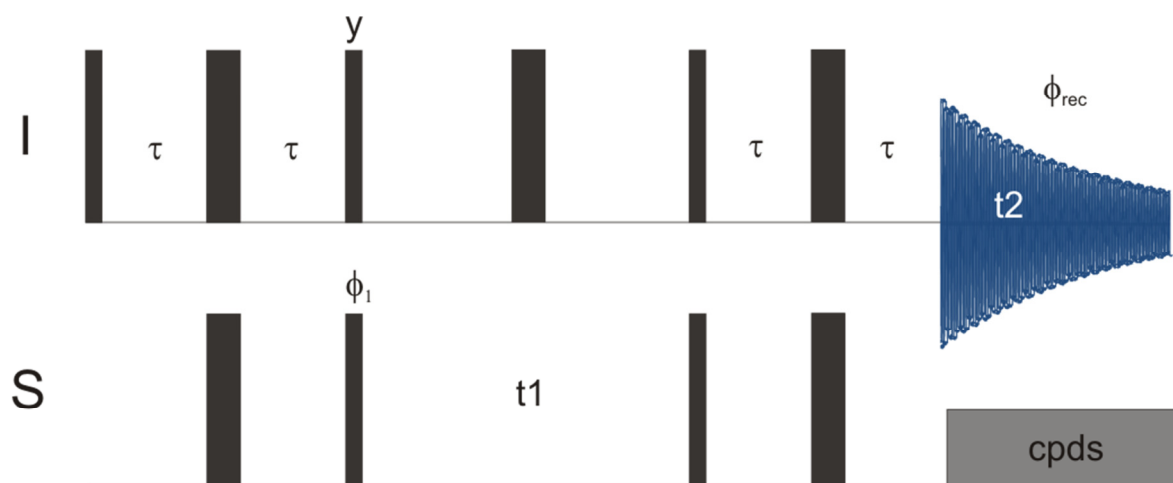
Figure 12 The experimental scheme for a common HSQC experiment (after (Bodenhausen et al., 1980)). The narrow bars depict 90° pulses and wide bars 180° pulses; the τ delay is adjusted to $1/4J_{IS}$, pulses phases are assumed to be x, unless otherwise stated; for purposes of coherence selection $\Phi_{1}= \Phi_{rec}=x,-x$. Two useful variations of the experiment employ different back-transfer schemes that transform both coherences present after the t1 evolution into observables (Kay et al., 1992), thus theoretically enhancing the sensitivity of the experiment by a ⎺ factor and a version in which water magnetization at the beginning of t2 acquisition is aligned along +Z axis, thus decreasing the interscan water saturation (Mori et al., 1995).

The complexity and number of interactions that influence the position of HSQC crosspeaks makes direct interpretation of protein HSQC spectra very difficult, however comparison of spectra recorded under different conditions (e.g. in the absence and presence of a ligand) is straightforward and provides important information on the changes in chemical environment of the nuclei (Pellecchia et al., 2002).

HSQC spectra recorded in presence of ligands yield important qualitative and quantitative information on the interaction. A more detailed analysis of various aspects of HSQC investigations of binding is described and discussed in the following subsections.

2.1.3.1   Chemical exchange timescale and binding affinity

The binding of a ligand to a protein may be considered as a two-site second-order exchange:

$$P + L \; \underset{k_{on}}{\overset{k_{off}}{\rightleftarrows}} \; PL$$
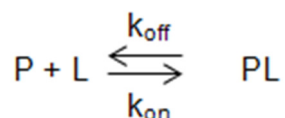
From the mass conservation law we obtain that the equilibrium constant for the reaction is:

$$K_D = \frac{[P][L]}{[PL]} = \frac{k_{off}}{k_{on}}$$

Equation 2

With the averaged lifetimes of the states as follows:

$$\tau_{PL} = \frac{1}{k_{off}} \quad \tau_L = \frac{1}{k_{on}[P]} \quad \tau_P = \frac{1}{k_{on}[L]}$$

The overall exchange frequency $1/\tau^*$ being the averaged frequency of chemical exchange occurrence may be defined for both the protein and the ligand as:

$$\frac{1}{\tau_P^*} = \frac{1}{\tau_{PL}} + \frac{1}{\tau_P} = k_{off} + k_{on}[L] = k_{off} + \frac{k_{off}[PL]}{[L]} = k_{off}\left[1 + \frac{[PL]}{[L]}\right]$$

Equation 3

27

$$\frac{1}{\tau_L^*} = \frac{1}{\tau_{PL}} + \frac{1}{\tau_L} = k_{off} + k_{on}[P] = k_{off} + \frac{k_{off}[PL]}{[P]} = k_{off}\left[1 + \frac{[PL]}{[P]}\right]$$

<div align="right">Equation 4</div>

Therefore, as seen from Equation 3 and Equation 4, the chemical exchange frequency is determined by both k_{off} and concentrations of the interaction players (Lian et al., 1994).

Comparing the timescale of chemical shift with exchange timescale, we may distinguish three situations (Cavanagh et al., 2007):

- "fast" chemical exchange when $1/\tau^* \gg \Delta\omega$ – NMR peaks move continuously during the titration with a ligand, position of the peak is related to concentrations of the "bound" and "free" forms of the ligand
- "intermediate" chemical exchange when $1/\tau^* \approx \Delta\omega$ – shape of the peaks is distorted and exchange broadening is observed in intermediate titration steps
- "slow" chemical exchange when $1/\tau^* \ll \Delta\omega$ – two forms of peaks originating from the "bound" and "free" forms are present; the intensity of the peaks is proportional to the concentration of each of the forms

Figure 13 depicts a simulation of spectral line shapes depending on the timescale of chemical exchange.

By neglecting the influence of concentrations and making assumption that the bimolecular association is limited only by diffusion for interactions of small molecules with proteins ($k_{on} \approx 10^9$ M^{-1}s^{-1}) (Fersht 1998), K_D of the interaction is commonly estimated from the timescale of chemical exchange observed in the system. As implied in Equation 2, for systems undergoing "slow" chemical exchange K_D is in submicromolar range, "intermediate" chemical exchange is a sign of K_Ds in low micromolar range and "fast" chemical exchange is typical for weak interactions with high-micromolar – millimolar K_Ds.
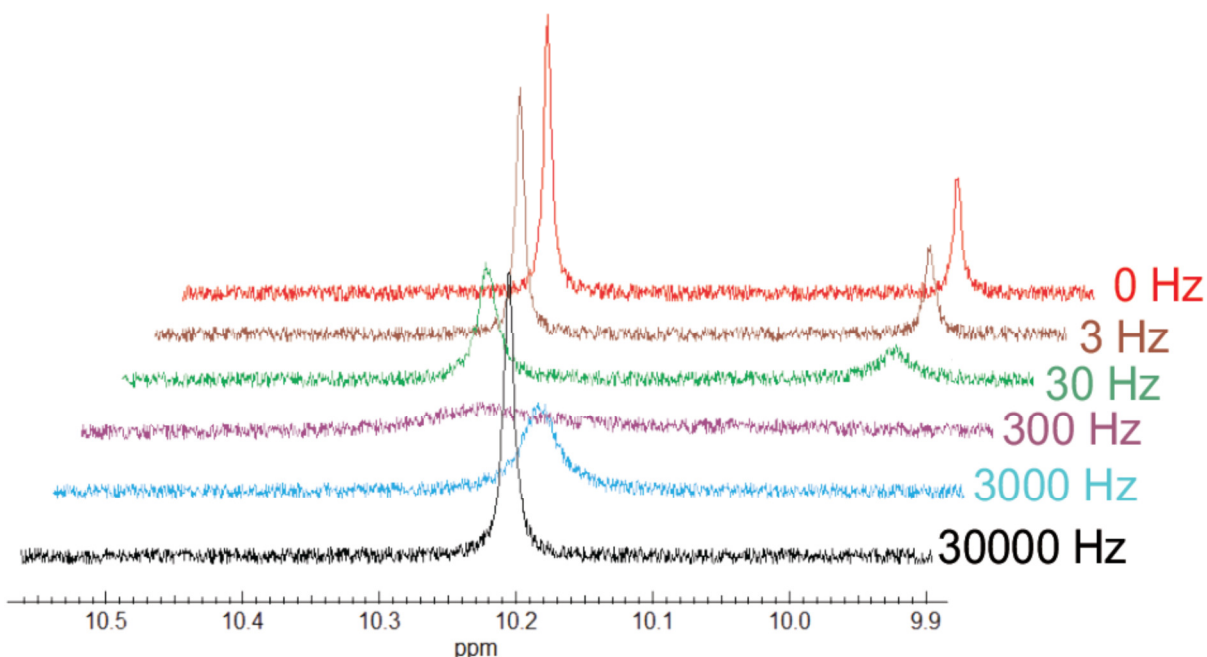
Figure 13 Simulation of NMR lineshapes in presence of chemical exchange. The simulation was performed for 300MHz ^{1}H frequency, with 70% of "free" and 30% of "bound" forms, that are separated by $\Delta\omega$ = 565 rad/s. Numbers on the right side are values of $1/\tau^*$. In order to depict the real situation, 2% of noise was added to the spectra. Simulation was performed with WinDNMR (Reich 1995). The simulation is performed by numeric elucidation of McConell equations (Mcconnell 1958).

It must be emphasized that the McConnell equations describing the magnetization evolution in the presence of chemical exchange (Mcconnell 1958) imply that the type of chemical exchange is not only a function of the k_{off}, but depends also on the difference in chemical shifts of the "free" and "bound" forms. Therefore, the HSQC crosspeaks that exhibit the largest chemical shifts perturbations upon addition of ligands are also more likely to exhibit "intermediate" or "slow" chemical exchange whereas crosspeaks originating from atoms, that undergo smaller changes in their chemical environments may be at the same time in typical "fast" exchange. This dependency may be used for rough estimation of K_D of the interaction; the lower the K_D, the smaller minimal frequency differences give rise to the "slow" or "intermediate" chemical exchange.

In a special (and quite frequent) case of "intermediate" time scale of chemical exchange combined with limited solubility of the compound, an interesting and deceiving case of disappearance of the crosspeaks from the spectrum may occur. Such

situation takes place, when solubility limits the maximal saturation of the protein with a compound to about 30%-70% (see Figure 13). Chemical exchange in this situation may cause broadening or weakening of the resonances beyond the detection level. Similar situation of the crosspeak broadening may be also a consequence of increasing the correlation time of the complex and thus, accelerating the transverse relaxation. This case is easy to distinguish from exchange broadening by spectral line shape analysis; pure non-exchanging NMR states give rise to Lorentzian shape of peaks whereas peaks originating from atoms undergoing chemical exchange have complex non-Lorentzian shapes (see Figure 13).

Another deceiving situation is observed when the protein is titrated with ligand batches containing impurities also binding to the protein or with racemic mixtures of the ligands (when affinities of diastereomers are similar). In case of such competition, even though the ligands are in "fast" exchange, apparent crosspeaks splitting may wrongly suggest "slow" chemical exchange timescale and high affinity of the ligand. Such situations may be easily resolved by employing other methods of K_D determination (i.e. by competition NMR binding experiments).

2.1.3.2 Mapping the binding site of the ligand

Spatial distribution of chemical shift perturbations induced by addition of a ligand allows for mapping the interaction interface. The method, even though powerful and sensitive for even weak (millimolar K_Ds) interactions (Shuker et al., 1996), gives rather low spatial resolution and care should be taken not to overinterpret the obtained results.

First of all, the amide nuclei are strongly involved in interactions with the solvent (i.e. by numerous hydrogen bonds) (Otting et al., 1991) and due to transient character and large complexity of their interactions, several crosspeaks tend to respond unspecifically to change in polarity of the buffer. The situation is even more deceiving by the fact that the most lipophilic areas of the protein are engaged in biologically important processes like protein-protein recognition or enzymatic catalysis and HSQC titrations of

a protein with organic solvents are even used to reveal the druggable sites on protein surfaces (Mattos et al., 1996; Dalvit et al., 1999).

Since binding of a ligand may induce a variety of conformational changes in the protein i.e. affecting the highly dynamic pattern of hydrogen bonds, special care should be taken not to interpret the secondary effects observed in HSQC spectra with direct evidence of ligand binding. To reduce the problem, the chemical shift perturbations of amide protons, that are distant from the solvent-accessible area should be filtered out from the analysis (the solvent accessibility may be determined i.e. using the program NACCESS (Hubbard 1996) (Dominguez et al., 2003).

Different parts of a ligand may induce different magnitudes of chemical shift perturbations; especially delocalized electrons from aromatic rings are able to induce large local magnetic fields (Wuthrich 1986). The consequence of this is twofold: the magnitude and pattern of chemical shift perturbations (that are observed in large excess of the ligand) depends rather on the structure of the ligand-protein complex and not on the actual affinity of the ligand. On the other hand, if a series of HSQC experiments is recorded for structurally similar ligands and the concentrations of the protein and ligands are the same for each spectrum, the magnitude of chemical shift perturbations would be inversely proportional to the K_D of the interaction (providing, that the protein has not been saturated with a ligand and the system undergoes "fast" chemical exchange).

Last but not least – molecular graphics programs are powerful tools for visualization of chemical shift perturbations in structural context, however, the most intuitive (and wrong) way of using those programs is selecting by default an entire amino acid that undergoes the largest chemical shift changes, rendering it with contrast colors and generation of molecular surface. As a consequence, by default the whole amino-acid (from the amide bond to the last side chain atom) is colored. Naturally, the chemical shift perturbation, most commonly measured for the amide group is a space-specific probe, not sequence-specific. Therefore the right way of depicting the ^{1}H-^{15}N-HSQC chemical shifts perturbation is to select the amide groups of proteins and atoms in close spatial proximity of them (from practical experience approximately 2Å - 4Å) and

then render those atoms with color, accordingly to magnitude of chemical shift perturbation.

2.1.3.3 Detecting compounds acting by protein denaturation or covalent modification

Denaturation of a protein leads to collapse of ^{1}H-^{15}N crosspeaks into chemical shifts around 8.2 ppm and 120 ppm for ^{1}H and ^{15}N, respectively. Alternatively, if denaturation is followed by the aggregation of the protein, NMR crosspeaks disappear due to the increase in the rotational correlation time and only few flexible side chain resonances remain visible (Rehm et al., 2002).

The case of covalent modification of the protein is often difficult to detect during HSQC titrations, may be easily mistaken with high affinity binding and spotting of covalent modifications to large extent relies on experience of an NMR spectroscopist and general knowledge of a particular protein-ligand system. Since the k_{off} constant for irreversible chemical modification is 0, an indication of covalent modification may be when slow timescale chemical exchange is prevalent throughout the whole spectrum and no intermediate exchange is observed. However, for very tightly binding ligands, the kinetic dissociation may take even years (Kaplan et al., 1991) and therefore for such cases the only way of distinguishing the reversible and irreversible binding may be i.e. mass spectrometry performed in denaturing conditions.

2.1.3.4 K_D determination from HSQC titrations

For the case of "fast" chemical exchange, plots of normalized chemical shifts perturbations against ligand concentration form a titration curve. K_D determination from such curves is straightforward and relies on fitting the experimental points to the binding isotherm (Equation 5) (Fielding 2007).

$$[PL] = \frac{(K_D + P_T + L_T) - \sqrt{(K_D + P_T + L_T)^2 - (4 \cdot P_T \cdot L_T)}}{2}$$

Equation 5

32

The general issues that must be kept in mind to properly design the NMR titration are:

- Using correct protein concentration

In order to get an analyzable binding curve, protein concentration should be similar to the expected K_D value (see Figure 14 derived from Equaition 5 and made by myself); therefore due to limited sensitivity of NMR experiments, the lower limit on K_D determination by HSQC titrations is ca. 10 µM.

Since this way of the K_D determination is performed in stoichiometric conditions, a factor critical for precision of the measurement is knowing the exact concentration of the protein. As can be easily seen from Equation 5, the error in protein concentration is strongly transferred to the determined value of K_D and considering that K_D may be also defined as the concentration of free ligand [L] at which the protein saturation is 50%, the obtained experimental K_D error may be estimated to at least 0.5 times the error in protein concentration.

- Compound solubility

Inability of determination of the resonance position of a fully "bound" form makes the analysis impossible and, as shown in Figure 16, changing the protein concentration has no influence on the maximal protein saturation that may be achieved during the titration; the maximal achievable saturation of a protein by a ligand is in that case a function of the solubility limit and K_D. An elegant, though experimentally demanding solution of this problem may be determination of chemical shifts of the "free" and "bound" protein forms by relaxation dispersion analysis (Hansen et al., 2008; Gardino et al., 2009).

Also, when solubility is the limiting factor, changing the concentrations does not influence the rate of chemical exchange (see Equation 3 and Equation 4). Thus, increasing the concentration of the complex would decrease the exchange lifetime and thus may be used to modulate the spectral line shapes in unfavorable cases of intermediate chemical exchange.
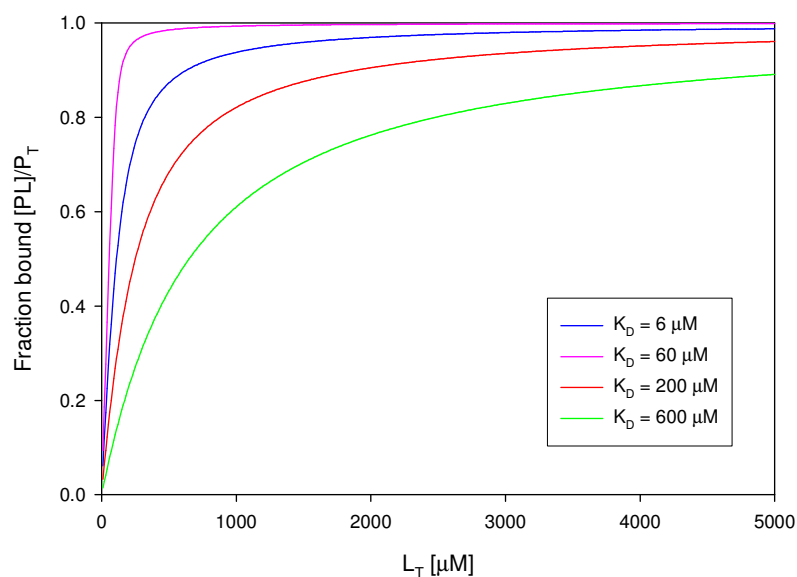
Figure 14 Simulation showing dependence of the bound fraction of the protein (that is equivalent to the chemical shift) on concentration of the ligand added and K_D of the interaction. Concentration of the protein is 100 μM. For weak interactions (high K_Ds), achieving full saturation requires very large excess of the ligand over the protein, for strong interactions, steepness of the titration curve at the beginning of the titration is too high to extract accurate value of K_D, additionally for the case of high protein concentration and low K_D of the interaction, large absolute uncertainties in protein concentration determination transfer to errors in determined K_D value. The most advantageous situation is when the protein concentration is similar to the expected K_D.
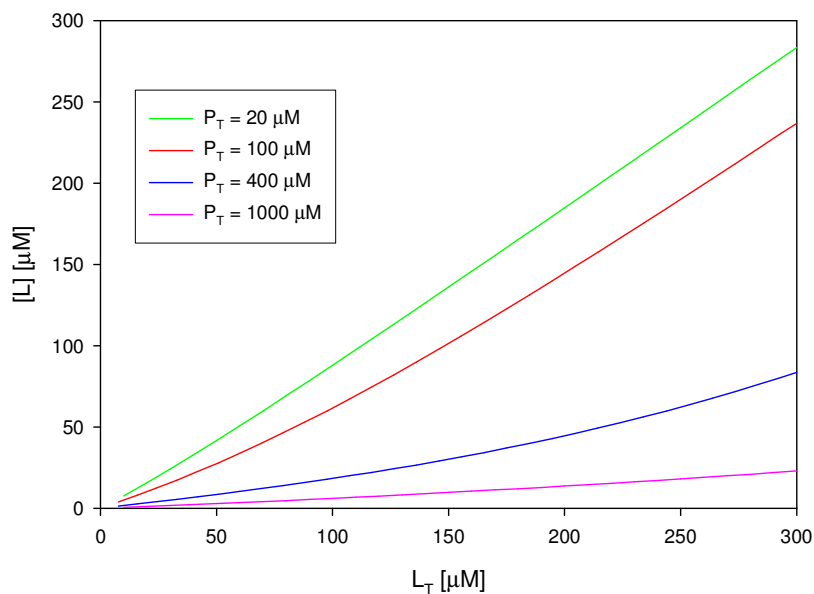
Figure 15 Simulation showing dependence of free ligand concentration on the total amount of ligand added carried out for various total protein concentrations. The K_D of the interaction was set to 60 μM. Total protein concentration has strong influence on free ligand concentration.
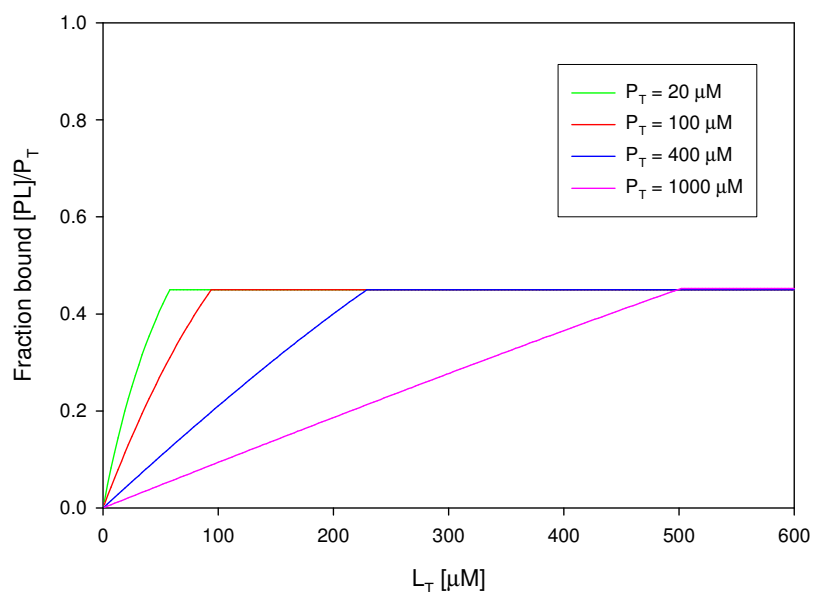
Figure 16 Simulations of HSQC titrations carried out for different total protein concentrations and $K_D = 60\ \mu M$. 50 μM solubility limit of the compound was assumed (equal to the maximal achieveable concentration of the unbound compound in the solution). Total concentration of the protein has no effect on the final saturation achieveable with specific solubility limit and K_D values.

2.1.4 Competition NMR experiments

Competition NMR experiments are powerful and alternative approach to the K_i (equivalent to K_D) estimation by NMR. This class of NMR methods allows for measurement of K_is even in presence of slow chemical exchange and is especially beneficial in case of protein-protein interactions, where the whole protein-protein-antagonist system may be reconstituted in vitro. Knowing the K_D of receptor-reporter interaction, total concentrations of the interaction players and the equilibrium concentrations of receptor-reporter or protein-antagonist complexes, it is possible to calculate the K_i of the receptor-antagonist interaction in a single-step titration (at least for a single-site and two competing ligands system, see section 8.3) (Wang 1995).

2.1.4.1 Antagonist Induced Dissociation Assays

The method, named AIDA-NMR (for the Antagonist Induced Dissociation Assay-NMR) (D'Silva et al., 2005) provides unambiguous information on whether an antagonist of a protein-protein interaction is strong enough to dissociate the complex and whether its action is through denaturation, precipitation, or release of a protein in its functional folded state. For effective antagonists, AIDA can also quantitatively characterize antagonist-protein and antagonist-protein-protein interactions in the form of K_is and fractions of the released proteins from their mutual binding. AIDA requires a large protein fragment (larger than ca. 30 kDa) to bind to a small protein (less than ca. 20 kDa). The principle of the method is explained in Figure 17.

The 2D NMR version relies on monitoring HSQC spectra of the ^{15}N and/or ^{13}C labeled reporter protein. For its 1D proton NMR variant (on unlabeled proteins, i.e. no ^{15}N or ^{13}C labeling required), one must have or must introduce an amino acid "reporter", that has at least one non-overlapped NMR signal which is sensitive to the binding of a ligand to the investigated protein. Since signal overlap in proton 1D spectra of proteins may present a problem, we have chosen to use tryptophan; this is because it is the only amino acid whose $^{N}H^{\varepsilon}$ indole side chain gives an NMR signal at approximately 10 ppm at physiological pH; the signal is hence well separated from the bulk of amide protons and can be easily monitored. To be used in our NMR assay, the Trp residue must be positioned near a potential antagonist binding site and, importantly, its indole side-chain must be flexible so, that its high motion gets restricted upon binding of the Trp-reporter protein to its proteinous target. The principle of one-dimensional version of the assay is explained in Figure 18.

The approach of using competition assays in search for PPI antagonists is advantageous over the traditional SAR by NMR (Shuker et al., 1996); in competition methods a real potency of a compound to inhibit the PPI interaction is assayed whereas classical NMR-aided drug discovery relies on checking only binary interactions between one of the protein partners and the ligand. Another advantage of the 1D version of the AIDA competition assay is that it allows for simultaneous quantification of both – the protein-partner-bound and free forms of the reporter protein in a single experiment.

Thanks to this, a reliable K_D estimation can be achieved in a one-step titration. For a 1D version of AIDA, a K_D determination can be achieved typically for protein concentrations as low as 40 µM for a ca. 0.5 h experiment in a 5 mm NMR tube using a cryogenically cooled probehead on the 600 MHz spectrometer.
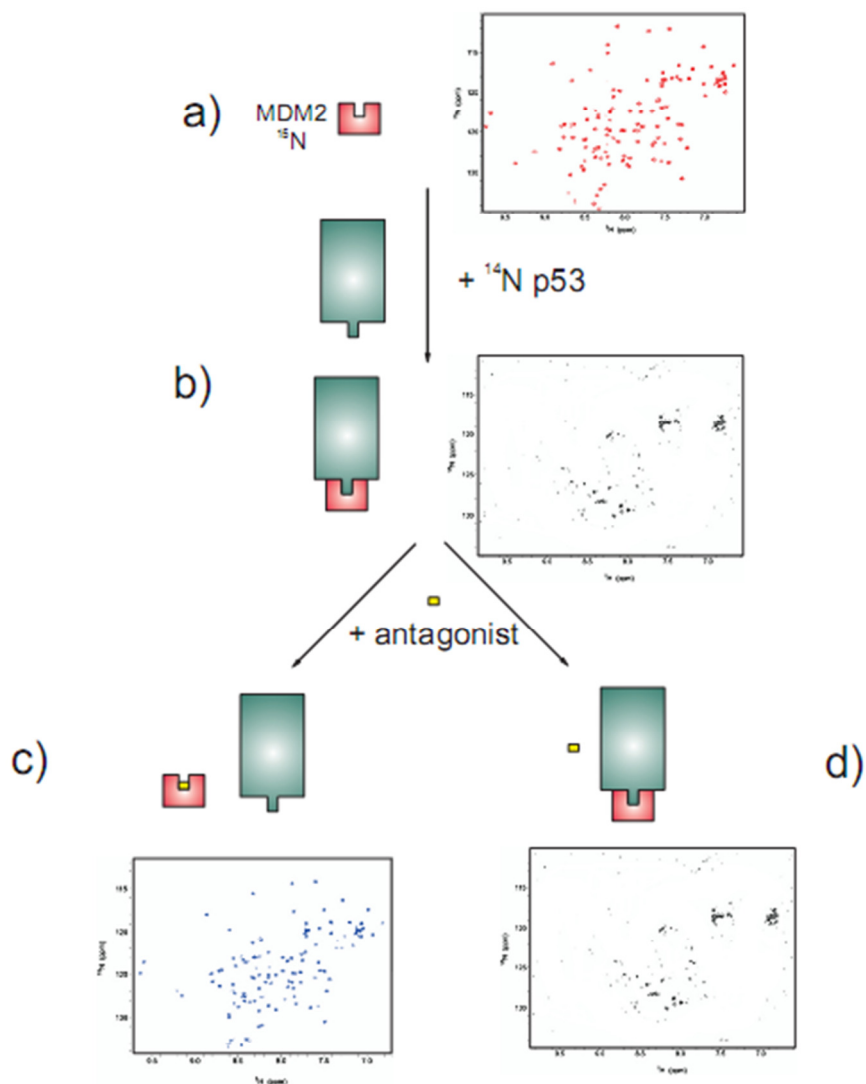
Figure 17 The 2D version of the AIDA (Antagonist-Induced Dissociation Assay) requires a small reporter 15N-labeled protein, that yields a 1H-15N-HSQC spectrum of good quality and a large (unlabeled) interaction partner protein (e.g. p53). (a) A 15N HSQC spectrum of a ca. 12 kDa uniformly 15N labeled MDM2 (each amino acid gives a cross peak for the N-H pair, the side chain N-H resonances are observed at around 7 ppm 1H and at 120 ppm 15N chemical shifts). (b) The cross-peaks disappear on addition of a large fragment of the p53 protein (ca. 35 kDa), that forms a complex with the smaller one. Due to increase in the rotational correlation time of the protein-protein complex, the HSQC signals are broadened beyond detection. (c) Addition of an effective antagonist of the protein-protein interaction releases the small 15N-labeled protein from the complex and recovers the HSQC signal. (d) A weak inhibitor does not dissociate the complex.
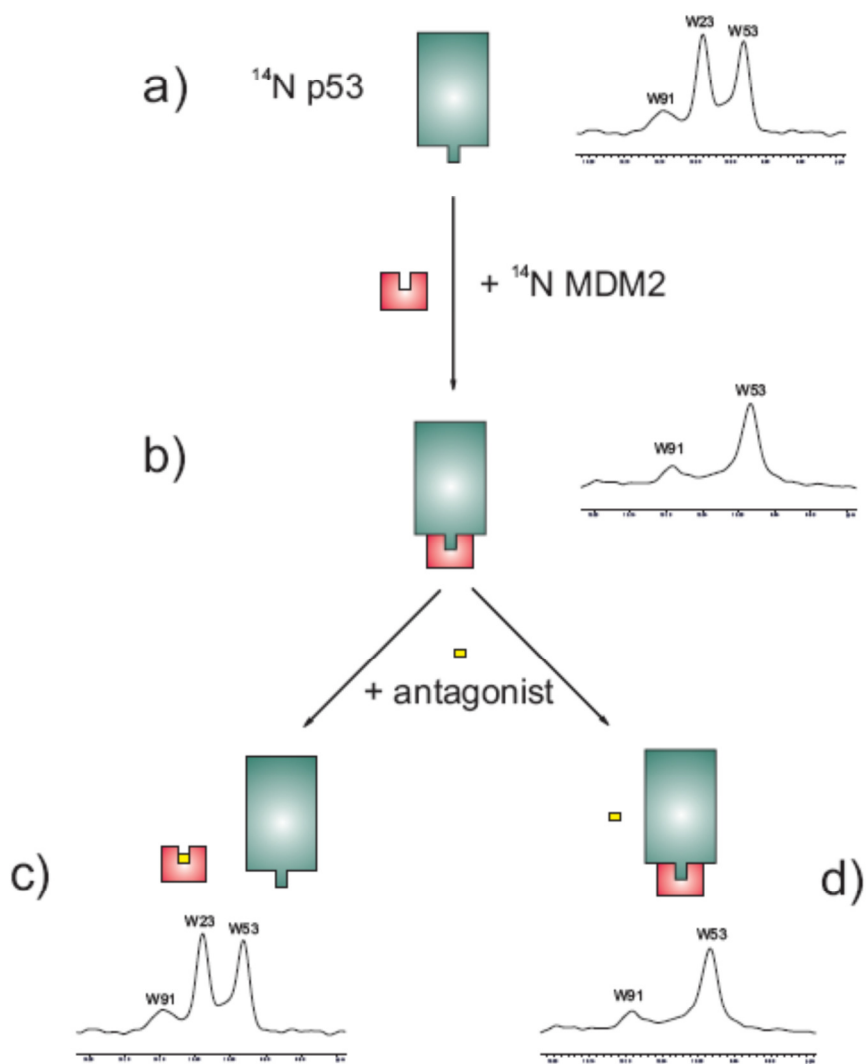
Figure 18 A 1D NMR version of the AIDA assay. (a) The 1D proton NMR spectrum of the side chains of tryptophans (W) of free p53 (residues 1-321). The N-terminal domain of p53 contains three tryptophan residues: W23, W53, and W91 (for NMR assignments refer to (Ayed et al., 2001); the N-terminal domain encompasses residues 1-94; the p53 domain structure is shown in Figure XX (Joerger et al., 2008) Because of a highly flexible nature of the very N-terminal segment of p53 between residues 1-73, the side chains of W23 and W53 give rise to sharp lines, because the very N-terminal segment of p53 comprising residues 1-73 has been shown to be very flexible (Lee et al., 2000; Ayed et al., 2001; Dawson et al., 2003). (b) Upon forming the complex with MDM2, the signal of W23 disappears. This is because W23, together with the p53 residues 17 to 26, comprise the primary binding site for MDM2. Upon binding, these residues participate in a well-defined structure of a large p53-MDM2 complex, whereas W53 is still not structured when p53 is bound to MDM2 (D'Silva et al., 2005; Krajewski et al., 2007; Rothweiler et al., 2008). Thus, the observed chemical shift is different and $1/T2$ transverse relaxation rate of the bound W23 in the complexes increases thus significantly and broadening of NMR resonances results in the disappearance of this signal in the spectra (D'Silva et al., 2005; Krajewski et al., 2007; Rothweiler et al., 2008). (c) Disruption of the MDM2-p53 interaction results in the release of free p53 and the recovery of the $W23^{p53\ N}H^{\varepsilon}$ signal. The height of W23 peak corresponds to the fraction of free p53 and thus, when total concentrations of the complex and the antagonist are known, the K_i of the MDM2-antagonist interaction can be determined from a single competition experiment (Wang 1995; Krajewski et al., 2007). (d) A weak inhibitor does not dissociate the complex.

2.1.4.2 Practical aspects of 1D AIDA-NMR

The philosophy of the quantitative AIDA assay is generally similar to other competition experiments. The main differences between the AIDA-NMR and, for example, fluorescence-polarization based assays are: the fact that NMR is less sensitive than fluorescence, the assay uses protein-protein complex, that is usually prepared by gel filtration and thus has native 1:1 stoichiometry. Also number of titration points that can be acquired by NMR is much lower than for automatized fluorescence methods and due to time limitations usually 1-3 steps of titration are performed.

Therefore optimal design of AIDA experiments is an important issue and general rules governing the measurements performed with the AIDA-NMR assay are more complex than for binary NMR titrations.

The main factors influencing the experiment are:

- Sensitivity limitations – decreasing the concentration of the protein two times increases the experimental time four times
- Dilution-related dissociation of the complex – observed in the absence of the inhibitor; for protein concentrations close to K_D value of the complex, dilution-related dissociation decreases the effectively measured signal and decreases the range of measureable K_is (see Figure 19); in order to avoid excessive protein complex dissociation, the protein concentration should be at least 10 times higher than the K_D value.
- Solubility of the compound – unlike in binary NMR titrations, competition experiments allow K_D determination also when full saturation of the protein with an antagonist cannot be achieved. As Figure 20 shows, concentration of the protein used in the assay has low influence on the concentration of the free antagonist in the solution (which is a quantity limited by the solubility of the compound). Simulations shown in Figure 21 that for a hyphotetical protein-ligand-antagonist system and in the presence of 50 μM solubility limit, the maximal dissociation of the complex induced by the antagonist would range from almost 100% for 1 μM protein complex to ca. 60% for 100 μM protein complex. For each of the cases it is possible to

determine the K_i of the interaction (as long as the concentration of the free antagonist is below the solublity level).

- The protein complex to antagonist molar ratio used for titrations – as Figure 22 shows, measurements performed at low antagonist to protein molar ratios give higher precision in K_i determination for tighter binding, whereas higher antagonist to protein molar ratios are appropriate to measure weaker binding. Therefore it is advisable to record at least two points of titration (with low and high antagonist to protein ratio) to cover both the high and low ranges of K_is.

The abovementioned rules might sometimes lead to contradictory conclusions and show limitations of the assay; i.e. quantitative measurement of binding of poorly soluble and weakly binding antagonists with AIDA-NMR might lead to large inaccuracies in the determined K_i; however, by using low protein concentration AIDA-NMR may still provide information on whether the antagonist is effective and capable of disruption of a protein-protein interaction.

2.1.5 Comparison: AIDA-NMR and HSQC-screening

The overall philosophy of binary NMR titrations and NMR competition experiments is different; methods are highly complementary and only usage of both methods allows for thorough characterization of PPI inhibition. Table 1 summarizes the main characteristics of the methods.

	HSQC	2D AIDA	1D AIDA
Isotope labeling	yes	one partner	no
Protein:drug ratio	equimolar	excess of the drug	excess of the drug
Typical protein concentrations	mM range	mM range	μM range
Measureable affinities range	Quantitative tens of μM-mM Qualitative: < tens of μM	No quantitative information	Quantitative: ca. $0.01\ K_D < K_i < 100\ K_D$ Qualitative: $K_i < 0.01\ K_D$
Binding site mapping	yes	yes	no
Potential to inhibit PPI	no	yes	yes
Quantitative affinity of poorly soluble drugs	no	no	yes
Detection of denaturing factors	yes	yes	limited
Detection of covalent modifications	limited	limited	limited

Table 1 Comparison of HSQC titrations, 2D version of AIDA and 1D version of AIDA in drug discovery.
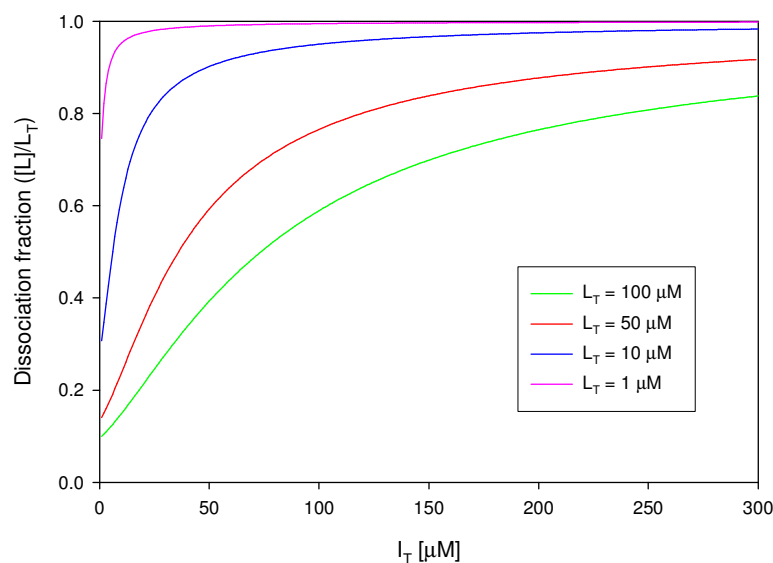
Figure 19 Simulation showing dependence of the released fraction of the ligand from the protein-ligand complex (that is equivalent to the chemical shift) on concentration of the antagonist added. KD of the protein-ligand interaction is set to 1 µM, K_i of protein-antagonist interaction is set to 0.5 µM. For low complex concentrations, large fraction of the ligand is dissociated because of complex dilution. In, that situation, the measured difference in dissociation in presence and in absence of antagonist is low. For higher complex concentrations, the maximal amplitude of measureable signal is higher, however more antagonist is required to induce complex dissociation, therefore the most optimal situation is when the complex concentration is ca. 10 times higher than the K_D of protein-ligand interaction. Simulations were performed according to equations from section 8.3.
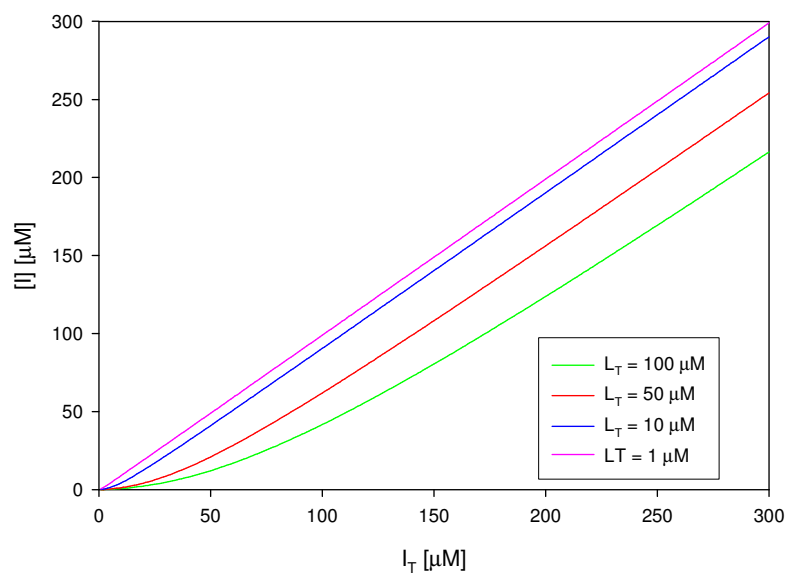
Figure 20 Simulation of a competition binding experiment (i.e. 1D AIDA-NMR) showing dependence of free inhibitor concentration on the total amount of added inhibitor, carried out for various total protein-ligand complexes concentration. The K_D of the interaction was set to 1 µM. For typically used compound concentrations, total complex concentration has low influence on the unbound inhibitor concentration. Simulations were performed according to equations from section 8.3.
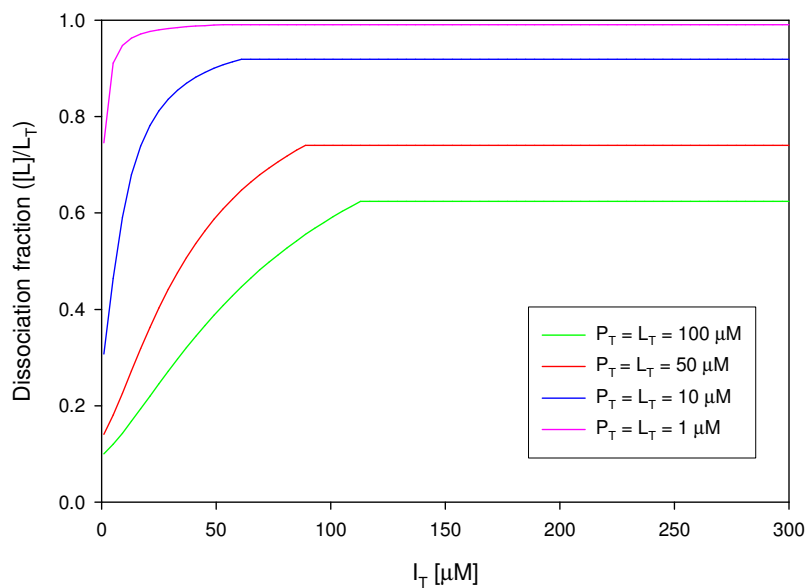
Figure 21 Simulation of a competitive assay (i.e. 1D AIDA-NMR) carried out for different protein-ligand complexes concentrations and K_D = 1 μM, K_i = 0.5 μM. 50 μM solubility limit of the compound was assumed (equal to the maximal achieveable concentration of the free compound in the solution). Total concentration of the protein complex has effect on the final saturation achieveable with specific solubility limit and K_D values; the lower the concentration of the complex, the higher maximal dissociation observed. Simulations were performed according to equations from section 8.3.

Figure 22 Simulation of a competitive assay (i.e. 1D AIDA-NMR) carried out for different protein-ligand to antagonist ratios. Concentration of the protein-ligand complex was set to 10 μM. For higher complex:antagonists ratios, K_is of weaker interaction may be determined more accurately. Simulations were performed according to equations from section 8.3.
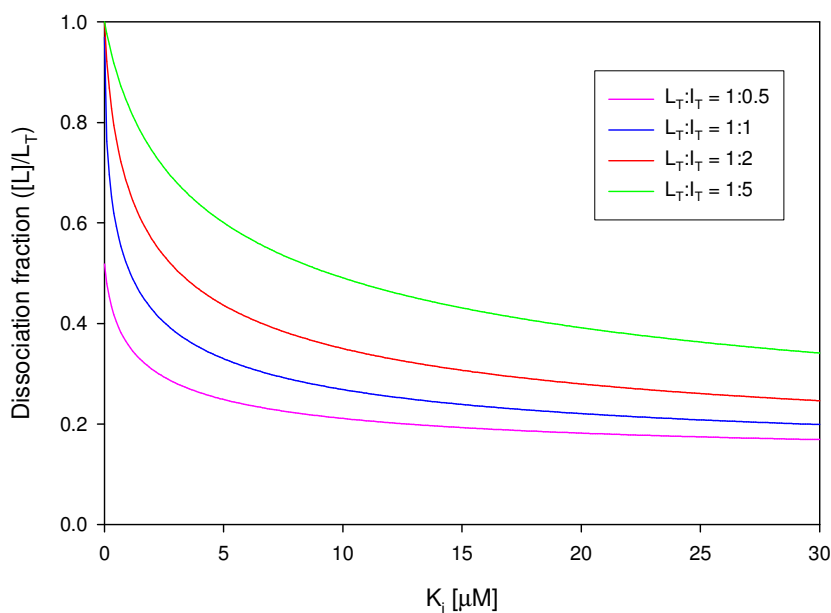
2.2 Results

2.2.1 Robust generation of new inhibitor scaffolds by multicomponent reaction chemistry

A virtual library of 30000 compounds accessible by multicomponent chemistry and based on commercially available or easy to synthetize substrates was generated using the ChemAxons REACTOR software (www.chemaxon.com). All compounds contained a tryptophan analogue (that was either an indole derivative or 4-chlorophenyl) at random positions. The virtual compounds were docked to MDM2 (1YCR) using Moloc software and as a method of overcoming the local minima problem during docking, tryptophan analogue was always initially placed in the space occupied by Trp23[p53].

The compounds were synthetized using various multicomponent reactions (see Chapter 5.1.4 and (Czarna et al., 2010)) and tested for binding to MDM2 by NMR. Several compounds from each class of inhibitors were checked and based on SAR data, preliminary optimization of binding affinity was carried out. Figure 24 and Table 2 depict the best hits derived for the total of 12 diverse scaffolds. Table 2 estimates also the "drug-likeness" of each of the compounds based on the classical rules by Lipinski et al. (Lipinski et al., 2001). According to them, orally active drugs are most likely to have molecular weight below 500 Da, logarithm of octanol-water partition coefficient below 5, less than 10 hydrogen bond acceptors (expressed as total number of oxygen and nitrogen atoms) and less than 5 hydrogen bonds donors (expressed as number of nitrogen or oxygen atoms with one or more hydrogens). Violations of Lipinski's rules are marked in the Table.

2.2.2 1,4-benzodiazepin-2,5-diones as MDM2-p53 interaction inhibitors

Seven-membered 1,4-diazepine ring-based scaffold is considered to be one of the "privileged" structures with a broad range of biological activities and applications in human medicine (Sternbach 1983), being able to target various classes of

pharmacologically relevant targets such as GPCRs, ion channels and enzymes. Therefore, several members of this compound family were synthetized using the combination of the Gewald three-component reaction and Ugi-Deprotection-Cyclization (Huang et al., 2010) and their biological activities were evaluated by NMR and fluorescence polarization assays. Two representative members of 1,4-benzodiazepin-2,5-diones were shown to be able to antagonize the MDM2-p53 interaction and bind to MDM2 with K_is in low µM ranges (see Figure 23).

2.2.3 Known antagonists of MDM2-p53 interaction

Nutlin-3a (Vassilev et al., 2004) and MI-63 (Ding et al., 2006) were used as reference examples of the most developed inhibitors of MDM2-p53 interaction and positive controls for the NMR assays used in the study (see Figure 24). Both compounds exhibited K_is in AIDA similar to those reported in the literature and "slow" chemical exchange during HSQC titrations.

Compound name	K_D/K_i [µM]	cLogP	MW [Da]	H acceptors	H donors
PB1	40±15[a]	7.93±0.66	416.73	3	1
PB2	3±1[b]	4.09±0.62	368.86	4	0
PB3	20±7[a,b]	3.16±0.70	340.44	5	2
PB4	30±10[a]	4.13±0.43	362.25	3	1
PB5	30±10[a]	3.86±0.88	337.81	5	0
PB6	Denaturation[a]	4.67±0.76	385.28	3	1
PB7	>100[a]	5.26±0.64	379.90	5	2
PB8	60±20[a]	6.57±0.28	365.90	2	2
PB9	60±30[a]	6.07±0.30	360.88	2	2
PB10	5±2[b]	7.63±0.93	507.04	5	2
PB11	0.8±0.4[a,b]	3.45±0.65	439.00	5	1
PB12	1.1±0.4[a,b]	7.02±0.62	462.33	5	2
Benzodiazepine 5a-7	30±20[b]	4.39±1.14	465.95	5	2
Benzodiazepine 5a-8	10±6[b]	5.95±1.15	534.84	5	2
Nutlin-3	0.09±0.03[a,b]	2.77±1.19	581.49	8	1
MI-63	0.015±0.05[a,b]	4.96±0.86	577.51	7	3

Table 2 Characteristics of MDM2-p53 interaction inhibitors discussed in the chapter. Values of octanol-water partition coefficient (cLogP) were calculated with ACD/ChemSketch software. The KDs/Kis of the interaction were determined in binary ^{1}H-^{15}N-HSQC titrations (a) or 1D competitive AIDA assay (b). The experimental error of the measured K_D / K_i values was assumed to be ca. 30%.
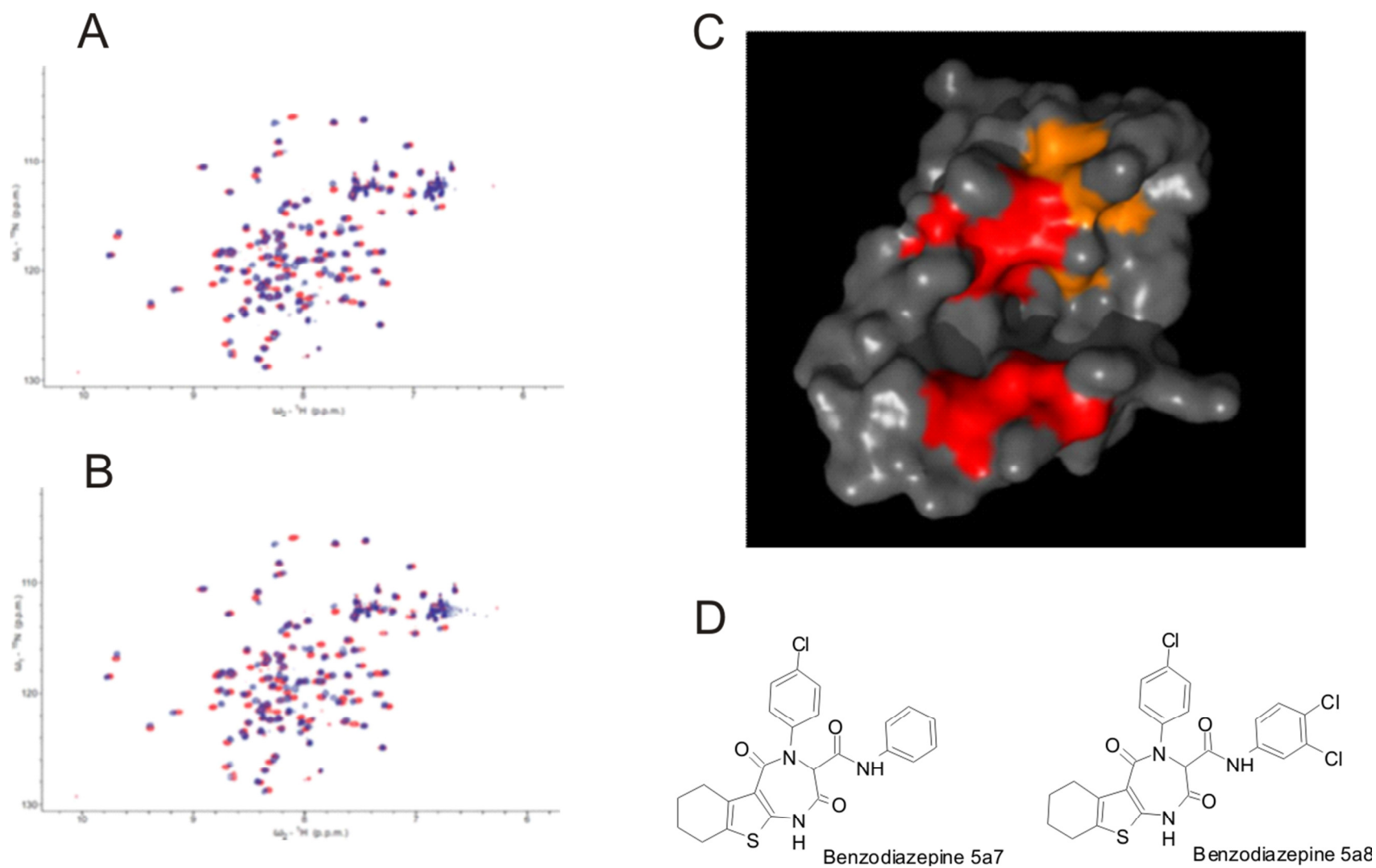
Figure 23 Benzodiazepine inhibitors of the MDM2-p53 interaction. ^{1}H-^{15}N-HSQC titrations with compound 5a7 (A) and 5a8 (B), respectively. Both compounds have similar structures and display very similar chemical shifts perturbation patterns. (C) NMR mapping of binding site of compound 5h. Atoms experiencing very large (> 0.08 ppm) and large (> 0.04 ppm) differences in chemical shifts upon addition of the molar excess of the compound are marked. Assignment of the N-terminal domain of MDM2 was published previously (Stoll et al., 2000). (D) Formulas of the compounds.

PB1   PB2   PB3

PB4   PB5   PB6

PB7   PB8   PB9

PB10   PB11   PB12

MI-63   nutlin-3a
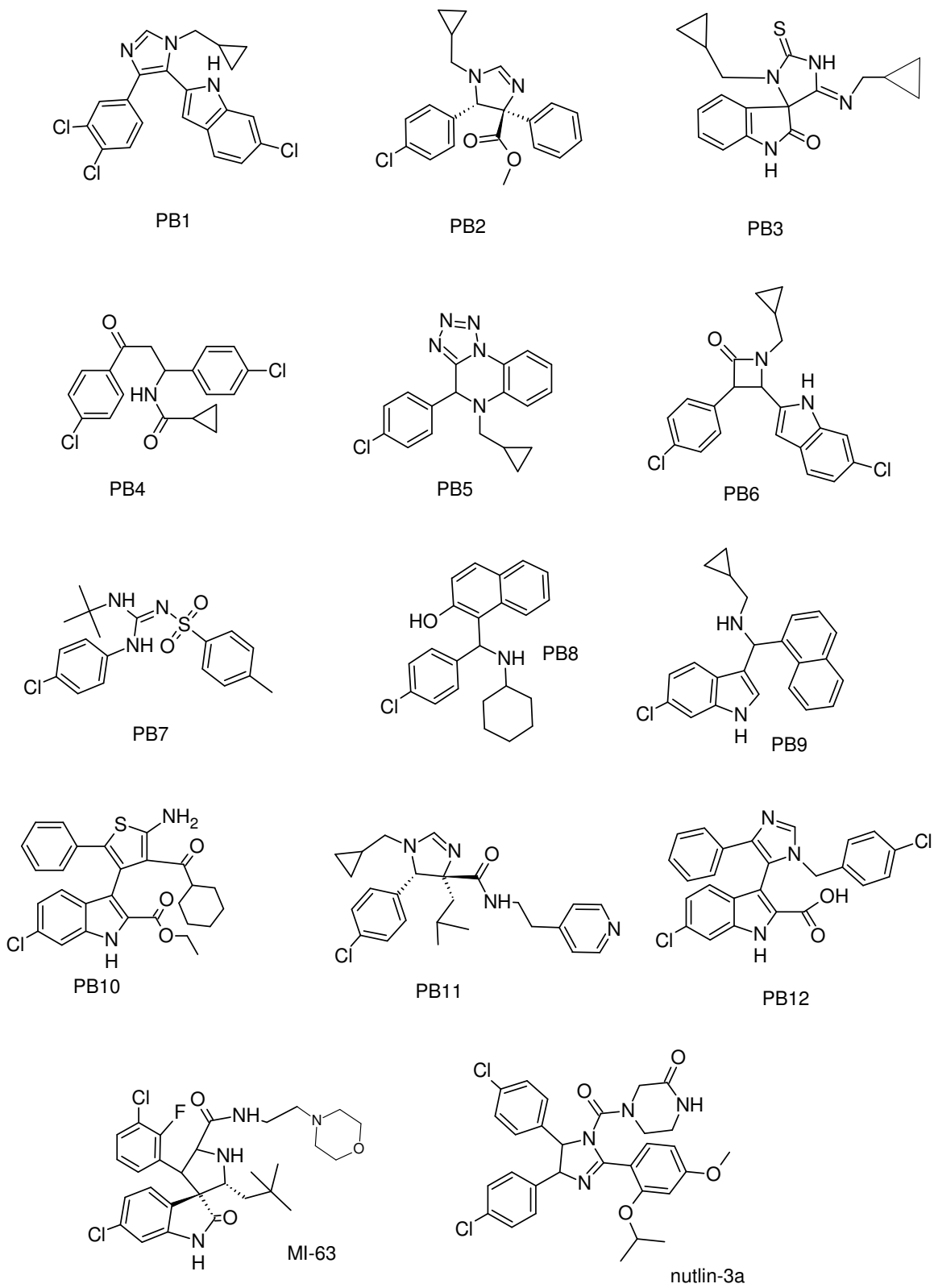
Figure 24 MDM2 inhibitors derived from multicomponent reactions and two reference compounds: MI-63 (Ding et al., 2006) and Nutlin-3 (Vassilev et al., 2004).

2.3 Discussion

2.3.1 The high-content NMR screening

Thanks to combination of binary ^{1}H-^{15}N-HSQC titrations with the competition 1D AIDA-NMR assay, a complex and thorough characterization of small molecule binding may be carried out.

The HSQC titrations allow for direct determination of K_Ds of weak interactions and provide information, whether a compound acts through conventional binding or denaturation of the receptor. The HSQC titrations are generally able to detect binding of also poorly-soluble ligands and furthermore the timescale of chemical exchange observed during the titrations allows also for qualitative assessment of binding strength.

The K_D/K_i of ligands being in intermediate or slow chemical exchange time scale in binary experiments can be accurately calculated using competitive 1D AIDA-NMR assay. The assay additionally shows ability of a ligand to really dissociate the protein-protein complex. Comparison of results derived from binary titrations and 1D AIDA-NMR shows that both methods give the same K_D/K_i values and for $K_D/K_i \leq 10$ μM, the compounds usually are in intermediate or slow time scale of chemical exchange. The agreement of both values may be also considered as an additional validation criterion and test of correctness of experimental screening. As discussed in the current chapter and shown in Chapter 3, the lack of consistency between the binary titration results and competition experiments is a warning sign suggesting some additional mechanism may accompany the binding.

The requirement of relatively high protein and compound concentrations is commonly regarded as a drawback of NMR screening. This feature may be, however, transformed into its benefit if we consider that the real drugs must in fact have considerable water solubility and the substances with serious solubility issues should be excluded from further optimization (Jorgensen et al., 2000). The practice (and simulations from previous part of the chapter) show that the minimal compound

solubility required for NMR (low µM) is in the same range as the solubility limitation of bioavailability.

2.3.2 Multicomponent chemistry as a robust method of lead generation

A relatively small database of 30000 compounds has led to development of 10 diverse scaffolds of PPI antagonists. Even though the affinities of the compounds are often moderate and do not ensure their biological activity, yet the molecules comply with the bioavailability rules by Lipinski (Lipinski et al., 2001) and have potential for development that is facilitated by their simple and combinatorial synthesis (Czarna et al., 2010).

Lead discovery and choice of compounds for further optimization is a critical step in drug development pipelines and, based on analysis of currently known drugs and protein ligands, several descriptors that guide choice of the compounds for further optimization have been derived. One of the parameters is the ligand binding efficiency, which is calculated by converting the dissociation / inhibition constant to the Gibbs energy of binding and relating it to the number of heavy atoms of the ligand (Kuntz et al., 1999).

$$LE = -\frac{RT \ln K_D}{\# \ heavy \ atoms}$$

Equation 6

The values of ligand efficiency for MDM2-p53 interaction inhibitors are shown in Table 3.

The ligand with the highest efficiency is PB2; the molecule is based on cis-imidazoline scaffold (similarly to Nutlin-3), however arrangement of substituents is different from that in Nutlin-3. Other ligands with efficiencies that are similar to the most developed MDM2-p53 inhibitors (Nutlin-3 and MI-63) are PB3, PB4, PB8, PB11, PB12; those hits may lead to the ligands of affinity similar to Nutlin-3 or MI-63. Benzodiazepine

inhibitors have lower ligand efficiency values than other inhibitors, which implies that they are not good lead candidates.

Compound name	ΔG [kcal/mol]	# heavy atoms	LE [kcal/mol of atoms]
PB1	-6.0	27	0.22
PB2	-7.5	26	0.29
PB3	-6.4	24	0.27
PB4	-6.2	24	0.26
PB5	-6.2	25	0.25
PB8	-5.8	26	0.22
PB9	-5.8	26	0.22
PB10	-7.2	35	0.21
PB11	-8.3	31	0.27
PB12	-8.1	32	0.25
Benzodiazepine 5a-7	-6.2	34	0.18
Benzodiazepine 5a-8	-6.8	36	0.19
Nutlin-3	-9.6	40	0.24
MI-63	-10.7	39	0.27
p53*	-8.6	40	0.23

Table 3 Ligand efficiencies of MDM2-p53 interaction inhibitors. X-ray structure of MDM2-p53 complex (PDB ID: 1YCR (Kussie et al., 1996)) shows,, that 40 heavy atoms of p53 are in direct van der Waals contacts with MDM2.

As it was shown by Kuntz et al. (Kuntz et al., 1999), the maximal value of ligand efficiency is about 1.5 kcal/mol for heavy atoms of small ligands, but the value drops down with size increase to about 0.7-0.4 kcal/mol for heavy atoms of ligands comprising 20-40 heavy atoms. Table 3 shows that the ligand efficiency for the already known MDM2-p53 ligands (and p53 itself) are relatively low. This suggests that both the native MDM2-p53 system and MDM2 antagonists are not perfect energetically. This tendency seems to be a general case for protein-protein interactions and their inhibitors (Wells et al., 2007) and may be explained by general inherent "wobbliness" of protein-protein interfaces (observed, for example, by paramagnetic NMR (Tang et al., 2006)) and relatively high entropy barriers that are related to the often encountered cases of folding upon binding (Mittag et al., 2010). The values of ligand efficiencies of our MDM2-p53 inhibitors are however in perfect agreement with other known antagonists of protein-protein interactions (Wells et al., 2007).

2.4 Materials and methods

2.4.1 Sample preparation

The human recombinant MDM2 (residues 1–118) and p53 (residues 1–321) were expressed and purified as described in section 4.4.1, page 83. Uniform ^{15}N labeling was achieved by growing the Escherichia coli BL21(DE3) RIL in M9 minimal medium containing ^{15}NH$_4$Cl as nitrogen source (Miller 1972). Nutlin-3 was purchased from Cayman Chemicals, MI.

Protein concentrations were determined by measurement of the absorbance at 280 nm. The extinction coefficient was calculated using the ProtParam tool at the Expasy server (Wilkins et al., 1999).

2.4.2 NMR spectroscopy

All NMR spectra were acquired at 300 K on a Bruker DRX 600 MHz spectrometer equipped with a cryoprobe. Typically, NMR samples contained 0.05-0.2 mM protein in 50 mM KH$_2$PO$_4$ and 50 mM Na$_2$HPO$_4$, pH 7.4., containing 150 mM NaCl and 5 mM DTT. To provide lock signal, 10% D$_2$O was added to NMR samples. Water suppression was carried out using the WATERGATE sequence (Piotto et al., 1992). NMR data were processed using the Bruker program Xwin-NMR version 3.5.

^{1}H-^{15}N HSQC spectra were acquired using the fast-HSQC pulse sequence (Mori et al., 1995). For the ^{1}H-^{15}N HSQC spectrum, typically a total of 2048 complex points in t2 and 192 t1 increments were acquired.

NMR ligand binding experiments were carried out typically on 500 µL of the protein sample, at a concentration of 0.05-0.3 mM, by titrating the sample with 100mM stock of the compound in DMSO-d6. The AIDA experiments were performed according to Bista *et al.*, 2009. Typically, 5-40 µM MDM2/p53 complex was mixed with compounds in 1:1 molar ratio; amount of p53 released from the complex by the compound was

estimated from 1D spectrum, and K_i of MDM2-inhibitor interaction was calculated according to (Wang 1995; Krajewski et al., 2007).

Normalized chemical shift perturbations were calculated according to equation (Stoll et al., 2001):

$$\Delta\delta = \sqrt{0.04\left(\delta_N^{\text{bound}} - \delta_N^{\text{free}}\right)^2 + \left(\delta_H^{\text{bound}} - \delta_H^{\text{free}}\right)^2}$$

3. Covalent inhibitors of MDMX-p53 interaction

3.1 Introduction

3.1.1 First inhibitors of MDMX? – an overview of publication by Reed et al. (2010)

A publication describing development of the first group of small molecule antagonists targeting the MDMX-p53 interaction appeared in 2010 in the Journal of Biological Chemistry. The paper describes results of a high-throughput assay performed by fluorescence polarization on the MDMX-p53 complex (Reed et al., 2010). The compound library used for screening contained 295 848 unique compounds from commercial sources.

The assays were carried out by preincubation of the compounds with the unlabeled GST-tagged N-terminal domain of MDM2, followed by addition of the fluorescently labeled p53 peptide and fluorescence anisotropy readout. The assay buffer contained 10 mM Tris (pH 8.0), 42.5mM NaCl, and 0.0125% Tween- 20. The control experiments performed for Nutlin-3 and the unlabeled competitive p53 peptide showed EC50 concentrations that were close to the literature values of K_Ds of those interactions.

The best compound selected in the screen was named SJ172550 and its EC50 for the MDMX-p53 interaction was 0.84 µM; this suggested a low-micromolar K_D for the MDMX-SJ172550 interaction. The compound was shown to interact also with MDM2, albeit 10 times weaker.

The researchers performed also an extensive characterization of their hits, which included: the redox activity determination using the resazurin-rezorufin system (Lor et al., 2007), the cellular activity assays, thermal-shift assay and reversibility assays using mass spectrometry. According to them, SJ-172550 was binding to MDMX reversibly,

was active in cell lines (triggering p53-dependent apoptosis) and had no detectable redox activity. Analysis of the effect of point mutations in MDMX on binding strength allowed even for predicting that the compound binds within the p53 pocket.
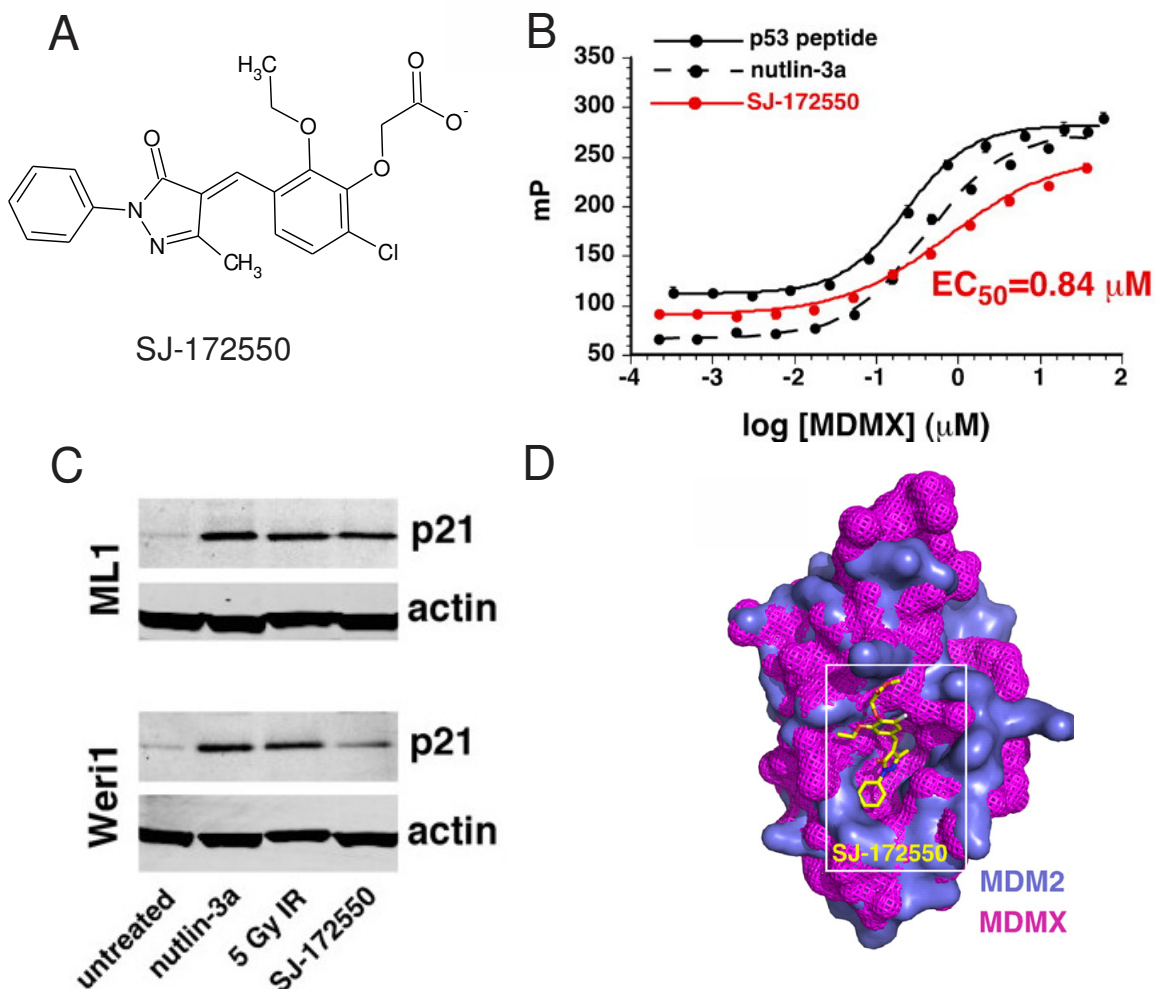
Figure 25 Summary of the findings presented in Reed et al. (2010). (A) Structure of SJ172550 - the best compound selected in the high-throughput screen. (B) Fluorescence polarization inhibition curves show strong, low- or submicromolar binding of SJ172550 to MDMX. (C) Immunoblotting showing induction of p21 – cyclin-dependent kinase inhibitor 1 – the main transcriptive target of p53 (el-Deiry 1998). The cell lines ML1 (derived from lymphoma) and Weri1 (derived from retinoblastoma) were treated with Nutlin-3a, ionizing radiation and SJ-172550. (D) Mutagenesis-derived docking proposed for SJ-172550. Figure combined from Reed et al. (2010).

The reversibility of the interaction was checked by both the MALDI mass spectrometry and dialyzing out the compound from the N-terminal domain of MDMX and checking its ability to bind p53.

3.2 Results

We have carried out biochemical characterization of a commercially available methyl ester of SJ172550, the compound designated by us as 4T14,

Fluorescence polarization on compound 4T14 (methyl ester of SJ172550, MW = 428.9 Da, see the Materials and Methods section for structure) performed according to (Czarna et al., 2009) gave results in agreement with the data published by Reed et al. (2010) and showed IC50 values in low micromolar ranges for both N-terminal domains of MDMX and MDM2. The compound was further subjected to NMR analysis of binding to MDM2 and MDMX by both the competition experiments (Bista et al., 2009) and binary HSQC titrations.

NMR investigations were begun with checking the water solubility of the compound. This test was performed by adding the compound to the phosphate buffer the same as the "non-reducing" buffer used for NMR experiments and taking a 1D ^{1}H NMR spectrum. Appearance of the signals originating from the compound (especially the aromatic protons around 6-10 ppm) confirmed that the compound is soluble in water and also allows for estimation of the solubility (from the signal intensity) and aggregation propensities (from the spectral line width). The compound turned out to be insoluble in the "non-reducing" buffer and formed a yellowish precipitate. Addition of a reducing agent (β-mercaptoetanol) caused immediate change of the color of the precipitate, followed by resolubilization of the material. Furthermore, a 1D ^{1}H NMR spectrum recorded in chloroform showed that the compound reacts with β-mercaptoetanol and forms a range of products (Figure 26).

The results obtained in the SEI-AIDA experiment (Bista et al., 2009) were inconclusive; the compound at the beginning was not able to release any p53 from the complex and after exceeding a threshold concentration, p53 was rapidly dissociated (Figure 27). Such immediate release of p53 from MDMX was rather an unexpected outcome of the competition experiment and suggested that the compound may either denature the MDMX after exceeding some critical concentration or react non-specifically with some other sample ingredients.
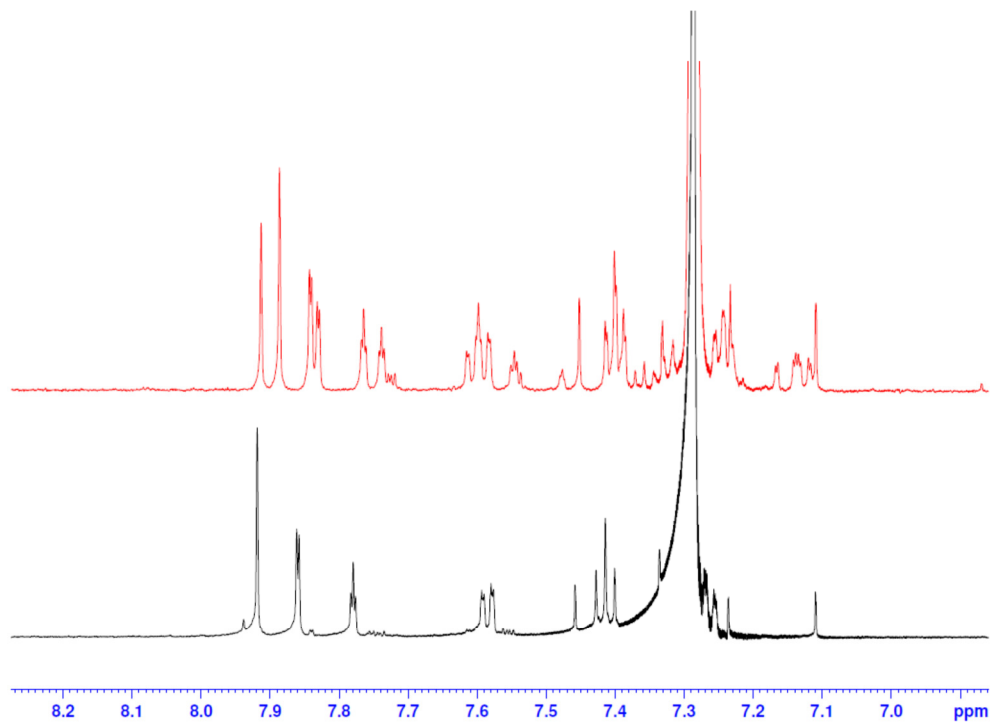
Figure 26 Aromatic regions of ^{1}H NMR spectra of 2 mM 4T14 in CDCl$_3$ (black) and after addiction of 10 mM β-mercaptoetanol (red). The compound reacts with thiols; however, even in the excess of β-mercaptoetanol, not all the 4T14 is modified.
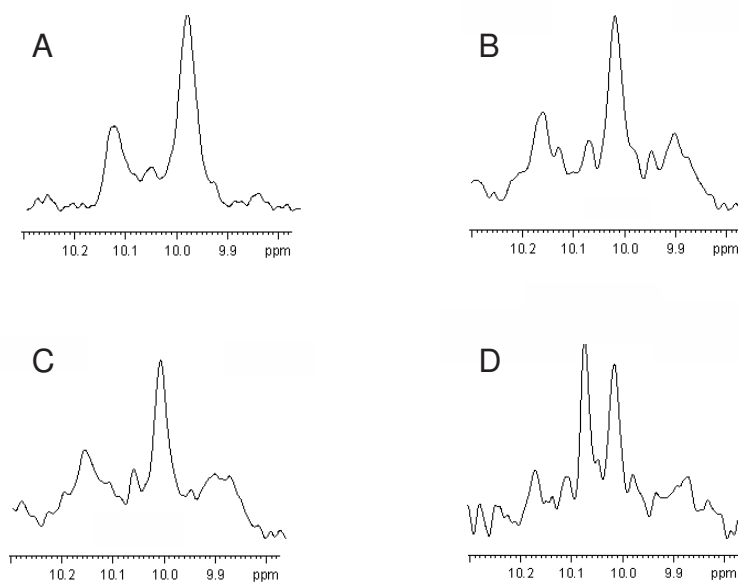
Figure 27 SEI-AIDA performed on the 40 μM MDMX-p53 complex in buffer containing ca. 0.5 mM DTT: (A) reference spectrum, (B) MDMX-p53 complex mixed with 4T14 in molar ratio compound : protein: 1:1, (C) 4:1, (D) 8:1, respectively.

In order to resolve this ambiguity, 4T14 was tested in the binary ^{1}H-^{15}N-HSQC titration of the ^{15}N-labeled N-terminal domain of MDMX. The results shown in Figure 29 show that in non-reducing conditions the compound is in "slow" on the chemical shift timescale chemical exchange; the peaks from the bound and unbound forms of the protein exist at the same time. The HSQC spectrum shows also that the compound does not denature the protein. Analogous NMR titration performed in reducing conditions (Figure 30) shows that the interaction of the compound is very different in presence of reducing agents; the compound does not induce so dramatic chemical shift perturbations and presence of "slow" chemical exchange is not observed.

Furthermore, HSQC titrations of ^{15}N-labeled MDMX show, that addition of reducing agents to the protein, that already had contact with the compound does not reverse the modification (not shown). Interestingly, in the partially modified by 4T14 N-terminal domain of MDMX, that was incubated for 48 hours at room temperature, crosspeaks originating from the modified form disappear (Figure 30). ^{1}H-^{15}N-HSQC titration of ^{15}N-labeled MDM2 shows that the compound interacts also with MDM2 (see Figure 31).

Liquid chromatography coupled with mass spectrometry shows, that 4T14 interacts covalently with the proteins. The reversed phase chromatograms, that were obtained after incubation of the protein with excess of the compound show appearance of additional peak eluting at higher acetonitrile concentration and mass spectrometry confirms, that the peak comes from the modified protein (see Figure 32). Similar tests performed on the N-terminal domain of MDM2 show, that the compound is also able to covalently modify this protein (see Figure 33). The difference in observed masses corresponds to double (MDMX) or single 4T14 mass (for MDM2). Both experiments show also,, that the yield of modification is less than 100%.

Analogous HPLC-MS assays were performed on the N-terminal domain of MDM2 (residues 18-125, C75V). This time, no covalent modification was observed (see Figure 34).
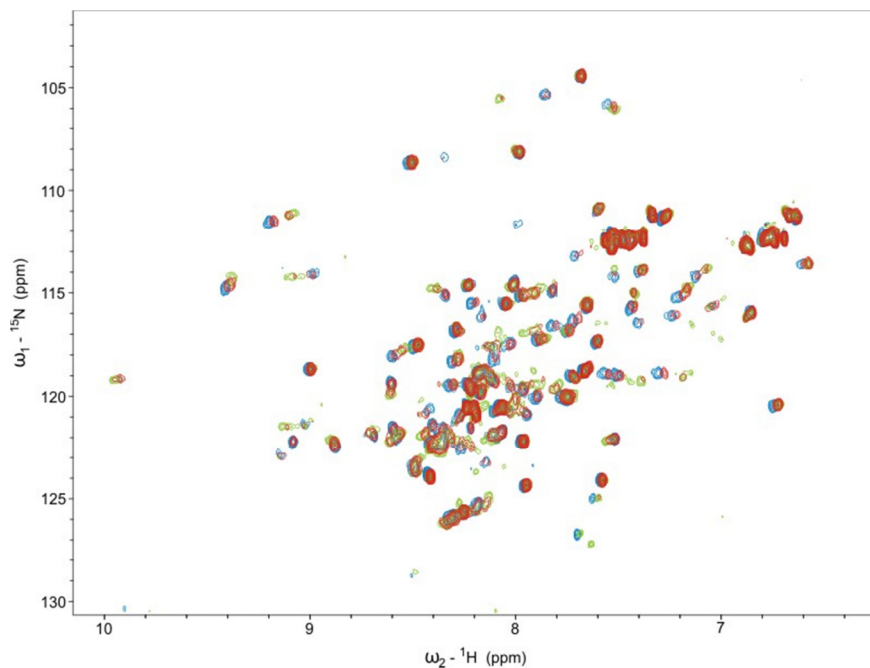
Figure 28 ^{1}H-^{15}N-HSQC spectra of MDMX (1-111) titrated with increasing amount of 4T14. Reference spectrum of apo-MDMX is plotted in blue, spectrum of MDMX-4T14 mixed in molar ratio compound : protein 1:2 is plotted in red, MDMX overtitrated with 4T14 is plotted green. Slow chemical exchange is observed for the intermediate titration step.
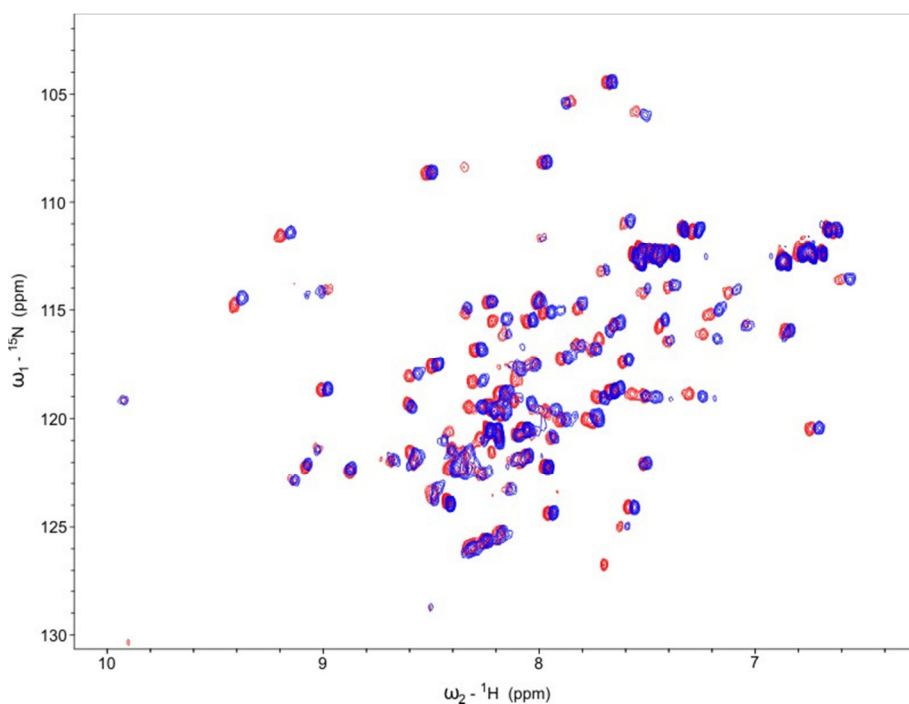
Figure 29 ^{1}H-^{15}N-HSQC spectra of MDMX (1-111) mixed with 4T14 in molar ratio 1:1 in presence of 20 mM DTT (blue) and reference spectrum of apo-MDMX (red).
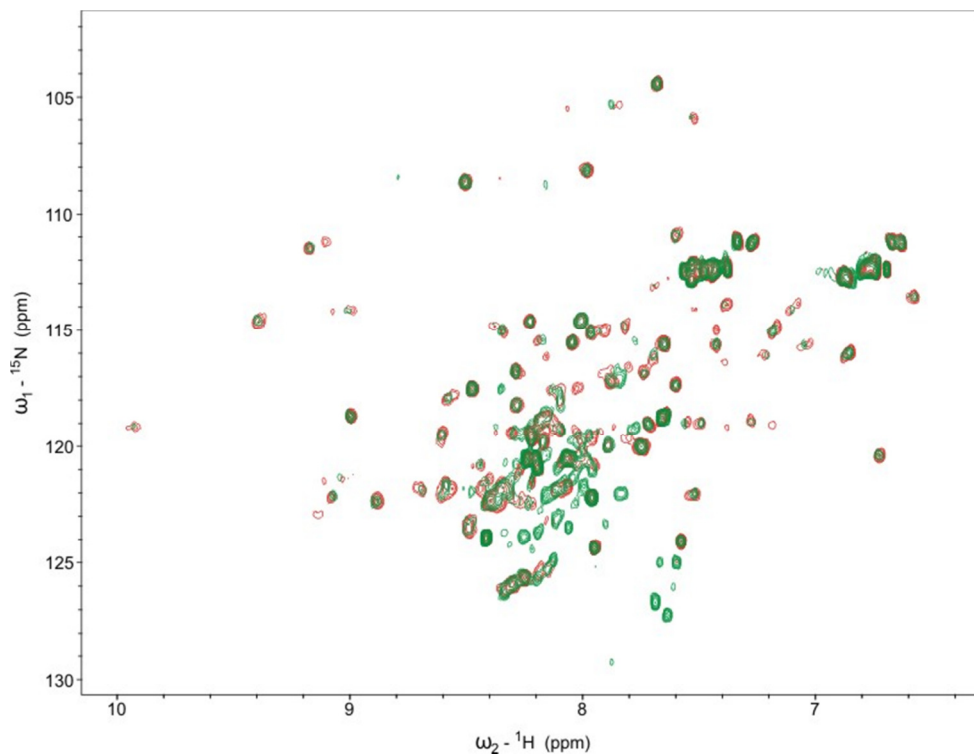
Figure 30 ^{1}H-^{15}N-HSQC spectra of MDMX (1-111) mixed with 4T14 in molar ratio compound : protein 1:2 (red) and spectrum of the same sample taken after 2 days of incubation at room temperature (green). The modified protein is less stable and the peaks originating from the modified MDMX disappear faster, green spectrum is a combination of the spectra of apo-MDMX and its denatured and proteolically degraded form.
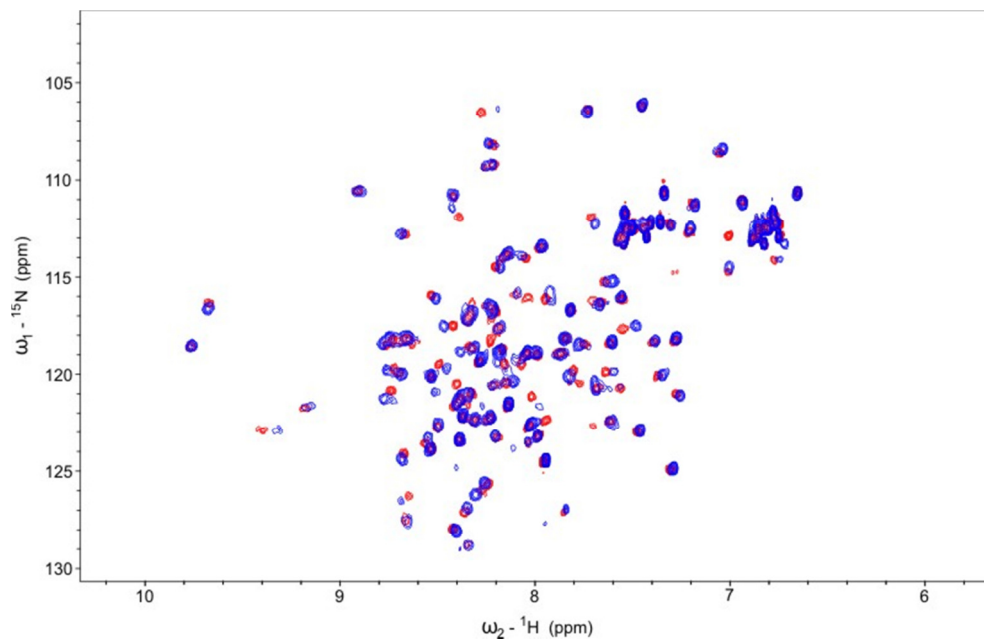
Figure 31 ^{15}N-MDM2 (1-125) mixed with 4T14 (molar ratio compound : protein 5:1) (blue) and reference spectrum of MDM2 (red).
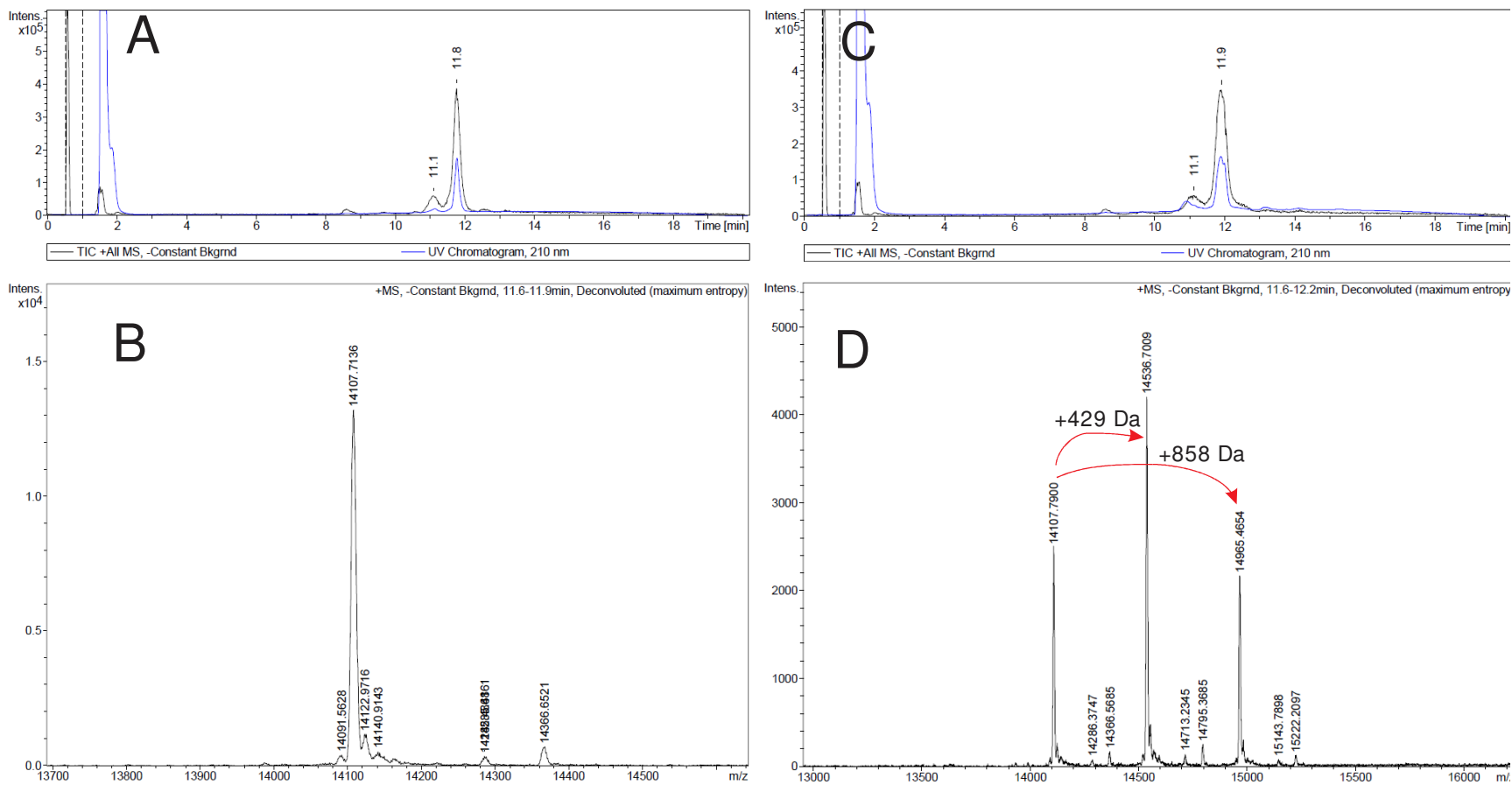
Figure 32 LC-MS analysis of the ^{15}N labeled apo-MDMX (1-111) (A-B) and the same protein mixed with tenfold molar excess of 4T14 (C-D).
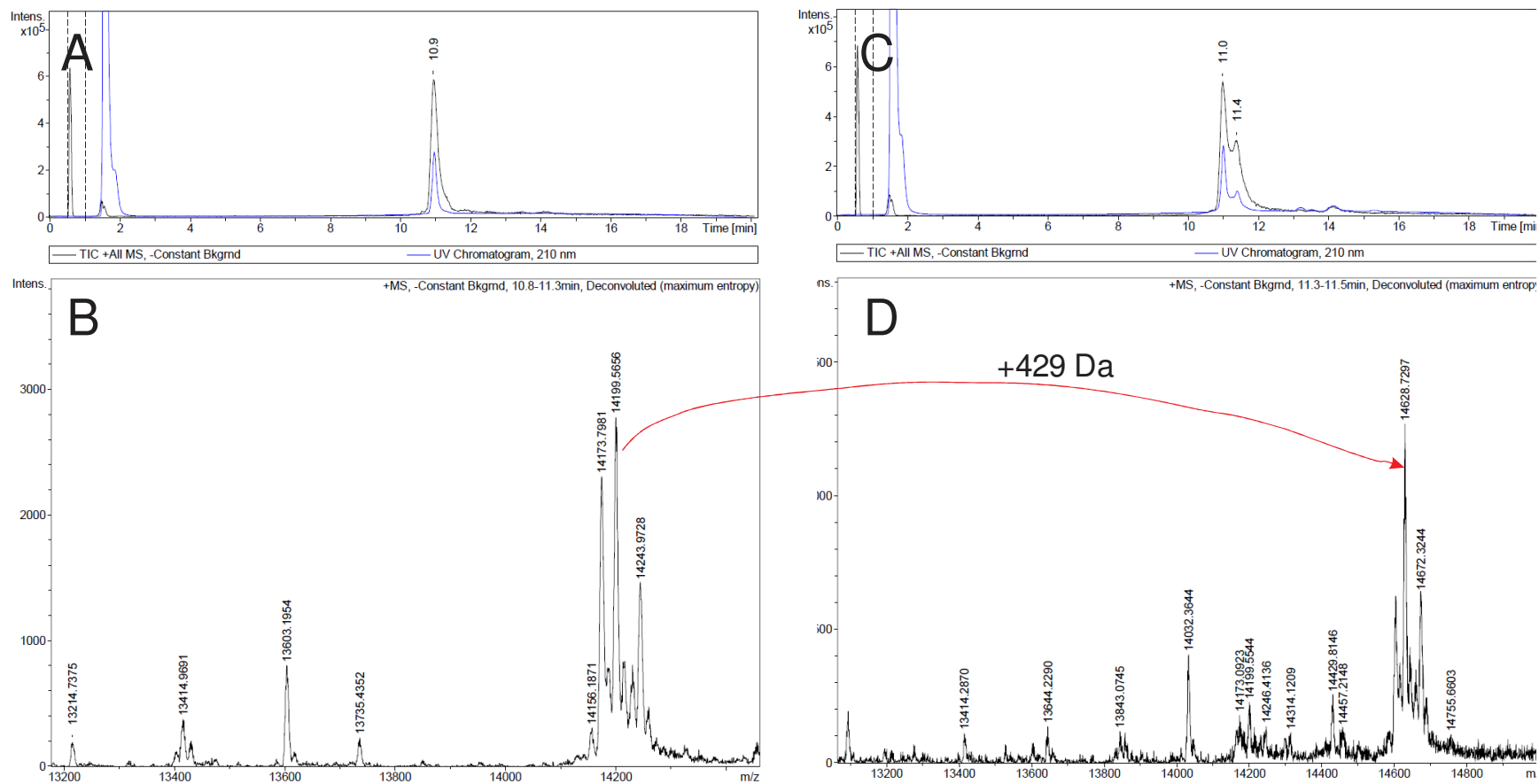
Figure 33 LC-MS analysis of the ^{15}N labeled apo-MDM2 (1-125) (A-B) and the same protein mixed with tenfold molar excess of 4T14 (C-D).
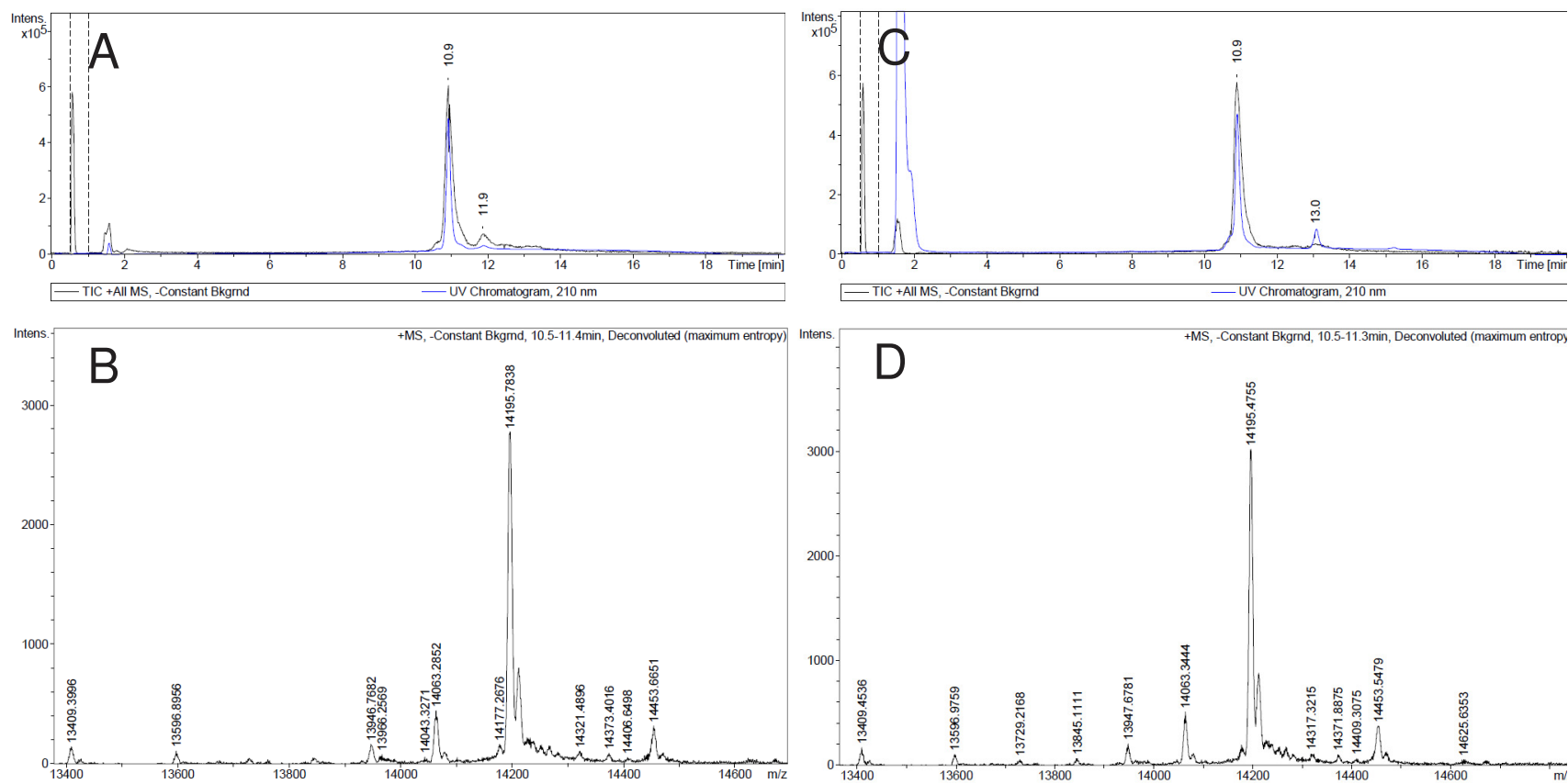
Figure 34 LC-MS analysis of C77V mutant of Mdm2 (18-125) (panels A-B) and the same protein mixed with tenfold molar excess of 4T14 (panels C-D)

3.3 Discussion

3.3.1 SJ172550 analogue modifies covalently variety of proteins

Unlike the results presented by Reed et al. (2010) in their Journal of Biological Chemistry paper, all the results presented here show that the compound acts through covalent modification and is able to react with nucleophiles containing free sulfhydryl group, particularly β-mercaptoetanol and free cysteines from proteins. The interaction seems to be non-specific, as it is not limited only to MDMX and both double covalent modifications and modifications of MDM2 are also observed by mass spectrometry.

Normally, usage of electrospray-ionization mass spectrometry as a proof of covalent interaction with a protein may be questionable; this type of ionization is rather gentle and may preserve strong non-covalent interactions (Siegel 2002). In this case, however, the presence of the covalent modification is not only demonstrated by increase in the mass of the protein (that corresponds to the mass of the compound), but also by the appearance of another chromatographic peak. Considering long time of chromatographic separation and harsh, strongly denaturing conditions of the elution (the modified protein elutes at approximately 60% of acetonitrile), the second chromatographic peak may be considered as the strongest proof of covalent reactivity of SJ172550.

The experiment in which MDMX-SJ172550 complex was preformed and incubated for 48 h at room temperature suggests that the modified form of the protein is less stable and more prone for aggregation; disappearance of NMR crosspeaks from the HSQC spectrum of the modified form is caused by increase in rotational correlation time resulting in peak broadening, and denaturation of the protein followed by proteolytic degradation, resulting in appearance of additional sharp crosspeaks at ca. 7.8 ppm and 125 ppm for ^{1}H and ^{15}N frequencies, respectively (Rehm et al., 2002). Additionally, the incomplete modification of the protein may lead to a false conclusion, that, since unmodified protein is still present after removal of the compound, the action of the drug is reversible.

The lack of redox activity of the compound in resazurin-rezorufin assay does not argue with ability of the compound to covalently modify cysteines; neither resazurin nor rezorufin contain sulfhydryl groups.

The correctness of the approach is further corroborated by several publications showing, that similar tests led other authors to giving up work on some of their hits; particularly Hajduk group has developed an ALARM-NMR assay, that is designed to warn against compounds acting covalently (Huth et al., 2005). The ALARM-NMR assay is based on similar principles, that I used in my investigations of SJ-172550 analogue; one of cysteines from the human La antigen protein turns out to be particularly nucleophilic and the compounds, that react with it in oxidizing conditions and do not bind in presence of reducing agents are considered particularly dubious (Huth et al., 2005).

Other recently published work identifies several classes of PAINs (Pan Assay INterference compounds); compounds, that appear as frequent hitters (promiscuous compounds) in many biochemical high-throughput assays (Baell et al., 2010). The authors of this paper suggest,, that compounds based on pyrazolidin-3,5-dione scaffold (like SJ172550) are highly likely to be potent Michael acceptors and react through Michael addition with nucleophiles. Therefore, a probable mechanism of covalent action of SJ172550 may be explained by reaction shown in Figure 35.
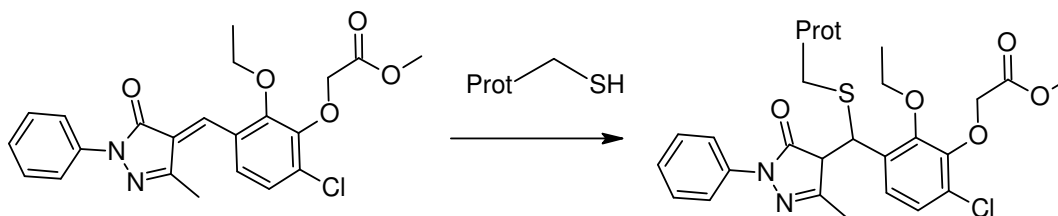
Figure 35 The suggested mechanism of covalent action of SJ172500 (based on (Baell et al., 2010)). Covalent addition of SJ172550 analogue to the protein results in increase of protein molecular mass by 429 Da,, that is equal to the value observed in mass spectrometry experiments shown in Figure 32 and Figure 33.

Analysis of X-ray structure of the N-terminal domain of MDMX in complex with p53 shows,, that the chemically modified residue responsible for loss of affinity of MDMX to p53 is Cys76^{MDMX}, whereas the other Cys10^{MDMX}, that is also modified by SJ172550 is in the N-terminal, unstructured part of MDMX (Popowicz et al., 2008; Sanchez et al., 2010) (see Figure 36). The distance between the modified cysteine

and closest p53 atom is about 10 Å, which is the distance comparable with the size of SJ172550 molecule (that for the extended conformation may exceed even 16 Å) and suggests that SJ172550 either sterically interferes with p53 binding or changes the conformation of MDMX so that it is no longer able to interact with p53. MDM2, the homologous protein to MDMX, also interacts covalently with the SJ172550 analogue has cysteine in analogous position.
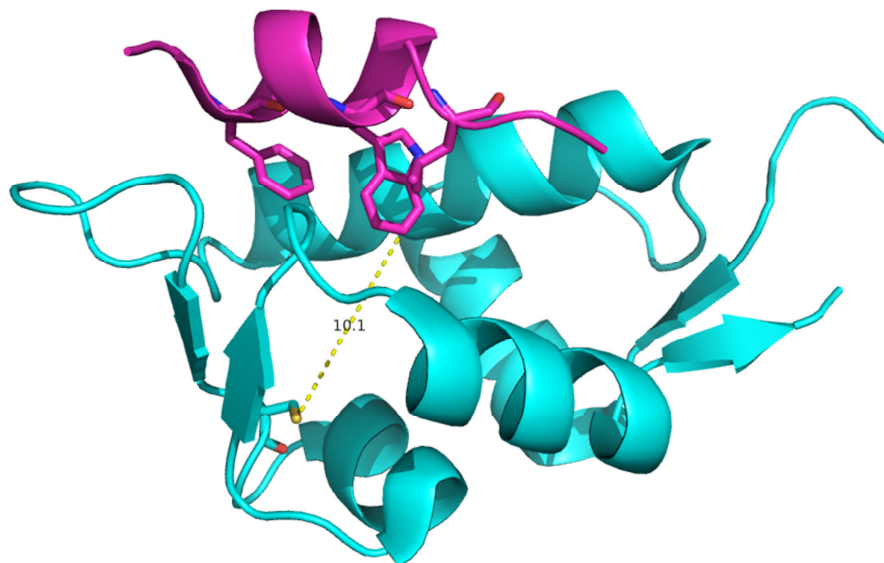
Figure 36 Structure of MDMX complexed with the p53 peptide (PDB ID: 3DAB, (Popowicz et al., 2008)). The distance between the cysteine and the p53 peptide is more than 10 Å.

3.3.2 Therapeutic potential of SJ172550

Even though the physicochemical evidence proving the covalent mechanism of action of SJ172550 is strong, the question whether it is a good drug candidate requires further discussion.

Searching for molecules that act through covalent modifications of their targets is an approach that is conceptually different from conventional, non-covalent drugs and additional factors like, for example, kinetics of chemical step, must be considered and added to traditional SAR studies. Even though covalent drugs raise serious safety concerns and increase the risk of idiosyncratic drug reactions and

may lead to direct tissue damage as well as haptenize their targets and raise autoimmunogenic response against them (Ju et al., 2002), there are numerous successful drugs that are widely used and turn out to act through the covalent mechanism. The most striking example of a covalent drug is Aspirin, that irreversibly modifies the cyclooxygenase, acetylating the serine residue in the active site of the enzyme (Roth et al., 1975). Furthermore, it is common that covalent mechanism of action of drugs is revealed only after their clinical utility has been established (Singh et al., 2011). Therefore covalent mechanism of action is not an absolute contraindication for the drug lead development.

On the other hand, the general aim of the rational drug development is to find molecules that would act specifically on the target protein. Selectivity requirement for covalent modifiers is achieved by high affinity of the drug and accurate initial binding that places the reactive group in proximity of its target site and is prerequisite for the second, chemical step. Therefore, the quality of the compound is determined by both its affinity and efficiency of the chemical step. Furthermore, achieving high selectivity is possible only when the intrinsic reactivity of the electrophilic motif of the inhibitor is low (Singh et al., 2011).

Our results of mass spectrometry show that the compounds from the SJ172550 family are rather reactive and able to modify multiple cysteine residues; furthermore, 4T14 is not absolutely specific for MDMX and modifies efficiently also MDM2. The actual K_i of non-covalent binding of a non-reversible PPI inhibitor is hard to measure, however a direct proof of high affinity of the compound to p53 pocket would be the synthesis of a non-covalent analogue that would bind to MDM2. Indeed, an analogue of SJ172550 that does not contain the reactive double bond is unable to covalently modify nucleophiles and still shows some affinity to MDMX (although lower, with EC50 in range of hundreds of μM) (Michael Dyer, personal communication). This suggests that SJ172550 might have some selectivity for MDMX and the data showing its ability for non-specific modifications may be not relevant for lower, physiological concentrations.

The general conclusions from physicochemical analysis of the interaction of SJ172550 with proteins are in some contrast with promising results of in-vivo tests, which were included in the paper describing discovery of the inhibitor. Since

biochemistry of the living cell is very complex, simple physicochemical experiments still cannot explain many of the phenomena occurring in the cell; many substances acting in a destructive and rather non-specific way (i.e. cis-platin) turn out to be widely used drugs (Jamieson et al., 1999). Such general toxicity of covalently acting SJ172550 may be another explanation of its potential to inhibit growth of tumor cells.

3.3.3 High-throughput screening and new pharmaceutical targets

Last problem that should be discussed in the context of the presented findings is applicability of high-throughput screening for development of protein-protein interaction inhibitors. This type of drug targets emerges rapidly as a consequence of research on human proteome and interactome. The rapidly growing knowledge of the subject is not followed by increase of drugs targeting those interactions. The problem that very often underlies the failure of the PPI-inhibitor design programs is bad choice of screening strategies and lead compounds. As the example from this chapter shows the universal libraries are based on already known drugs against well-established targets and may be not optimal for new class of protein-protein interactions (see i.e. Figure 47) (Sperandio et al., 2010).

3.4 Materials and methods

3.4.1 Protein production and purification

The N-terminal domain of MDM4 (residues 1-111) was cloned into the pET46 Ek/LIC vector (Novagen) and expressed and purified in *Escherichia coli* according to Popowicz et al. (2007). The ^{15}N uniform labeling was achieved by cultivating the bacteria in M9 minimal media (Miller 1972). Recombinant human p53 (1-312) and p53-MDMX complex were produced and purified analogously to Bista et al., 2009. Recombinant human MDM2 was produced according to paragraph 4.4.1, page 83.

Protein concentrations were determined by measurement of the absorbance at 280 nm. The extinction coefficient was calculated using the ProtParam tool at the Expasy server (Wilkins et al., 1999).

3.4.2 Chemicals

4T14 – SJ172550 analogue (MW = 428.9 Da) was bought from the company Enamine

4T14
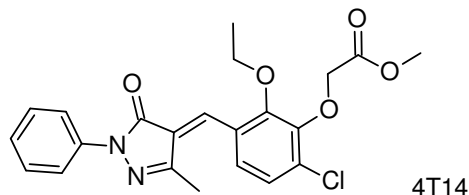
3.4.3 NMR spectroscopy

AIDA-NMR (Bista et al., 2009) was performed on 40 µM MDMX-p53 complex in 50 mM sodium phosphate, pH = 7.3, 100 mM NaCl, 0.5 mM DTT. ^{1}H-^{15}N-HSQC titrations were performed with fastHSQC pulse sequence (Mori et al., 1995). The non-reducing buffer of the sample contained 50 mM Sodium Phosphate, pH = 7.3, 100 mM NaCl, the reducing buffer contained 50 mM Sodium Phosphate, pH = 7.3, 100 mM NaCl, 10 mM DTT.

3.4.4 Mass spectrometry

HPLC-ESI analysis was performed on BRUKER microTOF mass spectrometer. The protein samples were dialyzed into 50 mM Sodium Phosphate, pH = 7.3, 100 mM NaCl and were mixed with tenfold molar excess of the compound and subjected to HPLC separation on a reversed phase C5 column and eluted with 20-80% gradient of acetonitrile (eluting at an approx. 60%/40% acetonitrile/water concentration).

4. Enhancing the sensitivity of NMR screening by rapid pulsing techniques

4.1 Introduction

NMR-based drug screening methods provide the most reliable characterization of binding propensities of ligands to their target proteins. Unique to NMR is its capability to detect weak µM-mM binding. NMR assays are, however, one of the least effective methods in terms of the amount of protein required and the time needed for acquiring the data. Therefore, there is a great need for improving the sensitivity and throughput of NMR screening and not losing the unique reliability of NMR at the same time.

Two main approaches that aim to reduce the measurement time of NMR experiments are alternative sampling and fast pulsing techniques. The alternative sampling approach allows speeding the acquisition up in multidimensional experiments by reducing number of indirect evolution increments needed for Fourier transformation (Orekhov et al., 2003; Kazimierczuk et al., 2010). Rapid pulsing, which is a more general approach, takes advantage of a fact that in solutions of slowly tumbling macromolecules longitudinal relaxation is much faster when only a fraction of the spins is manipulated during the preparation period. As a consequence, the "fast" experiments employing careful manipulation on limited populations of spins may be acquired much faster than their conventional counterparts employing non-selective pulses (Schanda 2009). Using soft NMR pulses instead of hard, both one-dimensional and multi-dimensional NMR methods may be adjusted to fulfill the principles of selective excitation and enable rapid pulsing.

4.1.1 Longitudinal relaxation in Bloch theory

In the vector description of NMR experiment, the longitudinal relaxation is a process of returning the Z component of magnetization (M_z) to its equilibrium value ($M_{z\,eq}$). The progress of this process is exponential and is characterized by the longitudinal relaxation constant (T1):

$$M_z(t) = M_{z\,eq} - \left(M_{z\,eq} - M_z(0) \right) \cdot e^{-\frac{t}{T1}}$$

Typical T1 values for amide protons of small proteins (100-150 amino acids) are ca. 0.2-1s (Markus et al., 1994), whereas magnetization of water recovers with T1 up to even 6s (Aso et al., 1988), however effectively, due to radiation damping, the real water magnetization recovery times are significantly shorter (but still in order of seconds) (Bloembergen et al., 1954).

The rate of longitudinal relaxation recovery is a limiting step dictating pace of NMR scans, and especially in case of observation of water-exchangeable protons, one must consider slowly relaxing magnetization of water as a bottleneck of NMR experiment.

4.1.2 Ernst angle excitation

Even intuitive qualitative analysis leads to conclusion that too quick pulsing in NMR experiments does not allow for full recovery of the magnetization between the scans whereas too slow pulsing makes NMR experiments excessively long. In both cases, sensitivity of the experiment per time unit is impaired. Additionally, by using pulses that leave the magnetization before acquisition at flip angle smaller than 90°, the amplitude of the signal is reduced, but on the other hand, the recovery time needed to return the magnetization to its equilibrium state is shortened.

For the simplest case of one-pulse experiment with the sum of acquisition and recycle delay t_{rec}, the optimal combination of flip angle α_{Ernst} and recycle delay was derived by Richard Ernst and is given by (Ernst et al., 1990):

$$\cos \alpha_{Ernst} = e^{-\frac{t_{rec}}{T1}}$$

<div align="right">Equation 7</div>
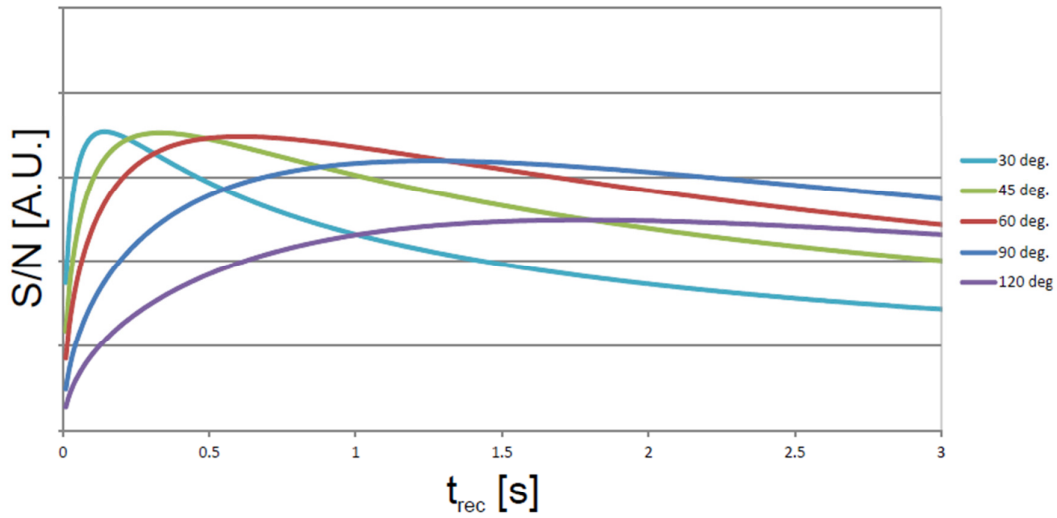
Figure 37 Dependence of the sensitivity of the one-pulse NMR experiment on the recovery delay t_{rec}. The data was simulated using equation derived in Chapter 8.4, five different values of flip angle were used (as shown on the right side of the plot). T1 value of 1s was assumed in all simulations.
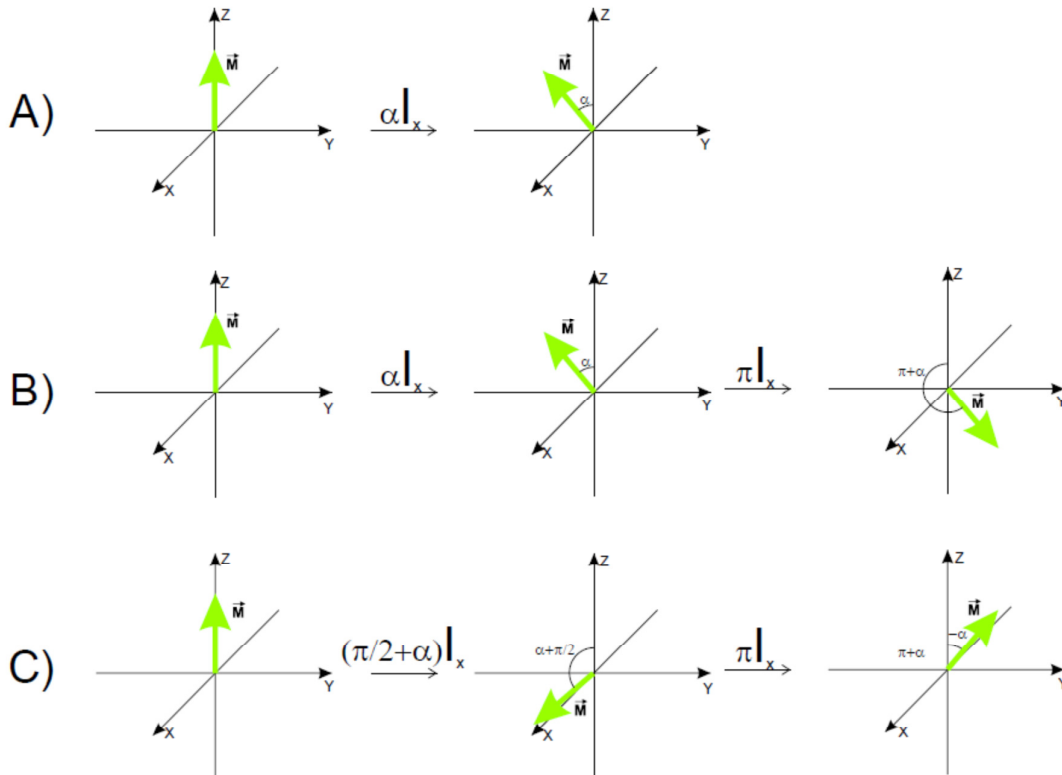
Figure 38 Dependence of effective value of Ernst angle from the number of pulses in NMR experiment. For one pulse experiment, the optimal angle is α (see Equation 7) (A), whereas in combination with inversion pulse, the first pulse should be of angle π/2+α (C), otherwise the pulse sequence will leave the magnetization in unfavorable orientation far from its equilibrium position (B).

Figure 37 shows the dependence of NMR sensitivity on the pulse angle and recycle delay. It is clear from the plot that the largest sensitivity per time unit is achieved for flip angles $\alpha < 90^O$.

Special consideration must be given when the Ernst angle excitation is used in conjunction with the 180° inversion pulses; in cases when the number of inversion pulses is odd, the optimal angle of the first pulse would be $90^O + \alpha_{Ernst}$ (see Figure 38).

4.1.3 Water exchange

Water molecules have big impact on magnetic properties of protein nuclei. From numerous NMR and crystallographic studies it is known that hydrogen bonds of water and polar groups of proteins have crucial impact on protein structure and dynamics (e.g. (Otting et al., 1991)). Water can influence relaxation of protein protons in two ways: by dipole-dipole cross relaxation and chemical exchange.

The timescale of water residence on protein surface is in range of ps-ns (Nucci et al., 2011) and therefore the cross-relaxation is generally not efficient way of magnetization transfer.

Contrary, the chemical exchange may play a major role in recovery of the magnetization of water-exchangeable protons (from amide, amine, guanidine and imine HN groups) of protons from protein is described by equation

$$HOH + HN \underset{k_2}{\overset{k_1}{\longleftrightarrow}} HOH + HN$$
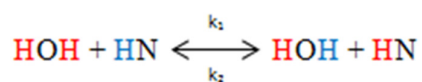
where the exchange rate of the process is defined as:

$$k_{ex} = k_1 + k_2.$$

Since the process may be both acid- and base-catalyzed, k_{ex} depends on pH; in example for indole H^N group in free tryptophan the k_{ex} value varies from 1 s^{-1} (at pH = 4) through 10^2 s^{-1} (at pH = 7.5) to 10^5 s^{-1} (at pH > 11) (Wüthrich 1986).

The effect of chemical exchange of labile protein protons is transfer of magnetization from water to protein and vice versa. In the example when water molecules have been saturated during the preparation phase of NMR experiment, saturation is transferred to protein and signals of water-exchangeable protons are attenuated. On the other hand, water magnetization that is in the Boltzmann equilibrium may take over the saturation of protein protons, thus enhancing the relaxation process.

The state of water magnetization during an NMR experiment is determined by water suppression technique employed in the experiment. The usual methods of removal of water signal employ presaturation of the water resonance, jump-return scheme, water flip-back pulses (that align the water magnetization along +Z axis) and a gradient echo scheme in which transverse magnetization of water is dephased by two gradients (Watergate) (Gueron et al., 1991; Piotto et al., 1992; Cavanagh 2007). The disadvantages of those experimental schemes are: low overall performance (presaturation, jump-return, water flip-back), saturation of water signal and suppression of exchangeable protons signals (especially presaturation, but also jump-return and gradient-echo) and difficult practical applicability (water flip-back). Usage of any of the aforementioned techniques requires introduction to NMR experiments long interscan delays during which water magnetization reeqilibrates. Therefore the best (though not always experimentally feasible) solution of water suppression problem is to design a selective pulse sequence that does not act on water magnetization.

4.1.4 Relaxation enhancement by selective spin manipulation

Magnetization recovery after excitation of a spin or set of spins is described by Solomon equations. Let us consider a simple example of a homonuclear system of two dipolar-coupled spins (IS). For this case, longitudinal relaxation after a non-selective excitation (moving the spins to transverse plane) of both spins is described by well-known equations:

$$I_z(t) = I_{z\,eq} - I_{z\,eq} \cdot e^{-(\rho+\sigma)t}$$
$$S_z(t) = S_{z\,eq} - S_{z\,eq} \cdot e^{-(\rho+\sigma)t}$$

where ρ and σ are auto-relaxation and cross-relaxation rates, respectively.

The longitudinal relaxation in this case is in agreement with simple macroscopic description of Bloch; the magnetization follows a mono-exponential decay with relaxation time constant $\frac{1}{T1} = \rho + \sigma$.
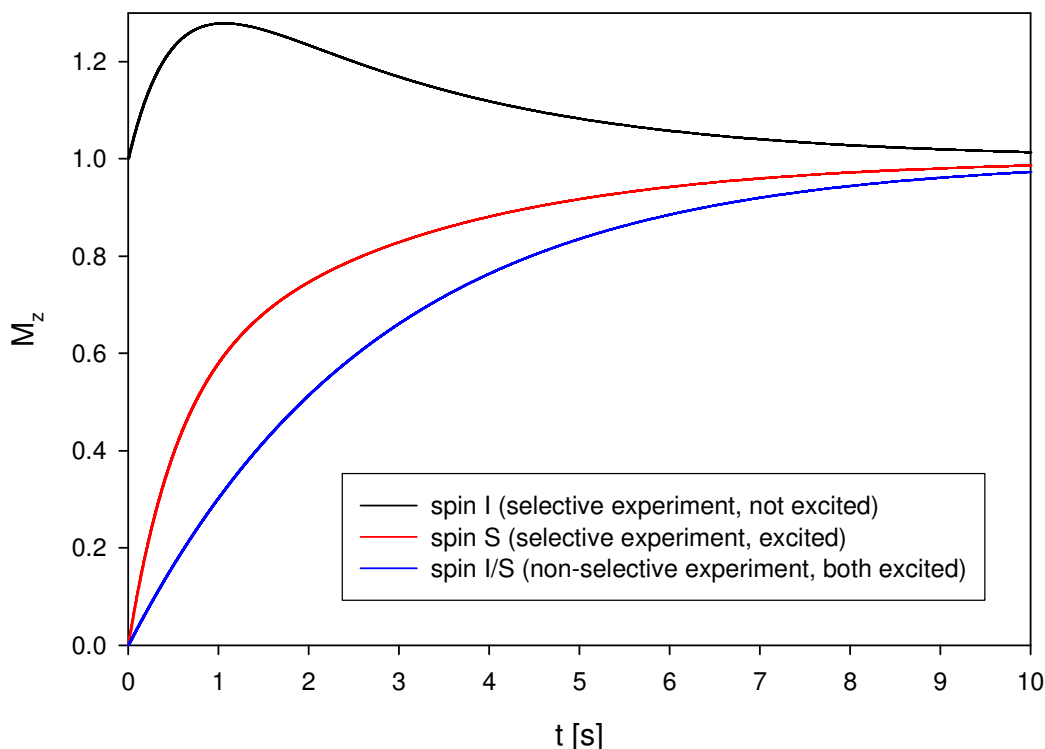
Figure 39 Longitudinal relaxation simulation for a two-dipolar-coupled, hydrogen spin system IS for cases of selective S excitation (spin is brought to transverse plane) and non-selective excitation of both spins. The values of σ and ρ (-0.8 s^{-1} and 1.16 s^{-1}, respectively) were calculated according to equations from Appendix Z for correlation time 1 ns ($\omega\tau_c$>>1), and intranuclear distance of 2 Å.

However, if we consider selective excitation of only the S spin in the same spin system, Solomon equation solution for that case is (see Chapter 8.5 for derivation):

$$I_z(t) = I_{z\,eq} + \frac{1}{2}S_{z\,eq} \cdot \left(e^{-(\rho-\sigma)\cdot t} - e^{-(\rho+\sigma)\cdot t}\right)$$

$$S_z(t) = S_{z\,eq} - \frac{1}{2}S_{z\,eq} \cdot \left(e^{-(\rho-\sigma)\cdot t} + e^{-(\rho+\sigma)\cdot t}\right)$$

We see that in this case the magnetization build up and decay have bi-exponential progress with two relaxation constants, one being sum of auto- and cross relaxation rates and the other being their difference. The overall outcome of the equation depends on the sign of σ; for large molecules in slow tumbling limit ($\omega\tau_c \gg 1$), σ is negative and the S spin relaxation would be increased when compared to non-specific inversion, for small molecules with $\omega\tau_c \ll 1$, σ is positive and relaxation is slowed down (see Chapter 8.6).

Since almost all biological polymers have long rotational correlation times $\omega\tau_c \gg 1$ they exhibit negative cross relaxation rates and after selective excitation or inversion, they recover in a biexponential mode with the fast decay constant $-(\rho - \sigma)$ and the slower decay constant $-(\rho + \sigma)$ (that is equal to inverse of T1 in classical understanding).

Simulation of magnetization recovery for a two-spin system is shown in Figure 39.

4.1.5 Effect of fast pulsing on saturation of protein resonances

The best candidates for selective excitation and manipulation are well separated amide and aromatic resonances. They resonance frequencies span from ca. 6 to 10 ppm and numerous excitation techniques may be used to achieve selective manipulation on these spins populations. The unperturbed aliphatic protons of proteins act as "relaxation sink" that quickly discharges the amide magnetization by spin-diffusion process, transiently becoming hyperpolarized (see Figure 39). As shown in Appendix Z, the larger the protein, the quicker the polarization transfer, therefore the relaxation boost is proportional to the size of the protein. The initial magnetization of amides or aromatics is quickly transferred and diluted over the whole protein spin population and finally reaches the quickly rotating methyl sidechains. Those groups have fast correlation times and large spectral densities at high frequencies and due to, that are very effective sources of longitudinal relaxation in proteins (Olejniczak et al., 1990; Schanda 2009).

The optimal pulsing rate must be determined experimentally and Ernst angle is a good criterion; in case of too fast pulsing, aliphatic protein resonances become saturated and spin diffusion becomes ineffective. As usually, the optimal pulsing rate should be a balance between unnecessarily long recycle delays and sample saturation with too large radiofrequency load.

4.2 Results

4.2.1 SEI methods for NMR screening

By using tryptophan-bearing proteins, it was shown that a 1D proton NMR version of AIDA-NMR is faster than the 2D version and can be used universally in competition experiments for monitoring ligand/protein-protein complexes (Krajewski et al., 2007). In addition, such tryptophan-containing proteins can be used for studying binary interactions between ligands and target proteins with 1D NMR (Rothweiler et al., 2008).

SEI methodology is an extension of the previously published NMR screening
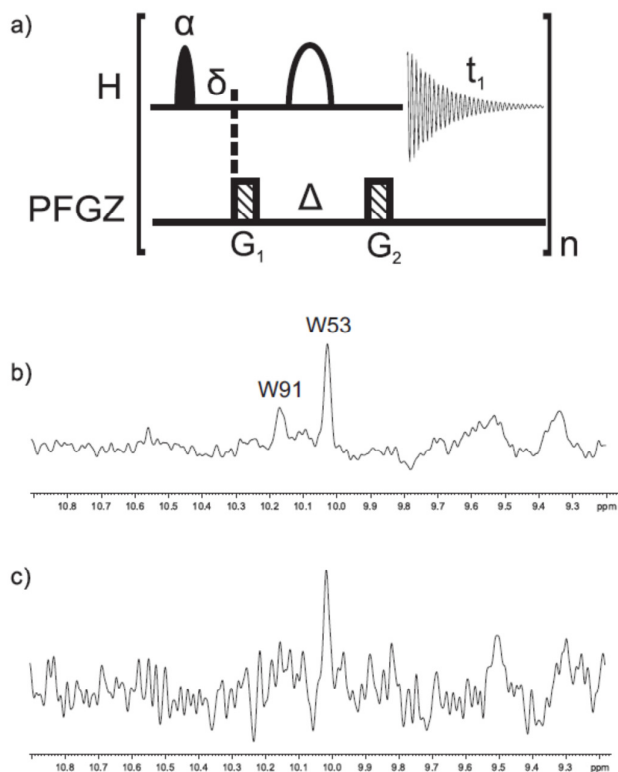
Figure 40 . (a) Experimental scheme of the SEI experiment. The pulse sequence incorporates a Gaussian-shaped pulse of angle $\alpha \geq 90^\circ$, followed by a modified WATERGATE sequence for residual water signal suppression. The rSnob profile (Kupce et al., 1995) is used for selective refocusing of downfield shifted protein resonances in the spin-echo part of the experiment (the 2 ms long rSnob is placed in the middle of the $\Delta = 4$ ms delay). The Gaussian-pulse has the duration of 1 ms and α of $\approx 110^\circ$. Selective pulses are applied at 10 ppm. Gradient strengths are 20% for both gradients, the gradient recovery delay and δ were set to 100 µs, and the acquisition time t_1 to 300 ms, giving the total scan time T_{scan} ~300 ms. (b) (c) 1D ^{1}H NMR spectra of the 35 µM MDM2-p53 complex; two $^NH^\varepsilon$ signals of Trp of p53 are visible (for the NMR properties of the complex see Figure XX). Both spectra were acquired in 2.5 min using (b) the SEI pulse sequence and (c) a 90° hard pulse followed by the WATERGATE-W3 sequence (Piotto et al., 1992).

methods. The SEI experiments achieve longitudinal relaxation optimization employing: relaxation enhancement of relaxation by spin diffusion, chemical exchange with water and excitation under the Ernst angle.

The SEI pulse sequence shown in Figure 40 employs selective pulses only on well-separated NMR signals (e.g. Trp $^H N^\varepsilon$ signals).

4.2.2 Applications to MDM2-p53 antagonists

Figure 41 shows examples of the assay for two antagonists of the MDM2-p53 interaction: Nutlin-3 (Vassilev et al., 2004) and compound PB10 (for formulas see Materials and Methods section). Since AIDA is a competition experiment, the K_i of protein-antagonist interaction can be determined in a single measurement. For Nutlin-3, the assay produces the K_i of binding to MDM2 of 90 nM, in agreement with the literature data (Vassilev et al., 2004). The SEI AIDA of Figure 41d indicates that compound PB10 binds weakly to MDM2, with the estimated K_i of 3 µM in agreement with the binary titration on the MDM2 T101W mutant using also the SEI pulse sequence (Figure 44a-d).

Figure 41 The $^N H^\varepsilon$ indole Trp region of 1D ^{1}H NMR spectra of the MDM2-p53 complex. The signal of W23p53 is used for monitoring the ligand/MDM2-p53 interactions (details of the diss/re-appearance of NHε signals are explained in Figure S2). (a) free p53. (b) The MDM2-p53 complex. (c) The Mmd2-p53 complex titrated with Nutlin-3; the protein : inhibitor molar ratio 1 : 2. (d) The Mmd2-p53 complex titrated with compound PB10; the protein : inhibitor molar ratio 1 : 2. All the spectra were acquired using the SEI pulse sequence, complex concentration was 36 µM, acquisition time 2 min. Corresponding 1D 1H spectra recorded using hard pulses are shown in Figure 42.
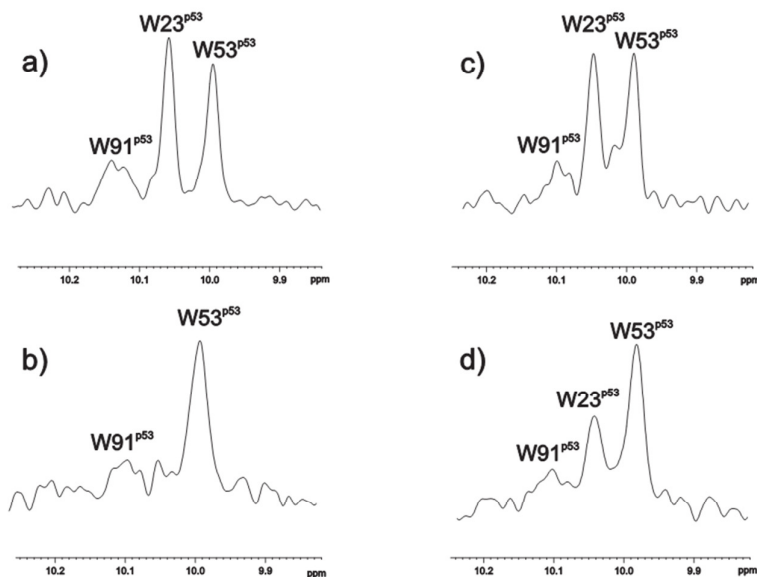
4.2.3 Comparison of spectra acquired with SEI and hard pulses
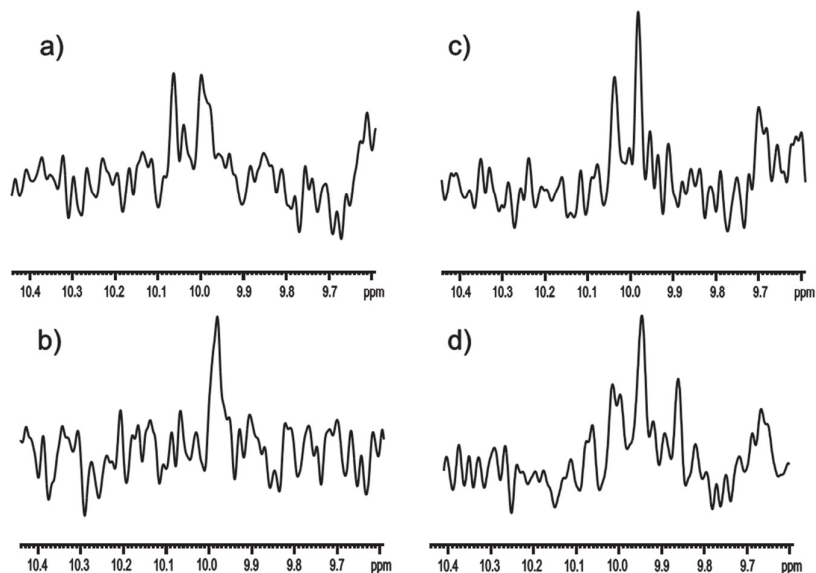
Figure 42 The NHε indole Trp region of 1D ^{1}H NMR spectra of the MDM2-p53 complex. The signal of W23^{p53} is used for monitoring the ligand/MDM2-p53 interactions (a) Free p53. (b) The MDM2-p53 complex. (c) The Mmd2-p53 complex titrated with Nutlin-3; the protein : inhibitor molar ratio 1 : 2. (d) The Mmd2-p53 complex titrated with compound PB10; the protein : inhibitor molar ratio 1 : 2. All spectra were acquired using the 90° hard pulse followed by WATERGATE-W3 sequence with an acquisition time of 2 min. Corresponding spectra acquired in the same experimental time using the SEI sequence are shown in Figure 41.
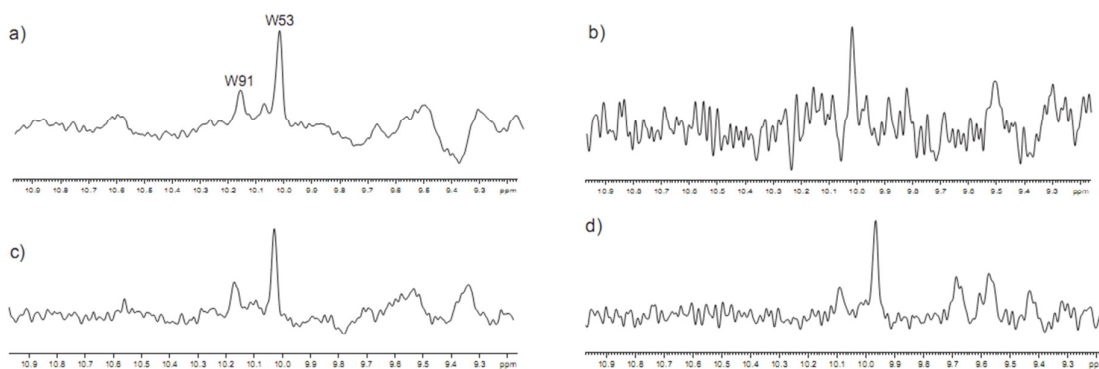
Figure 43 1D ^{1}H NMR spectra of the MDM2-p53 complex. Two visible peaks originate from the W91^{p53} ^{N}H^ε (broadened, pH-dependent) and the W53^{p53} ^{N}H^ε. (a) Spectrum of the 35 μM solution of the MDM2-p53 complex recorded using a 90° hard pulse followed by a WATERGATE-W3 sequence (acquisition time: 0.5 h). (b) Spectrum of the 35 μM solution of the MDM2-p53 complex recorded using a 90° hard pulse followed by a WATERGATE-W3 sequence (acquisition time 2.5 min). (c) spectrum of the 35 μM solution of the p53-MDM2 complex recorded using the SEI pulse sequence (acquisition time 2.5 min). (d) Spectrum of the 3.5 μM solution of the MDM2-p53 complex recorded using the SEI pulse sequence (acquisition time 1 h).

4.2.4 Applications to tryptophan mutants: MDM2 and CDK2 inhibitors

CDK2, together with its associated cyclin, controls the passage of the cell through different phases the cell division. Inhibiting CDKs in tumor cells should arrest or stop the progression of the uncontrolled tumor cell division (Knockaert et al., 2002). Figure 44e-g show the application of the SEI to roscovitine (Appendix W), an extensively characterized small molecule inhibitor of CDK2 with nanomolar affinity.
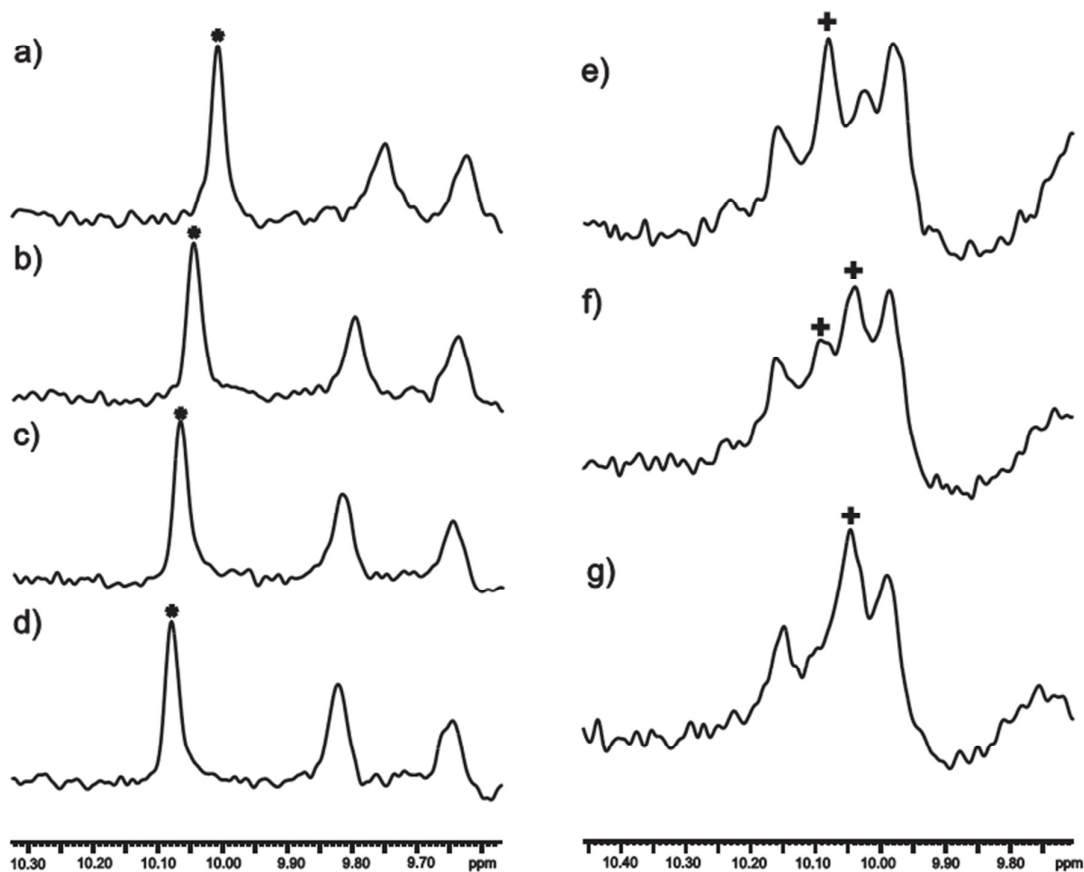
Figure 44 Binary NMR titrations of small molecule ligands with the 20 µM solutions of the MDM2-T101W and the CDK2-A93W mutants using the SEI pulse sequence. The experimental time for each step was 10 min; the SEI pulse sequence gives approximately tenfold reduction in experimental time compared to the corresponding proton spectra acquired using 90° hard pulses. (a) – (d) Titration of the 20 µM solution of the MDM2 T101W mutant with increasing amounts of compound PB10 (the compound : protein molar ratio = (a) 0:1, (b) 1:1, (c) 2:1, (d) 5:1), respectively. The compound is in fast exchange on the NMR timescale with MDM2, thus the $^{N}H^{\varepsilon}$ peak of W101^{MDM2} (indicated with an asterisk) moves continuously from its initial to final position. The estimated K_D is 3 µM, in agreement with the SEI-AIDA of Figure 41d. (e) – (g) Titration of the 20 µM CDK2 A93W mutant with increasing amount of roscovitine (the compound: protein molar ratio = (e) 0:1, (f) 0.5:1, (g) 1:1). The compound is in slow exchange with CDK2 and, thus, the $^{N}H^{\varepsilon}$ peak originating from the newly introduced W93^{CDK2} (indicated with a cross) is split into 2 peaks originating from the bound and free fractions of CDK2 A93W.

4.3 Discussion

4.3.1 Pulse sequence optimization

Choice of shapes of the pulses used in the SEI sequence was empiric; the combination of a Gaussian and rSnob pulses turned out to be the most advantageous. The main advantage of using the Gaussian pulse is the fact that its excitation profile is very clean, does not show any "winglets" or sidelobes, therefore the effect of the pulse on water and other protons is minimized (see Figure 45). The disadvantage is the unfavourable linear phase evolution that occurs during excitation with the pulse and leads to baseline distortions (Kessler et al., 1991). However, since the effective bandwidth needed to obtain the information on K_i in SEI-AIDA experiments is only about 200 Hz, the unfavourable phase properties of the pulse may be neglected and efficiently corrected by manual phasing of the spectra and by applying polynominal baseline correction.
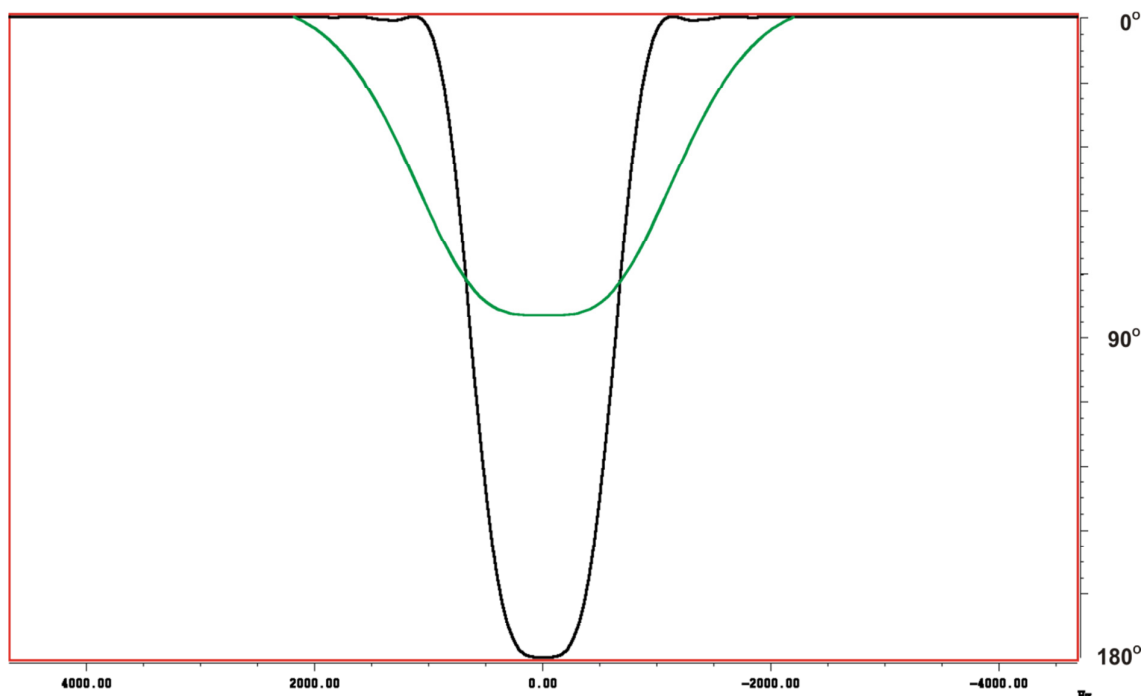
Figure 45 Excitation and inversion profiles calculated for shaped pulses used in the SEI pulse sequence. Green lines show the excitation profile (X2+Y2) for the 90° 1 ms Gauss shape and black lines show refocusing profile of 180° 2ms rSNOB profile. Simulations were carried out with the Bruker NmrSim software.

Usage of other pulse shapes, like E-Burp (Geen et al., 1991), is theoretically also possible, however, practice shows that the sidelobes present in their excitation

profiles impair water suppression and decrease the overall sensitivity, by both the saturation of water, and consequently, chemical exchange of saturated water with then indole H^N protons and by overflowing the digitizer with poorly supressed water signal.

4.3.2 Advantages of the SEI scheme

The pulse sequence shown in Figure 40 has several advantages that enable its efficient use in various NMR assays. Firstly, it is possible to adjust selective pulses' bandwidths and offsets so that the water magnetization is not moved from the +Z axis and excellent water suppression is achieved in a single scan. Moreover, since the slowly relaxing water magnetization is not saturated, no long recycle delays are necessary and the Ernst-angle excitation (Ernst et al., 1990) is possible. Considering that only a small fraction of spins of a macromolecule is in a non-equilibrium state, the dipole interactions between the excited spins and other spins in the protein and chemical exchange with bulk water significantly speed up the longitudinal relaxation (Pervushin et al., 2002; Schanda et al., 2005). For a "normal" 1D version of AIDA, we found that a reliable K_D determination can be achieved typically for protein concentrations as low as 40 µM for a ca. 0.5 h experiment in a 5 mm NMR tube using a cryogenically cooled probehead on the 600 MHz spectrometer. For the SEI sequence, the duration of a single scan can be decreased down to 300 ms without significant reduction in the signal to noise ratio per scan. With faster acquisition, the experimental time is reduced by an order of magnitude or protein concentration may be decreased by ca. 70% compared our 1D proton "Trp" version of AIDA described previously (see also Figure 42 and Figure 43) (D'Silva et al., 2005; Krajewski et al., 2007).

Since only a narrow fragment of the proton NMR spectrum is detected in the SEI method, sample may contain protonated buffering substances and additives and unless they give NMR signals at ca. 10 ppm, they are not detected and do not overflow the receiver.

Other advantage of the presented pulse sequence is its robustness. Usage of a typical Watergate element requires always proper calibration of pulse lengths and offsets, whereas the spin echo element used in the SEI sequence is insensitive to change in the frequency of water resonance and misadjustment of the pulse power

decreases the overall sensitivity of the experiment but does not result in the digital receiver overflow by a poorly supressed water signal.

4.3.3 Conclusions

To my knowledge, the SEI pulse sequence is the first application of rapid pulsing techniques for NMR screening. Analogous pulse sequences were successfully applied to optimize two-dimensional and three-dimensional experiments employing amide protons (particularly sofastHMQC (Schanda et al., 2005) and BEST-set of triple resonance experiments (Brutscher et al., 2007) are recently gaining popularity in the NMR community). According to my experience within the SEI and sofast- methods, the SEI experiments give significantly larger sensitivity gain, probably because of the less complex pulse sequence and simpler coherence transfer. Additionally, since only soft, relatively short low-power pulses are applied, there is no danger of hardware damage by too short duty cycles, like in the case of the heteronuclear rapid pulsing methods.

As shown in Figure 43, the SEI pulse sequence may in some cases successfully replace conventional ^{1}H 1D NMR spectroscopy and give spectra almost identical to those recorded with hard pulses, but significantly faster, or with much larger sensitivity.

Thus, the combination of a simple SEI pulse sequence with 1D AIDA NMR screening is a straightforward, robust alternative to the traditional NMR screening methods. Due to increased sensitivity, the SEI experiment is beneficial for the NMR of proteins difficult to obtain, whereas the reduction of experimental time can significantly increase the throughput of NMR screening. SEI AIDA-NMR can be used universally for monitoring ligand/protein–protein complexes because by introducing tryptophan residues through site-directed mutagenesis the method can also be applied to proteins that do not contain tryptophan in their natural amino acid sequence. Our method is suitable also for chromophoric and fluorescent aromatic small molecule compounds and thus may complement assays based on the intrinsic fluorescence of tryptophan, which usually fail in these cases.

4.4 Materials and Methods

4.4.1 Protein production and purification

The recombinant human MDM2 (residues 1-118) was obtained from an *E. coli* BL21(DE3) RIL expression system using pET-46Ek/LIC vector (Novagen). Cells were grown at 37°C and induced with 1 mM IPTG at an OD_{600nm} of 0.7. After induction the cells were cultured for additional 4.5 h at 37°C and the recombinant protein was purified from inclusion bodies. After washing with PBS containing 0.05% Triton X100 with subsequent low-speed centrifugation (12000G), the inclusion bodies were solubilized in 6 M GuHCl in 100 mM tris-HCl, pH 8.0 including 1 mM EDTA and 10 mM DTT. The protein was then dialyzed against 4 M GuHCl, pH 3.5. For renaturation, the protein was diluted (1:100) into 10 mM Tris-HCl, pH 7.0, containing 1 mM EDTA and 10 mM DTT, by adding the protein in several pulses to the refolding buffer. Refolding was performed overnight at 4°C. Following, ammonium sulphate was added to the final concentration of 1.5 M and after 3 h the sample was mixed with 10 ml of the Butyl Sepharose 4 Fast Flow (Pharmacia, FRG). The protein was eluted with 100 mM Tris-HCl, pH 7.2, containing 5 mM DTT, and further purified on HiLoad 16/60 Superdex200 gel filtration (Pharmacia) into buffer containing 10 mM Na_2HPO_4, 1,8 mM KH_2PO_4, 140 mM NaCl, 2,7 mM KCl, 0,05% NaN_3, 5 mM DTT, pH 7.2.

MDM2 mutant T101W, and p53 (residues 1-321) were obtained form an *E. coli* BL21 (DE3) RIL expression system using the pET-46Ek/LIC vector. Cells were grown at 37^0C and induced with 1 mM IPTG at an OD_{600nm} 0.7. Both proteins were expressed for 12 h at 20^0C and purified under native conditions using Ni-NTA (Qiagen). The final purification of MDM2, MDM2 T101W mutant and p53 was carried out via HiLoad 16/60 Superdex200 gel filtration (Pharmacia) into buffer containing 10 mM Na_2HPO_4, 1,8 mM KH_2PO_4, 140 mM NaCl, 2,7 mM KCl, 0,05% NaN_3, 5 mM DTT, pH 7.2.

The MDM2-p53 complex was prepared by mixing p53 and MDM2 in ratio 1:3 and applied on HiLoad 16/60 Superdex200 gel filtration (Pharmacia) into buffer containing 10 mM Na_2HPO_4, 1,8 mM KH_2PO_4, 140 mM NaCl, 2,7 mM KCl, 0,05% NaN_3, 5 mM β-mercaptoethanol, pH 7.2 in order to remove the excess of MDM2.

The CDK2 mutant A93W (residues 1-298) was overexpressed at 20°C overnight in *E. coli* BL21 (DE3) RIL using pET-28 vector. The protein was purified under native conditions via Ni-NTA (Qiagen) and finally by HiLoad 16/60 Superdex200 gel filtration (Pharmacia) into buffer containing 10 mM Na_2HPO_4, 1,8 mM KH_2PO_4, 140 mM NaCl, 2,7 mM KCl, 0,05% NaN_3, 5 mM DTT, pH 7.2.

4.4.2 NMR Spectroscopy

All NMR spectra were acquired at 300K on a Bruker DRX 600 MHz spectrometer equipped with a cryoprobe. Typically, protein samples obtained from gel filtration were concentrated or diluted to the desired concentration and mixed with up to 8% (v/v) of D_2O or D_6-dimethyl sulfoxide. Stock solutions of the compounds used in titrations were prepared in D_6-dimethyl sulfoxide. The spectra were processed with XwinNMR 3.5 software. 1D ^1H spectra were recorded using a hard 90° pulse followed by the WATERGATE-W3 sequence (Piotto et al., 1992) and total 3 s of acquisition and relaxation delay or the SEI pulse sequence and total 300 ms of acquisition and relaxation period. For both cases, a total of 4k points were acquired during t1 evolution, zero filled to 32k and subjected to Fourier transform and polynominal baseline correction.
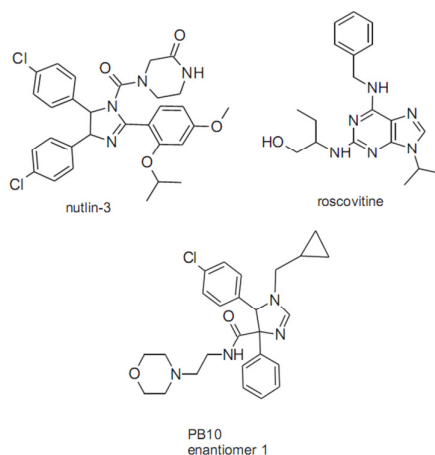
4.4.3 Chemicals

Figure 46 Chemical structures of the compounds used in this study. Only the more active enantiomer of PB10 was used.

5. AnchorQuery and acyclic inhibitors of MDM2-p53 interaction

5.1 Introduction

5.1.1 "Hot spots" and "anchors" of protein-protein interaction

Binding of two proteins may be in frequent cases dissected to only few points in molecular space that contribute to the most of free energy. In a protein-protein interaction, those amino acids that contribute energetically to binding are defined as the "hot spots" of the interaction (Kortemme et al., 2002). The estimation of their energetic contributions may be done experimentally, by mutagenesis (Bottger et al., 1997) or computationally, using for example computational alanine scanning, which employs well established force fields with molecular dynamics simulations (Massova et al., 1999). Analysis of the MDM2-p53 interaction shows that the "hot spots" are Phe19^{p53}, Trp23^{p53} and Leu26^{p53} (Bottger et al., 1997; Kortemme et al., 2002; Meireles et al., 2010) and the rest of the p53 helix may be to good approximation considered as a skeleton that places the side chains in correct positions.

Molecular dynamics simulations provide important insights into dynamic sides of the protein-protein interaction. The works of Camacho group (Rajamani et al., 2004; Meireles et al., 2010) show that the residues that undergo the largest decrease in the solvent accessible area upon binding to other proteins may be considered the "anchors" of the interaction; i.e. they are the first elements that are recruited to the interaction partner and acquire their ultimate position already at the beginning of the simulations. Due to this, these elements act as the stabilizers of transient substates that are passaged by the system during the recognition (Rajamani et al., 2004). The stability and importance of the "anchoring" has obvious implications also in drug development; the inhibitors acting on the basis of molecular mimicry should contain elements chemically similar to the amino-acids and particularly the "anchor" residue analogue is a good starting point in antagonists development (Rajamani et al., 2004; Czarna et al., 2010; Meireles et al., 2010).

Furthermore, since "anchor" residues are surrounded by the receptor atoms and thus, conformationally constrained, the "anchor" analogue might be also considered as the most conserved element of the interaction that occupies the same space as the natural "anchor" and may therefore be used to guide docking of the inhibitor molecule to the protein (Czarna et al., 2010).

5.1.2 Pharmacophore conception

The pharmacophore is defined as an ensemble of steric and electronic features that are necessary to ensure the optimal supramolecular interactions with a specific biological target and to trigger (or block) its biological response (Wermuth et al., 1998). In modern medicinal chemistry, pharmacophore models are derived computationally or manually by comparison and structural alignment of known protein ligands (Leach et al., 2010).

The MDM2-p53 complex has been thoroughly studied in the last decade and more than 30 known high-resolution structures of the N-terminal domains of MDM2 bound to various classes of ligands are available. This should aid the development of a pharmacophore model.

The structures and extensive computational analysis demonstrate that the forces stabilizing the binding of MDM2 and p53 are mostly the delocalized hydrophobic interactions and only one hydrogen bonding between the carbonyl Leu54^{MDM2} oxygen and the indole H^N Trp23^{p53} proton is prevalent for the whole time of the interaction (Dastidar et al., 2009). An additional interaction interface around Asn29^{p53} is also stabilized by 4 hydrogen bonds, however, molecular dynamics and experimental data show that this area contributes positively to the free energy of binding, generates repulsive interactions and the hydrogen bonds in that area are not stable (Dastidar et al., 2008; Joseph et al., 2010). Trp23^{p53} undergoes the largest difference in the solvent-accessible area upon the binding and therefore may be considered as the main "anchor" of the interaction (Rajamani et al., 2004; Meireles et al., 2010).

Based on this data, a simple, but useful pharmacophore model for MDM2-p53 interaction implementing the "anchor" feature contains only three requirements: two hydrophobicity features that are placed in spaces occupied by the Leu26[p53] and Phe19[p53] side chains and an "anchor" feature that is located in the place occupied by the Trp23[p53] side chain (Domling 2008). Placing a tryptophan analogue in the space defined as "anchor" feature retains the hydrogen bonding pattern of the MDM2-p53 complex. Such a crude model is used as a basis and may be a subject of further development and refinement.

5.1.3 AnchorQuery

AnchorQuery (http://achnorquery.cbb.pitt.edu) is a web-based technology aimed as an aid in rational drug discovery. The software uses a user-defined pharmacophore model to search its own database for compounds that fulfill the pharmacophore constraints (see Figure 47A).

The database included in AnchorQuery currently contains products of 21 million virtual multicomponent reactions. The compounds were prepared *in sillico* using the ChemAxon REACTOR software (www.chemaxon.com) and simple, commercially available (or easy to synthetize) substrates. All the compounds contain "anchor" analogues. OpenEye Omega software (www.openeye.com) was used to generate 1.5 billion of conformers. The search algorithm employs spatial alignment of the compounds with pharmacophore features that is guided by proper positioning the anchor analogue. The program does not perform full conformational search, but uses only the preexisting structural ensembles and thus is not demanding computationally, normally providing full search results within several seconds. The AnchorQuery does not implement any scoring or energy minimization functions and therefore the results must be downloaded for in-house refinement using one of the available molecular modeling packages (Koes et al., 2011, submitted). Since the database was created by virtual chemical reactions, a custom synthesis scheme together with literature references is available for each of the compounds.
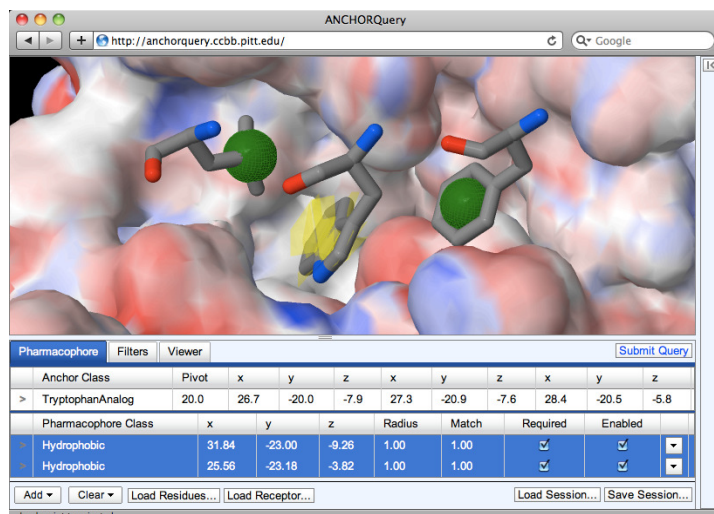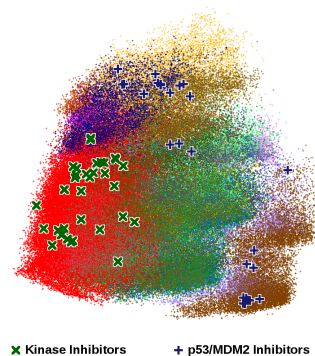
(a)   (b)

Figure 47 (a) AnchorQuery web interface with pharmacophore model of MDM2-p53 interaction loaded. Green spheres are used to define position of hydrophobic groups whereas yellow area defines position, that must be occupied by anchor analogue. (b) A representation of the chemical diversity of the multi-component reaction-biased libraries (different chemotypes shown in different colors) relative to the ZINC database (shown in red). The diversity space is visualized by plotting the top two principal components of the OpenBabel FP2 (http://openbabel.org) fingerprints of 200,000 compounds randomly selected from the 17.5-and-21 million compounds of ZINC and the AnchorQuery database, respectively. The PPI-biased compounds are focused on a different region of chemical space than the historically-biased ZINC database. Indeed, a library of kinase inhibitors, some containing a tryptophan analog, falls squarely in the space covered by ZINC, while inhibitors of p53/MDM2, including inhibitors without a tryptophan analog, are located in the space covered by the new libraries.

5.1.4 Multicomponent reactions

Multicomponent reactions are convergent reactions in which three or more components form a single product containing majority of the atoms of the substrates. The molecular mechanism underlying the multicomponent chemistry is diverse, but usually involves bimolecular formations of reaction intermediate that in further bimolecular processes lead to formation of the final product. The multicomponent reactions are therefore performed as one-pot, single-step procedures and are relatively easy and efficient way of obtaining complex drug-like molecules (Ugi et al., 1994; Domling 2006).

Since multicomponent reactions are type of the combinational chemistry that employs at least three starting components, the chemical diversity of their products is very large and the chemical space explored by the AnchorQuery database exceeds about 4 times the diversity of the most popular high-throughput database ZINC (Irwin et al., 2005) (see Figure 47b). Furthermore, multicomponent reactions

are very efficient way of producing α-helix imitators and the AnchorQuery database contains 75% of already known inhibitors of the MDM2-p53 interaction, whereas popular high-throughput databases are often biased toward classical drug targets (i.e. kinase inhibitors) and do not explore the newly emerged area of PPI inhibitors (see Figure 47 B).

a)

b)

c)
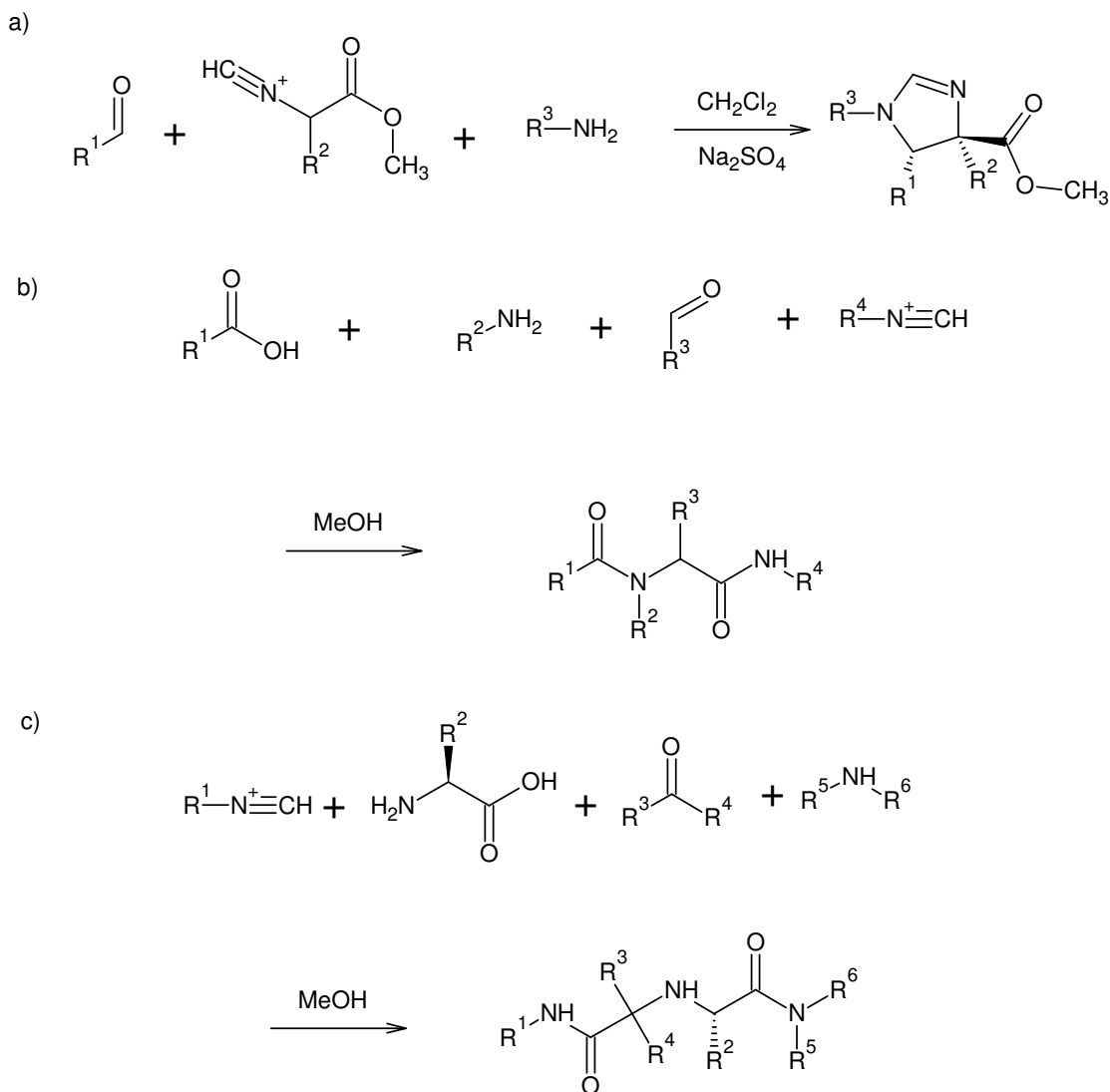
Figure 48 Examples of multicomponent reactions. a) Three component Orru reaction combines isocyanide, aldehyde and primary amine to yield a 2-imidazoline scaffold; the reaction is performed at room temperature and is diastereoselective (Bon et al., 2003). b) Classical four-component Ugi reaction combines carboxylic acid, amine, aldehyde and isocyanide into a peptide-based scaffold (Domling et al., 2000) c) In a four-component reaction named U4C5Cr (Ugi 4 compounds, 5 reactive groups) isocyanides react with α-amino acids, ketones (or aldehydes) and primary or secondary amines to yield complex peptidomimetic products. Both reactions do not require harsh conditions and are conducted at room temperature in methanol (Ugi et al., 1996).

5.2 Results

5.2.1 Results of the AnchorQuery screen

The approach of combining the AnchorQuery and multicomponent reactions leads to an assembly of very diverse chemotypes of the MDM2-p53 inhibitors. The direct proof of effectiveness of the approach are 80 anchor-based inhibitors of the MDM2-p53 interaction with K_Ds < 60 μM that were synthetized and validated by fluorescence polarization and NMR. Figure 49 depicts representatives of 6 different scaffolds based on the tryptophan anchor and synthetized by multicomponent reactions.

A
K_i = 0.7 μM
MW = 629.6 Da
cLogP = 4.95 ± 1.02

B
K_i = 5 μM
MW = 508.0 Da
cLogP = 5.49 ± 0.94

C
K_i = 1.1 μM
MW = 462.3 Da
cLogP = 7.02 ± 0.62

D
K_i = 2 μM
MW = 730.7 Da
cLogP = 5.81 ± 0.77

E
K_i = 6 μM
MW = 490.0 Da
cLogP = 6.53 ± 0.61

F
K_i = 1.5 μM
MW = 570.1 Da
cLogP = 4.12 ± 0.91
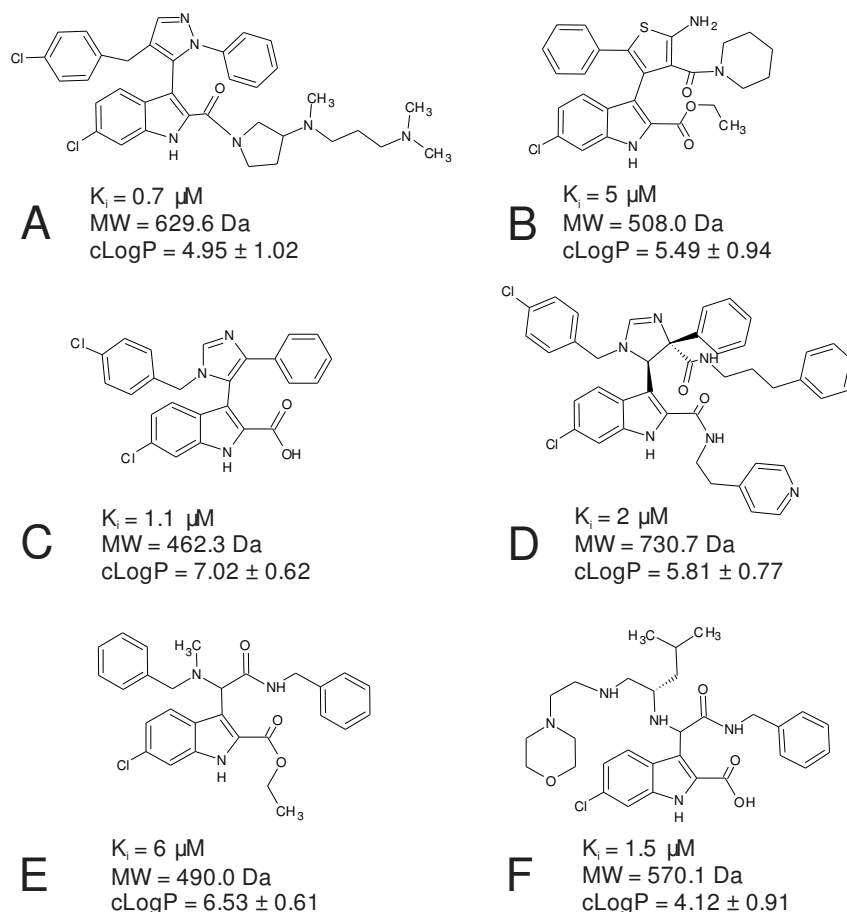
Figure 49 Anchor-based compounds derived from AnchorQuery screen. K_i values were determined by fluorescence polarization assay (Czarna et al., 2009), values of octanol-water partition coefficient (cLogP) were calculated with ACD/ChemSketch software.

5.2.2 First classes of acyclic MDM2-p53 inhibitors

The results of the AnchorQuery screen are highly enriched in representatives of new acyclic scaffolds (shown in Figure 49 E and F, synthetized by reactions depicted in Figure 48 B and C, Figure 51). Characterization of binding of the compounds by AIDA-NMR and ^{1}H-^{15}N-HSQC titrations shows that their affinity to MDM2 is in range of low micromolar (or submicromolar) K_Ds (Figure 50 and Table 4). The compounds are in the slow to intermediate chemical exchange timescales in the binary HSQC titrations.
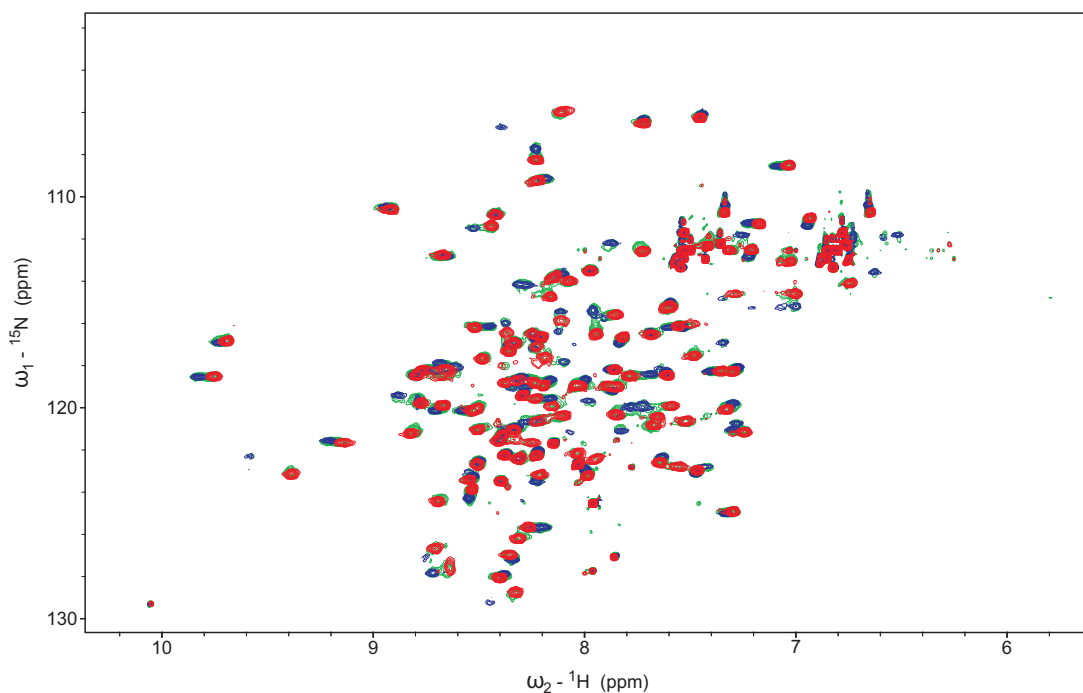
Figure 50 ^{1}H-^{15}N-HSQC titration of ^{15}N-MDM2 (1-125) with increasing amounts of the representative of acyclic scaffold inhibitors - KK271. Reference spectrum (apo-MDM2) is plotted red, intermediate step (MDM2:KK271 in 1:0.5 molar ratio) is plotted green and final step (MDM2:KK271 in 1:2 molar ratio) is plotted blue. Splitting of NMR crosspeaks in the intermediate step is demonstration of "slow" chemical exchange typical for interactions with submicromolar K_Ds.

Table 4 summarizes the results of structure-affinity studies performed on the acyclic MDM2-p53 interaction inhibitors. NMR shows that the compounds belonging to the class shown in Figure 49F do not interact with MDMX.
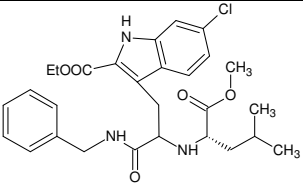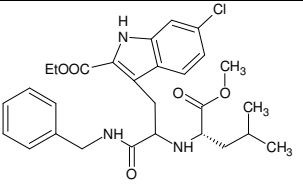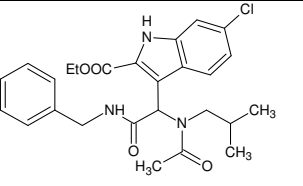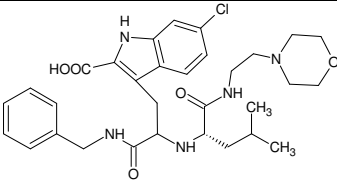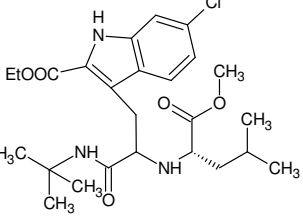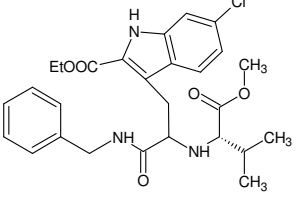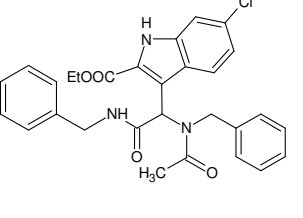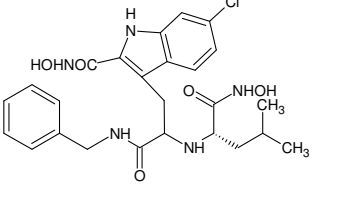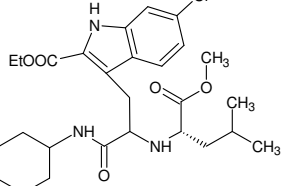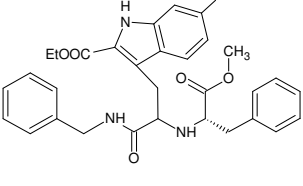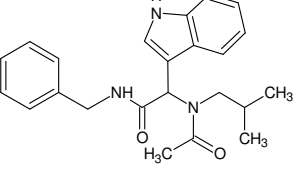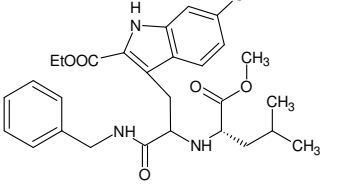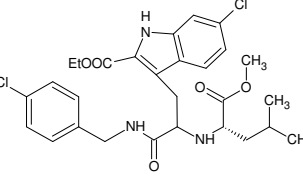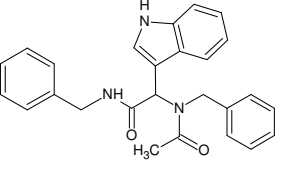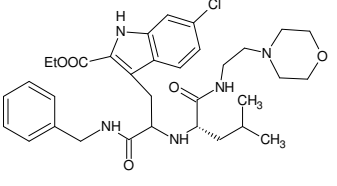
Structure-affinity relationships in acyclic inhibitors of MDM2							
Isocyanide variation	K_i	Amino acid variation	K_i	Anchor variation	K_i	Ester variation (indole and amino acid)	K_i
	(A) 1.4 µM		(E) 1.7 µM		(H) 1.8 µM		(L) 0.4 µM
	(B) >50 µM		(F) 3 µM		(I) 17 µM		(M) 1.2 µM
	(C) >50 µM		(G) >50 µM		(J) 30 µM		(N) 1.4 µM
	(D) >50 µM				(K) >50 µM		(O) 8 µM

Table 4 Structure-activity relationships in acyclic inhibitors of MDM2-p53 interaction. The K_is of the interaction were determined by a 1D SEI-AIDA experiment (Bista et al., 2009).
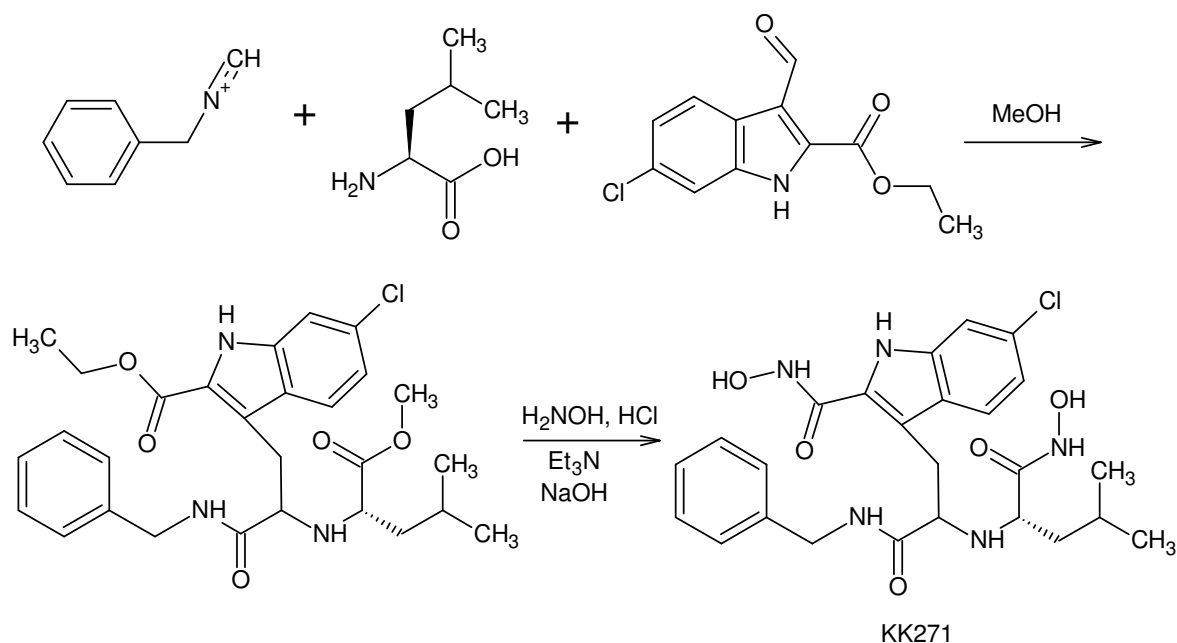
Figure 51 Synthesis of KK271. The first step is Ugi 4C5Cr reaction of 6-chloro-3-formyl-1H-indole-2-carboxylate, L-leucine, bensylisocyanide and methanol. The doubly-esterified intermediate is then derivatized by reaction with hydroxamine hydrochloride to dihydroxamic acid.

5.2.3 Structure of MDM2 in complex with KK271

One of the compounds, named KK271 (see Figure 51) was cocrystallized with the N-terminal domain of MDM2. The KK271-protein complex crystallized in space group P 6_5 2 2 and the crystals diffracted to 2.14 Å. The asymmetric unit contained one protein and two inhibitor molecules. One of the inhibitor molecules mediates important crystal contacts, as shown in Figure 52. This example shows that the choice of the ligand may be often a critical factor in crystallization trials and in fact, before growing MDM2-KK271 crystals, many other members of the same inhibitor family were subject to unsuccessful crystallization trials.

Figure 52 Hydroxame groups of KK271 form important crystal contacts and the inhibitors form in crystal lattice clusters containing 4 KK271 molecules.

The fact that two molecules of the compound interact with one protein molecule is surprising and has not been observed for the MDM2 inhibitors so far, however, more detailed analysis of the interactions pattern and comparison with other cocrystal structures of MDM2-inhibitor complexes shows that only one molecule of the ligand (referred later as Drg1) is binding in the classically targeted MDM2 area and the second molecule (referred as Drg2) explores a new hydrophobic pocket revealed by unusual arrangement of several amino acid side chains.
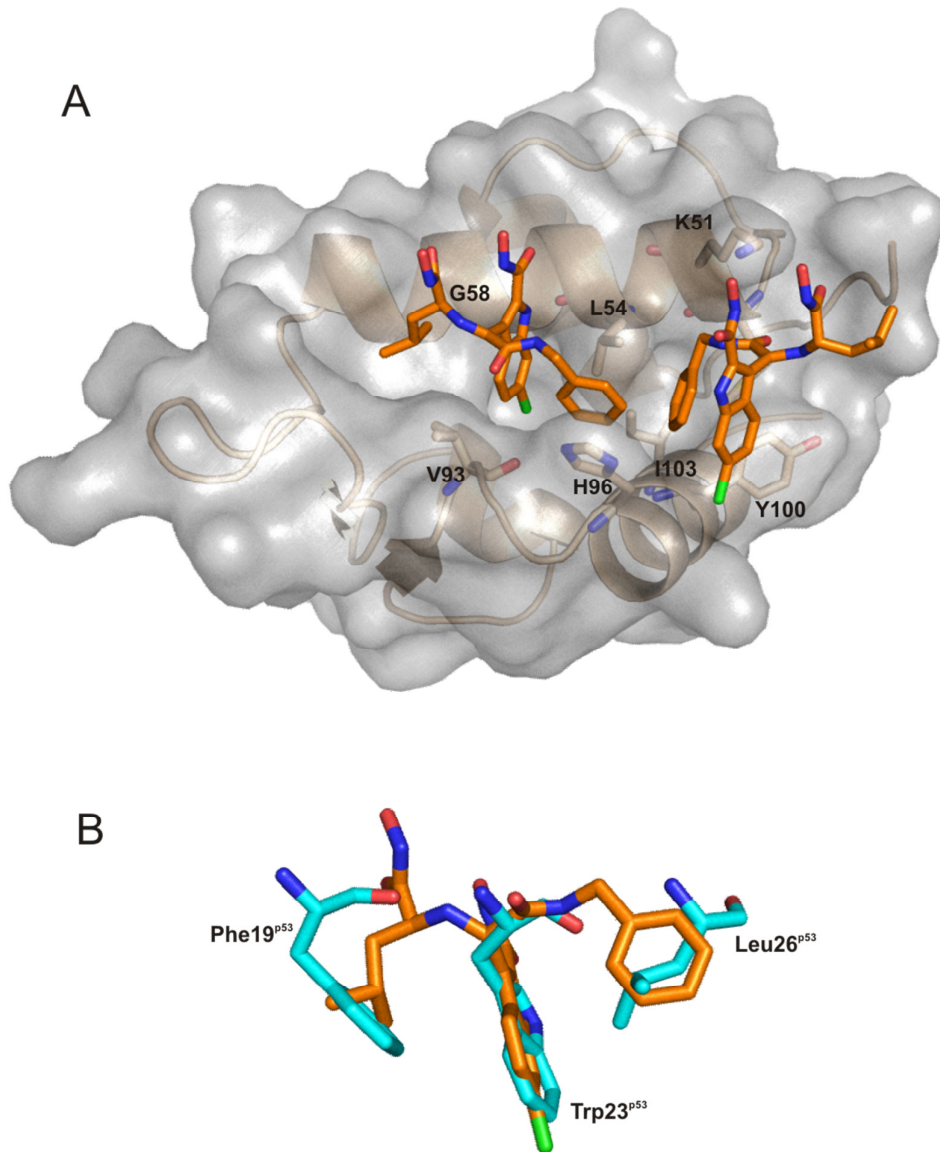
Figure 53 (A) Structure of the KK271-MDM2 complex determined by X-ray crystallography. MDM2 residues involved in recognition of the ligands are labeled. (B) Structural alignment of KK271 with the p53 peptide. Figure was created by aligning the crystallographic structure of the MDM2-KK271 complex with the structure of the N-terminal domains of the MDM2-p53 complex (PDB ID: 1YCR (Kussie et al., 1996)). The p53 residues are labeled. For clarity, the non-interacting part of the p53 helix as well as the second inhibitor molecule were removed.

5.2.4 Structure of the ligand

The structure shows that the compound in its bound form mimics the p53 peptide and the positions of the three p53 side chains critical for recognition overlay with structural elements of KK271; the phenyl ring of the compound replaces 26Leu^{p53}, 6-chloroindole ring overlays well with the 23Trp^{p53} side chain and the leucine part of the compound acts as the 19Phe^{p53} replacement. The alignment of the compound with side chains of the p53 peptide is shown in Figure 53.

A detailed analysis of the iKK271-MDM2 nteractions depicted in Figure 54 shows that the chloroindole ring of the first molecule of the inhibitor fills the tryptophan pocket of MDM2 and is stabilized by hydrophobic interactions and the hydrogen bonding with the Leu54^{MDM2} carbonyl oxygen. The ring has extensive hydrophobic contacts to Leu54^{MDM2} and Gly58^{MDM2} and Val93^{MDM2}. The isobutyl leucine side chain occupies (but does not fill completely) the phenylalanine pocket and keeps weak hydrophobic contacts to Val93^{MDM2} and Gly58^{MDM2}. The phenyl ring of the first KK271 molecule occupies the Leu^{p53} pocket and is engaged in many important contacts: a stacking interaction with aromatic His96^{MDM2} ring (with a distance approximately 3.5 Å, that is typical for π-π interactions (McGaughey et al., 1998)), numerous van der Waals contacts to the side chain of Leu54^{MDM2} and is also in the close proximity of the phenyl ring of another KK271 molecule (the distance between the closest carbon atoms is 3.5 Å).

The scaffold atoms of the first ligand molecule are in an extended conformation and their polar parts are solvent exposed, bind numerous water molecules and are engaged in crystal contacts. This part of the molecule is not in direct contact with the protein surface.

The second molecule of the ligand binds around the space that in the MDM2-p53 complex is occupied by Pro27^{p53}, Glu28^{p53} and Asn29^{p53}. This time only the phenyl ring of the compound is involved in multiple hydrophobic contacts with Leu54^{MDM2}, Tyr100^{MDM2}, Met50^{MDM2} and weak contact to the Ile103^{MDM2} side chain. The remaining part of the inhibitor molecule is solvent exposed and additionally stabilized by two hydroxamic groups forming hydrogen bonds with the Lys51^{MDM2} side chain. Both inhibitor molecules have the same configuration in their asymmetric centers.

The average B-factor for the Drg1 molecule of inhibitor is 23.8 Å^2 and for the Drg2 molecule – 38.4 Å^2.
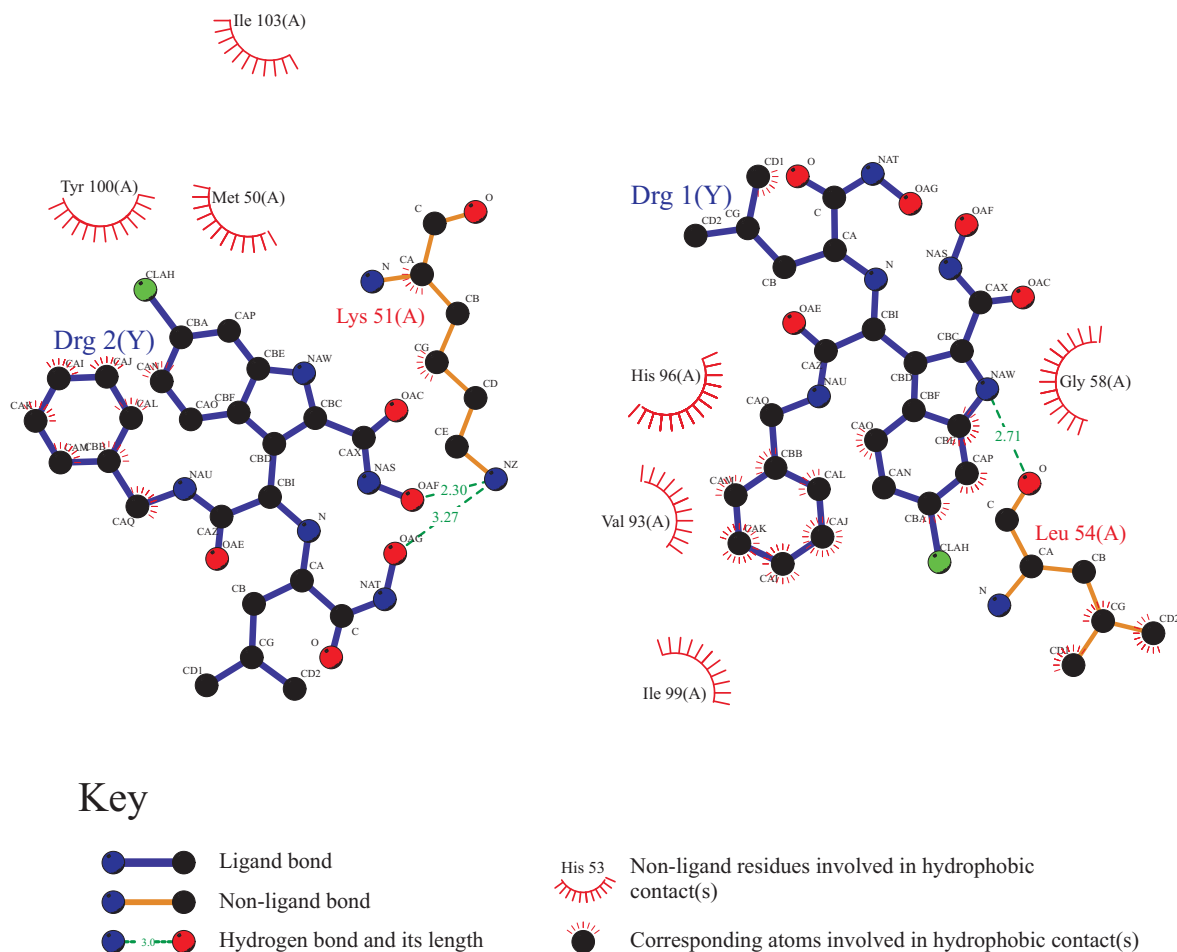
Figure 54 Binding pattern analysis for both KK271 molecules. The figure was produced with program LIGPLOT (Wallace et al., 1995).

5.2.4.1 Structure of the protein

The overall fold of MDM2 in the complex with KK271 is identical to the other known structures of other MDM2-p53 or MDM2-inihibitor complexes. The RMSD of backbone atoms of MDM2 complexed with the p53 peptide (PDB ID: 1YCR (Kussie et al., 1996)) and the MDM2-KK271cocrystal structure is 0.7 Å.

Variations of conformations observed in the already known MDM2 structures and in the new MDM2 coordinates can be divided into two groups: originating from differences in configurations of solvent-exposed amino acid side chains (that take part in formation of the crystal lattice) and the differences being due to the ligand

binding. The latter group is naturally more interesting and will be discussed in more detail.

The arrangement of amino acids in the Phe19^{p53} binding pocket is typical and the same as in majority of the known X-ray structures of MDM2 with its antagonists. Also the unusual stacking interaction of the inhibitor with His96^{MDM2} does not induce large rearrangements of the side chain; the amino acid remains in a position that may be found also in the cocrystal structures with other inhibitors that do not exhibit the stacking interaction.

PDB ID	χ1 Tyr100	χ1 Leu54	Ligand
KK271	-171	-160	Acyclic inhibitor
1rv1	-83	-74	Imidazoline inhibitor (Vassilev et al., 2004)
1t4e	134	-82	Benzodiazepine inhibitor (Grasberger et al., 2005)
1t4f	-89	-76	Optimized p53 peptide (Grasberger et al., 2005)
1ycr	-162	-66	Wild type p53 (Kussie et al., 1996)
2axi	-84	-67	β-hairpin (Fasan et al., 2006)
2gv2	-83	-74	High-affinity peptide (Sakurai et al., 2006)
3eqs	-92	33	High-affinity peptide (Pazgier et al., 2009)
3g03	-85	-75	High-affinity peptide (Czarna et al., 2009)
3iux	-89	-88	Apamin-analogue (Li et al., 2009)
3iwy	-75	-62	D-peptide (Liu et al., 2010)
3jzk	-97	-85	Chromenotriazolopyrimidine (Allen et al., 2009)
3jzr	-100	-177	High-affinity peptide (Phan et al., 2010)
3jzs	-91	-70	High-affinity peptide (Phan et al., 2010)
3lbk	-99	-76	Novartis-101 analogue (Popowicz et al., 2010)
3lbl	-141	-85	MI-63 analogue (Popowicz et al., 2010)
3lnj	-78	-51	D-peptide (Liu et al., 2010)
3lnz	-78	167	High-affinity peptide (Li et al., 2010)

Table 5 χ1 angles values for selected amino-acids in available structures of MDM2 with various ligands bound.

The largest rearrangements are observed at the interface of Trp23^{p53} and the Leu26^{p53} binding pockets and in the part of the N-terminal domain of MDM2 that is occupied by the C-terminal part of the p53 transactivation domain. The latest area has not been explored with small molecules so far and this is the first example showing a non-peptide antagonist bound there. Presence of the second inhibitor molecule induces large conformational rearrangements of the side chains forming this part of the binding pocket: Tyr100^{MDM2} and Leu54^{MDM2}. As Table 5 shows, the χ$_1$ angles of those amino acids have extreme values that are rarely (or at all) found in other structures of MDM2 complexes.

5.3 Discussion

5.3.1 General structure features

The X-ray structure of an acyclic inhibitor KK271 with MDM2 provides important information on structural basis of the p53-MDM2 PPI inhibition by this new class of compounds.

The central part of the inhibitor, the 6-chloroindol ring, fills the tryptophan pocket as it may be expected; all the already known small-molecule inhibitors explore this pocket with the 4-chlorophenyl or 6-chloroindol elements. Surprisingly, the Phe^{p53} pocket is filled by a leucine-like element and the Leu^{p53} pocket is filled by the phenyl ring. Such a 180° flip of the inhibitor has been observed already in the structure of the MI-63 analogue bound to MDM2 (Popowicz et al., 2010) and is evidence of a high functional symmetry of the p53-binding pocket. Furthermore, in all known structures of small molecular inhibitors bound to MDM2, the isoleucine pocket is occupied by phenyl derivatives.

Two molecules of the inhibitor bound to a single protein chain site are an unexpected finding. However, higher B-factors for the second molecule of the inhibitor suggest that the interaction is weaker and analysis of the nhibitor-protein contacts and B-factors shows that the only element of the second KK271 molecule relevant for binding is the phenyl ring and the rest of the molecule is to a large degree flexible. Two hydrogen bonds between hydroxamate groups and the solvent-exposed Lys51^{MDM2} side chain are the only apparent interaction weakly restraining and stabilizing the rest of the inhibitor.

Due to large degree of conformational plasticity of KK271 unusual interactions within the 26Leu^{p53} pocket are promoted. Thanks to the extended structure of the KK271 scaffold, the phenyl ring of KK271 is able to reach further toward helix IV and be involved in stacking interaction with His96^{MDM2}. This unprecedented π-π interaction of the small molecule inhibitor with MDM2 provides yet a new starting point for further diversifying the search for novel classes of inhibitors. Other known antagonists of the MDM2-p53 interaction with cyclic scaffolds have their phenyl-like

elements more constrained and attached closer to the tryptophan binding site and therefore their interaction pattern in this part is different.
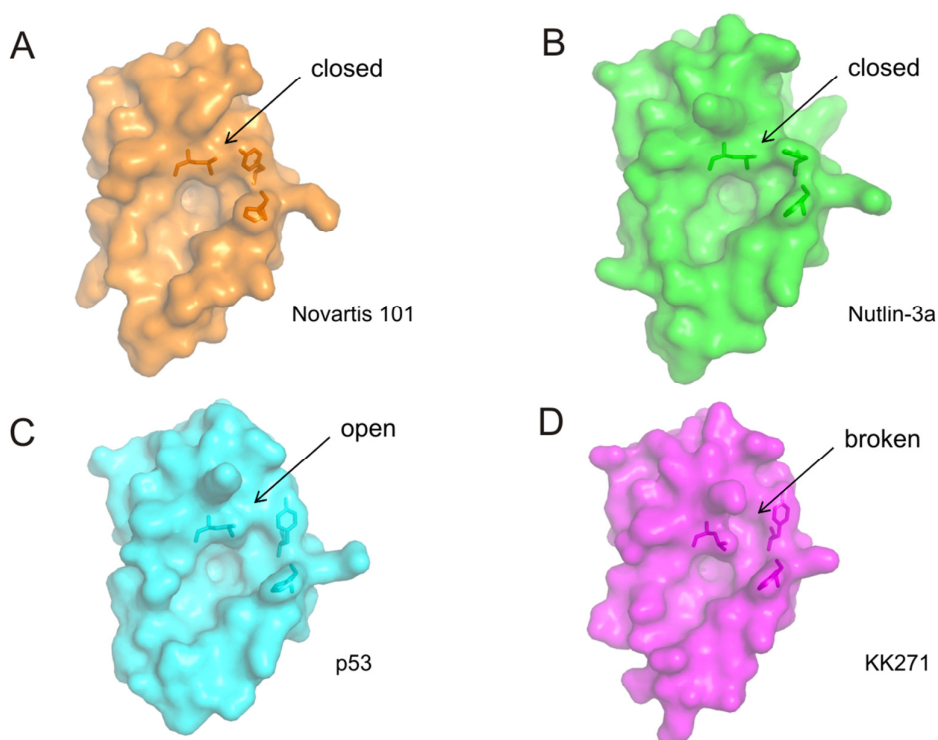
Figure 55 Surfaces of MDM2 in complex with the imidazole-indole inhibitor (vel Novartis-101 analogue) (A; PDB ID: 3LBK), Nutlin-3a (B; PDB ID: 1RV1) (both structures show the "closed" Tyr100-Leu54 gate). p53 (C; PDB ID: 1YCR) (showing the "open" Tyr100-Leu54 gate) and KK271 (C) (with the "broken" Tyr100-Leu54 gate). Amino acids depicted in the Figure are Leu54, His96 and Tyr100.

5.3.2 The Leu54-Tyr100 gate "breaking"

The Leu54^{MDM2zaq12wsx} and Tyr100^{MDM2} side chains are considered to be a gate that can modify the size of the p53 binding pocket by being in either the "closed" (with Tyr100^{MDM2} and Leu54^{MDM2} $\chi1 \approx -80^{O}\pm20^{O}$) or "open" configurations (with Tyr100$^{MDM2} \approx 180^{O}$). The fully "open" configuration has been observed only for the MDM2 structure with the native p53 peptide and all small molecular antagonists have crystallized with the "closed" Leu54^{MDM2}-Tyr100^{MDM2} gate. Surprisingly, binding of KK271 induces very large structural rearrangements; the ring of Tyr100^{MDM2} is in the most "open" conformation ever observed (χ_1 angle $= -171^{O}$), whereas the Leu54 side chain is flipped by 180° when compared to majority of the structures. Due to those uncommon configurations, the shape of the MDM2 surface is slightly different than in

other known structures of the MDM2 complexes; the ligand-binding cleft is longer and expanded more toward the fourth helix, as shown in Figure 55. This unprecedented side chain arrangement defines a third state of the Leu54^{MDM2}-Tyr100^{MDM2} gate referred as "broken". Figure 55 depicts positions of the side chains defining the Leu26^{p53} pocket in various structures.

5.3.3 X-ray structure in context of protein dynamics

The discussed crystal structure is a proof of large conformational plasticity of MDM2. Thanks to high-resolution NMR studies it is becoming recently clear that proteins are dynamic systems and the classical "key and lock" mechanism does not describe well the complex phenomena underlying protein-ligand recognition. The current view is that the ligands stabilize one of preexisting conformations (Henzler-Wildman et al., 2007; Lange et al., 2008). Therefore the structures from Figure 55 may be also considered as "snapshots" taken from the dynamic trajectory of the N-terminal domain of MDM2.

The question whether the MDM2 substate stabilized by KK271 is favorable or unfavorable energetically needs analysis of other known X-ray structures and performing molecular dynamics simulations. As the Table 5 shows, in all the cocrystal structures of high-affinity peptides and small molecule inhibitors with MDM2, the Tyr100^{MDM2}-Leu54^{MDM2} "gate" remains in the "closed" conformation that ensures a "cozier" fit for the ligand (Dastidar et al., 2008; Dastidar et al., 2009). Ensemble of NMR structures of MDM2 shows that also in the unliganded form of the protein, the "closed" state of Tyr100^{MDM2} is predominating, as it minimizes the solvent exposition of the side chain (Uhrinova et al., 2005). Molecular dynamics simulations suggest however that excursions to the "open" state are also possible and may be facilitated by the interaction with a pseudo-substrate "lid" motif (Dastidar et al., 2009; Dastidar et al., 2011), which suggests that the differences in the "open" and "closed" energy levels on the energy landscape of the N-terminal domain of MDM2 are relatively small and the KK271-competent conformation may be also an interesting starting point to search for MDM2-specific inhibitors with a new pharmacophore model.

5.3.4 Structure as a validation of AnchorQuery

Comparison of the X-ray structure with the AnchorQuery-derived model shows good agreement of the predicted and actual binding poses. The largest differences occur within the Leu^{p53} binding pocket; the stacking interaction was not predicted *in sillico*. The program did not also find the second inhibitor molecule. Considering the fact that the pharmacophore search is a ligand-oriented approach and conformational rearrangements of the protein are not considered during the search, the agreement between the predicted and experimentally obtained data is a validation of the pharmacophore model used to find the compound and proves the efficiency and accuracy of the AnchorQuery approach.
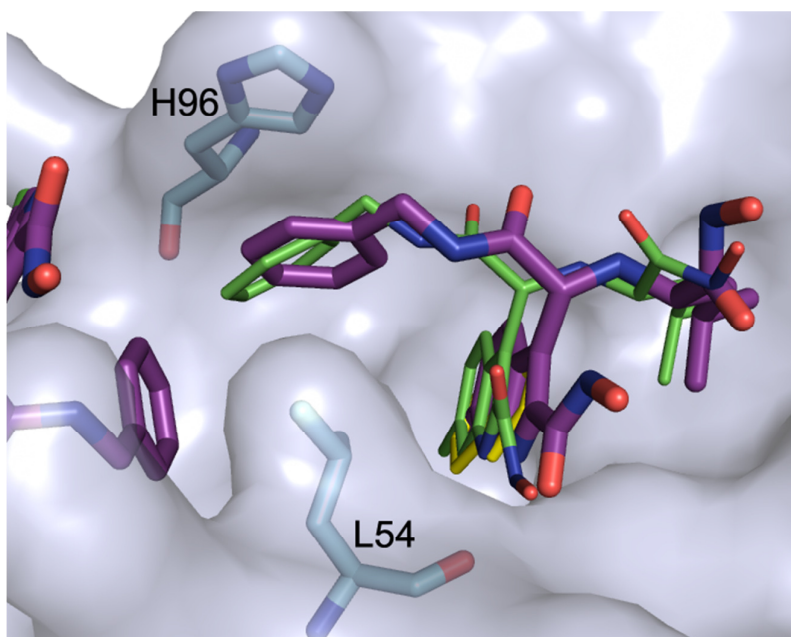
Figure 56 Comparison of an AnchorQuery derived structure (green) with the experimentally determined X-ray structure of KK271 in complex with MDM2 (violet).

5.3.5 Structure-affinity relationships and rational binding optimization

Knowing the high resolution structure of the KK271-MDM2 complex, the structure-activity data for similar compounds may be interpreted more deliberately. The structure-activity studies on a highly similar group of compounds show that the 6-chloroindole ring plays a major role in the affinity; removal of chlorine from the ring impairs the binding significantly (Table 4 H-K). The change in the anchor residue has the most pronounced effect on the binding, because the 6-chloroindol ring is

engaged in the largest number of van der Waals contacts and only large, hydrophobic elements can effectively fill this pocket.

Two other important elements of the interaction that are supposed to fulfill the hydrophobicity pharmacophore constraints are the amino acid and isocyanide components. These elements have also pronounced effect on affinity, are also engaged in numerous van der Waals contacts and their variation is the best way to optimize the binding strength of the compound; however, more variability should be introduced in these places in order to get a detailed picture of the structure-activity relationships in this area. From the data acquired so far, the benzyl isocyanide is preferable over non-aromatic derivatives and p-chlorobenzyl (Table 4 A-D) and small hydrophobic amino acids (Leu or Val) are preferable over bulky phenylalanine (Table 4 E-G). Particularly the leucine fragment of KK271 is engaged in small number of contacts and this element may be optimized; many known high-affinity inhibitors explore the Phe[p53] pocket with larger hydrophobic groups (Vassilev et al., 2004; Popowicz et al., 2010).

The SAR studies show also that esterification of 6-chloro-3H-indole-2-carboxylic acid group weakens the binding (Table 4 L, O). Other carboxyl groups originating from the amino acid element is also easily accessible for modifications and, as shown in Table 4 L, this place may be used to introduce new elements, i.e. modifying solubility and pharmacokinetic properties without affecting the affinity of the compound.

The hydroxamic acid group attached to the 6-chloroindol ring points toward the solvent and for the first inhibitor molecule is not engaged in any interactions with the protein. However, the second inhibitor is hydrogen bonded through the indole-hydroxame group and esterification of it impairs this interaction, thus leaving the second pocket unfilled and increasing the inhibitory concentration of the compound. The other hydroxamic group coming from the amino-acid part is also solvent-exposed may be modified without effect on affinity.

KK271 violates the Lipinski's rule of five (Lipinski et al., 2001) having too many hydrogen bond donors (7) due to presence of hydroxamic acid groups. Carboxylic acid analogues of KK271 would fulfill the Lipinski's rules better and would be more bioavailable.

5.3.5.1   Fragment-based optimization

The presence of the Drg2 molecule is an important information on how to optimize the isocyanide element. As the interaction pattern shown in Figure 54 and crystallographic B-factors suggest, the second ligand molecule may be reduced to the phenyl fragment and the structure suggest that by means of the traditional fragment-based drug development (Shuker et al., 1996; Ciulli et al., 2006), a more potent inhibitor should be obtained by connecting the two phenyl rings of the molecules with approximately 2 atoms-long covalent linker (the intermolecular distance between the closest carbons from the aromatic rings is 3.5 Å, whereas the length of the N-butyl group is approximately 3.9 Å). By covalently joining two fragments occupying independently adjacent binding sites, the entropic cost of binding is reduced and therefore the affinity of the binding is expected to increase significantly (Shuker et al., 1996).

5.3.6 MDM2-selectivity of KK271

Surprisingly, the compounds similar to KK271 do not interact (or interact very weakly) with MDMX. Majority of other known inhibitors (i.e. Nutlin-3, imidazo-indole or spiro-oxindole scaffolds) were shown to interact about 10-100 fold weaker with MDMX, giving K_Ds in ranges of tens of µM (Popowicz et al., 2007; Popowicz et al., 2010). This fact may be explained by replacement of His96^{MDM2} by Pro in MDMX.

5.4 Materials and methods

5.4.1 Protein production, purification and crystallization

Human MDM2 (residues 18-111) was cloned into the pET26 vector and expressed in the *Escherichia coli* BL21(DE3) Rosetta strain (Invitrogen). Cells were grown at 37°C and induced with 1 mM IPTG at an OD_{600nm} of 0.8 and grown for additional 4 h at 37°C. The recombinant protein expressed into inclusion bodies. The inclusion bodies were isolated by centrifugation of the bacterial lysate and washed with PBS containing 0.05% Triton-X100 and subsequently solubilized in 6 M GuHCl in 100 mM tris-HCl, pH 8.0, including 1 mM EDTA and 10 mM β-mercaptoethanol. The protein was then dialyzed against 4 M GuHCl, pH 3.5, 10 mM β-mercaptoethanol. For renaturation, the protein was diluted (1:100) into 10 mM Tris-HCl, pH 7.0, containing 1 mM EDTA and 10 mM β-mercaptoethanol, by adding the protein in several pulses into the refolding buffer. Refolding was performed overnight at 4°C. Following, ammonium sulphate was added to the final concentration of 1.5 M and after 3 h the sample was mixed with 10 ml of the butyl sepharose 4 Fast Flow (Pharmacia, FRG). The protein was eluted with 100 mM Tris-HCl, pH 7.2, containing 5 mM β-mercaptoethanol, and further purified on the HiLoad 16/60 Superdex200 gel filtration (Pharmacia) into buffer containing 5 mM Tris/HCl pH = 8.0, 50 mM NaCl, 10 mM β-mercaptoethanol. After addition of the molar excess of the small molecule inhibitor, KK271, the protein complex was concentrated to about 20 mg/ml and subjected to the crystallization screening with the sitting drop vapor diffusion method. The crystals of the MDM2-KK271 complex appeared after several days at 4°C in 0.2 M ammonium nitrate, 20% (w/v) PEG 3350 forming hexagonal bipyramides. All crystals were plunged frozen with 30% glycerol added to the mother liquor.

5.4.2 Diffraction data collection and structure solution

The dataset was collected on the SLS beamline PXII at Paul Scherrer Institut, Villingen, Switzerland. The collected data was indexed, integrated, scaled and merged with XDS and XSCALE (Kabsch 1993).The MDM2-KK271 crystal belonged to $P6_522$ space group and diffracted to 2.15 Å. One complex containing one protein molecule and two inhibitor molecules was present in the asymmetric unit. Phase

problem was solved by molecular replacement using the Molrep program from the CCP4 suite (Vagin et al., 1997). MDM2 molecule from MDM2-Nutlin cocrystal structure (1RV1; (Vassilev et al., 2004)) was used as a search model. The model was then subsequently improved by Arp/Warp (Lamzin et al., 1993) and manually rebuild by iterative electron density fitting in MIFit program (http://code.google.com/p/mifit/) and refinement with Refmac5 (Murshudov et al., 1997). Ligand molecule and Refmac5 dictionary restraints were created using the dictionary module in MIFit. Water molecules were added by Arp/Warp solvent module. The electron densities for residues 18-24 and 109-111 were missing and thus, those residues were not included in the model. Additionally, several side-chains' atoms without clear electron density were omitted in the model. Data collection and refinement statistics are summarized in Table 6.

Space group	P 6_5 2 2
Cell constant:	
a	53.520
b	53.520
c	122.270
Resolution range (Å)	46.350 - 2.14
Observed reflections	63031
Unique reflections	11501
Whole resolution range:	
Completeness (%)	97.6%
Rmerge	2.6%
I/σ (I)	32.03
Last resolution shell:	
Resolution range (Å)	2.24-2.14
Completeness (%)	84.2%
Rmerge	10.0%
I/σ (I)	9.83
Refinement:	
No. of reflections	10366
Resolution (Å)	18.467-2.140
R factor (%)	20.42
R_{free} (%)	22.79
Average B (Å^2)	28.691
rms bond length (Å)	0.0098
rms angles (°)	1.317
Content of asymmetric unit:	
No. of complexes	1
No. of protein residues/atoms	84/794
No. of solvent atoms	37

Table 6 Data collection and refinement statistics.

6. Summary

The work presented in this thesis was carried out in the NMR spectroscopy group at the Max Planck Institute of Biochemistry in Martinsried, Germany, from September 2007 to July 2011. The research described herein is part of a collaborative project on the development of new anti-cancer therapies. Specifically, the main research objective was the experimental investigation of protein-small molecule interactions by means of biophysical techniques: the solution-state NMR spectrometry and X-ray crystallography - to find antagonists of the MDM2-p53 and MDMX-p53 interactions.

The p53 protein is the most important tumour suppressor that is mutated in 50% of all human cancers. In the remaining 50% of the tumours, p53 retains its wild-type sequence, but is deregulated, mostly by the interaction with its main negative regulators: MDM2 and MDMX. A low-molecular-weight antagonist capable to disrupt the p53-MDM2/X interaction would activate p53 and inhibit or reverse tumour formation.

A combination of traditional protein-oriented NMR screening techniques - like the ^{1}H-^{15}N-HSQC binary titrations - with a set of newly developed techniques of the longitudinal-relaxation optimized NMR assays for the tryptophan-containing proteins were employed to detect and characterize the binding of hundreds of compounds belonging to more than ten new classes of antagonists of the MDM2-p53 and MDMX-p53 interactions. The new inhibitors discovered with the help of NMR spectroscopy were obtained by multicomponent reactions and turned out to have affinities to MDM2 ranging from submicromolar to tens of micromoles. The compounds belong to chemically diverse classes. Additionally, the recently discovered compounds claimed to be the first MDMX-p53 inhibitors were found to act through covalent modification of cysteine residues of MDMX.

The screening method that we have developed is named SEI AIDA-NMR (SEI, for Selective Excitation-Inversion, and AIDA for the Antagonist Induced Dissociation Assay) and is based on ^{1}H 1D NMR spectroscopy. This competition

NMR assay provides information on potency of a compound to disrupt a protein-protein interaction and allows the determination of K_i from one-step titration. By selectively exciting only the proton NMR signals of the $^NH^\square$ indole side chain of tryptophans, the acquisition time of the SEI AIDA-NMR experiment is reduced by an order of magnitude relative to the traditional 1D NMR pulse sequences employing hard pulses and water suppression schemes.

During the progress of my work on the MDM2/X-p53 antagonists, the AnchorQuery platform has been developed. This new web-based technology integrates the pharmacophore search with the multicomponent reaction chemistry and was introduced to help in discovery of antagonists of protein-protein interactions. NMR and X-ray crystallography were used to experimentally validate the results of the drug discovery with the AnchorQuery and the X-ray structure of MDM2 bound to one of the new inhibitors was determined. The inhibitor belongs to a new class of the MDM2-p53 interaction antagonists with an acyclic scaffold. The structure shows that the AnchorQuery is an effective tool of searching for new protein-protein interaction antagonists and is able to accurately predict the binding poses of small molecules. Additionally, the X-ray structure revealed that the interaction with the inhibitor induces unusually large conformational rearrangements in MDM2, creating a new druggable pocket nearby the area traditionally targeted with small molecules. The structure provided not only important insights on how to optimize the acyclic antagonists of the MDM2-p53 interaction, but also suggested new possibilities in designing the inhibitors of the MDM2-p53 interaction.

7. Zusammenfassung

Die hier vorgelegte Doktorarbeit wurde in der NMR-Spektroskopie Gruppe des Max-Planck-Instituts für Biochemie im Zeitraum vom September 2007 bis Juli 2011 durchgeführt. Die Forschung ist Teil eins kollaborativen Projekts für die Entwicklung neuer Anti-Krebstherapien. Insbesondere galt das Hauptforschungsziel der experimentellen Forschung an der Wechselwirkung von Proteinen mit niedermolekularen organischen Molekülen mittels biophysikalischer Techniken wie der NMR-Spektroskopie in Lösung und der Röntgenstrukturanalse. Das Ziel war es, Antagonisten der MDM2-p53 und der MDMX-p53 Interaktion zu finden.

p53 ist der wichtigste Tumorsupressor und ist in 50% aller menschlicher Tumore mutiert. Die übrigen 50% von Tumoren besitzen zwar noch die p53 Wildtyp Sequenz, jedoch ist dieses herunter- oder dereguliert, meistens durch die Interaktion mit dessen negativen Regulatoren – MDM2 und MDMX. Ein niedermolekularer Antagonist der in der Lage ist, die p53-MDM2/X Interaktion aufzuheben, würde p53 aktivieren und somit die Tumorentwicklung hemmen und/oder umkehren.

Eine Kombination aus traditionellen Protein basierter NMR Screening Verfahren, wie ^{1}H-^{15}N-HSQC Titrationen, und einer Reihe neu entwickelter Techniken der longitudinalen relaxationsoptimierten NMR Experimente für Tryptophan enthaltende Proteine wurde verwendet, um die Bindung von hunderten von Verbindungen aus mehr als zehn neuen Klassen an MDM2-p53 und MDMX-p53 Antagonisten zu entdecken und zu untersuchen.   Die neuen mittels NMR-Spektroskopie entdeckten Inhibitoren wurden durch Multikomponenten Reaktionen synthetisiert und binden mit Dissoziationskonstanten im Bereich von 10-0.1 µM an MDM2. Die Verbindungen gehören zu chemisch verschiedenen Klassen.

Das von uns entwickelte Screening Verfahren, SEI AIDA (SEI steht für *selective excitation-inversion*) basiert auf ^{1}H 1D NMR Spektroskopie. Das Kompetitions NMR-Verfahren gibt Informationen über die Stärke der Interaktion mit der eine Verbindung eine Protein-Protein Interaktion inhibiert und ermöglicht somit die Ermittlung des K_i durch eine einmalige Titration. Durch eine selektive Anregung

des H^N Indolproton NMR Signals der Tryptophanseitenkette wird die Acquisitionszeit bei der SEI AIDA um eine Größenordung relativ tu einer traditionellen 1D NMR Pulssequenz verkürzt, unter Verwendung von harten Pulsen und Wasserunterdrückungsmethoden.

Während der Untersuchungen mit dem MDM2/X-p53 Antagonisten wurde die AnchorQuery Plattform entwickelt. Diese neue Web-basierte Technologie integriert die Pharmakophor Suche mit der Multikomponenten Reaktions Chemie und wurde für die Entdeckung von Protein-Protein Interaktion Antagonisten eingeführt. NMR und Röntgen-Kristallographie wurden zur experimentellen Validierung der Ergebnisse angewandt. Die Kristallstruktur von einem MDM2-Inhibitor Komplex wurde gefunden. Der Inhibitor gehört zu einer neuen Gruppe an MDM2-p53 Antagonisten mit einer azyklischen Verbindung. Die Stuktur ist der Beweis dafür, dass AnchorQuery ein effektives Werkzeug zur Suche von neuen Protein-Protein Interaktionsantagonisten ist und fähig ist, die Bindungsweise von kleinen Molekülen präzise vorherzusagen. Zusätzlich zeigt die Kristallstruktur, dass die Interaktion mit dem Inhibitor große strukturelleelle Veränderungen in MDM2 induziert, wodurch eine neue Bindungsstelle in der Nähe der bisher durch Inhibitoren benutzten Bindungstelle entsteht. Die Struktur liefert nicht nur wichtige Einblicke, wie man azyclische Antagonisten der MDM2-p53 Interaktion optimieren kann, sondern weist auch auf neue Möglichkeiten in der Entwicklung von MDM2-p53 Inhibitoren hin.

8.   Appendix

8.1 Protein sequences

8.1.1 Human p53

Uniprot accession number: P04637

```
        10         20         30         40         50         60
MEEPQSDPSV EPPLSQETFS DLWKLLPENN VLSPLPSQAM DDLMLSPDDI EQWFTEDPGP

        70         80         90        100        110        120
DEAPRMPEAA PPVAPAPAAP TPAAPAPAPS WPLSSSVPSQ KTYQGSYGFR LGFLHSGTAK

       130        140        150        160        170        180
SVTCTYSPAL NKMFCQLAKT CPVQLWVDST PPPGTRVRAM AIYKQSQHMT EVVRRCPHHE

       190        200        210        220        230        240
RCSDSDGLAP PQHLIRVEGN LRVEYLDDRN TFRHSVVVPY EPPEVGSDCT TIHYNYMCNS

       250        260        270        280        290        300
SCMGGMNRRP ILTIITLEDS SGNLLGRNSF EVRVCACPGR DRRTEEENLR KKGEPHHELP

       310        320        330        340        350        360
PGSTKRALPN NTSSSPQPKK KPLDGEYFTL QIRGRERFEM FRELNEALEL KDAQAGKEPG

       370        380        390
GSRAHSSHLK SKKGQSTSRH KKLMFKTEGP DSD
```

8.1.2 Human MDM2

Uniprot accession number: Q00987

```
        10         20         30         40         50         60
MCNTNMSVPT DGAVTTSQIP ASEQETLVRP KPLLLKLLKS VGAQKDTYTM KEVLFYLGQY

        70         80         90        100        110        120
IMTKRLYDEK QQHIVYCSND LLGDLFGVPS FSVKEHRKIY TMIYRNLVVV NQQESSDSGT

       130        140        150        160        170        180
SVSENRCHLE GGSDQKDLVQ ELQEEKPSSS HLVSRPSTSS RRRAISETEE NSDELSGERQ

       190        200        210        220        230        240
RKRHKSDSIS LSFDESLALC VIREICCERS SSSESTGTPS NPDLDAGVSE HSGDWLDQDS

       250        260        270        280        290        300
```

```
VSDQFSVEFE VESLDSEDYS LSEEGQELSD EDDEVYQVTV YQAGESDTDS FEEDPEISLA

        310        320        330        340        350        360
DYWKCTSCNE MNPPLPSHCN RCWALRENWL PEDKGKDKGE ISEKAKLENS TQAEEGFDVP

        370        380        390        400        410        420
DCKKTIVNDS RESCVEENDD KITQASQSQE SEDYSQPSTS SSIIYSSQED VKEFEREETQ

        430        440        450        460        470        480
DKEESVESSL PLNAIEPCVI CQGRPKNGCI VHGKTGHLMA CFTCAKKLKK RNKPCPVCRQ

        490
PIQMIVLTYF P
```

8.1.3 Human MDMX

Uniprot accession number: O15151

```
         10         20         30         40         50         60
MTSFSTSAQC STSDSACRIS PGQINQVRPK LPLLKILHAA GAQGEMFTVK EVMHYLGQYI

         70         80         90        100        110        120
MVKQLYDQQE QHMVYCGGDL LGELLGRQSF SVKDPSPLYD MLRKNLVTLA TATTDAAQTL

        130        140        150        160        170        180
ALAQDHSMDI PSQDQLKQSA EESSTSRKRT TEDDIPTLPT SEHKCIHSRE DEDLIENLAQ

        190        200        210        220        230        240
DETSRLDLGF EEWDVAGLPW WFLGNLRSNY TPRSNGSTDL QTNQDVGTAI VSDTTDDLWF

        250        260        270        280        290        300
LNESVSEQLG VGIKVEAADT EQTSEEVGKV SDKKVIEVGK NDDLEDSKSL SDDTDVEVTS

        310        320        330        340        350        360
EDEWQCTECK KFNSPSKRYC FRCWALRKDW YSDCSKLTHS LSTSDITAIP EKENEGNDVP

        370        380        390        400        410        420
DCRRTISAPV VRPKDAYIKK ENSKLFDPCN SVEFLDLAHS SESQETISSM GEQLDNLSEQ

        430        440        450        460        470        480
RTDTENMEDC QNLLKPCSLC EKRPRDGNII HGRTGHLVTC FHCARRLKKA GASCPICKKE

        490
IQLVIKVFIA
```

8.2 Sequential alignment of MDM2 and MDMX

Global alignment of the human MDM4 and MDM2 proteins. The "Lid" sequence of MDM2 is marked in blue, the N-terminal p53-binding domains are marked green, the zinc binding domains – violet, the RING domains – red. The alignment was produced using the neddle tool from the EMBOSS suite (Rice et al., 2000) using the matrix EBLOSUM62, gap penalty 10 and gap extension penalty 0.5. 31.3% of positions are identical and 50.1% are similar.

```
MDM2     1 --------MCNTNMSVPTDGAVTTSQIPASEQETIVRPKPLLLKLLKSVG
             .|:|       :|.|...|  |.  |...||||..|||:|.:.|
MDMX     1 MTSFSTSAQCST-----SDSACRIS--PG--QINCVRPKLPLLKILHAAG

MDM2    43 AQKDTYTMKEVLFYLGQYIMTKRLYDEKQQHIVYCSNDLLGDLFGVPSFS
           ||.:.:|:|||:.|||||||.|:|||::||:|||..||||:|.|..|||
MDMX    42 AQGEMFTVKEVMHYLGQYIMVKQLYDQQEQHMVYCGGDLLGELLGRQSFS

MDM2    93 VKEHRKIYTMIYRNLVVVNQQESSDSGTSVSENRCHLEGGSDQKDLVQEL
           ||:...:|.|:.:|||.:  ...:||:..::+...|......|.|.|..
MDMX    92 VKDPSPLYDMLRKNLVTI-ATATTDAAQTLALAQDHSMDIPSQDQLKQSA

MDM2   143 QEEKPSSSHLVSRPSTSSRRRAISETEENSDELSGERQR---KRHKSDSI
           :|                |::||:|.  ||::...|.....:   .|...|.|
MDMX   141 EE------------SSTSRKRT---TEDDIPTLPTSEHKCIHSREDEDLI

MDM2   190 -SLSFDESLALCV----------------IREICCERSSSSESTGTPSN
           :|:.||:..|.:                :|.....||:.  ||...:|
MDMX   176 ENLAQDETSRLDLGFEEWDVAGLPWWFLGNLRSNYTPRSNG--STDLQTN

MDM2   222 PDLDAGVSEHSGD--WLDQDSVSDQFSVEFEVESLDSEDYSLSEEGQELS
           .|:...:...:.|  |...:|||:|..|..:||:.|:|  ..|||..:|
MDMX   224 QDVGTAIVSDTTDDLWFLNESVSEQLGVGIKVEAADTE--QTSEEVGKVS

MDM2   270 DEDDEVYQVTVYQAGESD------TDSFEEDPEISLADYWKCTSCNEMNP
           |:       .|.:.|::|      :.|.:.|.|::..|.|:||.|.::.|.
MDMX   272 DK-------KVIEVGKNDDLEDSKSLSDDTDVEVTSEDEWQCTECKKFNS

MDM2   314 PLPSHCNRCWALRENWLPEDKGKDKGEISEKAKLENS----------TQA
           |...:|.||||||||::|           .|:.:||.:|           .:.
MDMX   315 PSKRYCFRCWALRKDW----------YSDCSKLTHSLSTSDITAIPEKE

MDM2   354 EEGFDVPDCKKTI---VNDSRESCVEENDDKITQASQSQESEDYSQPSTS
           .||.|||||::||  |...:::.:::.:.|:.....|.|..|.:..|.|
MDMX   354 NEGNDVPDCRRTISAPVVRPKDAYIKKENSKLFDPCNSVEFLDLAHSSES

MDM2   401 SSIIYSSQEDVKEF--EREETQDKEESVESSLELNAIEPCVICQGRPKNG
           ...|.|..|.:...  :|.:|::.|:.  .|.::||.:|:.||::|
MDMX   404 QETISSMGEQLDNLSEQRTDTENMEDC------QNLLKPCSLCEKRPRDG

MDM2   449 CIVHGKTGHLMACFTCAKKLKKRNKPCPVCRQPIQMIVLTYFP
           .|:||:||||:.||.||::|||....||:|::.||:::.:..
MDMX   448 NIIHGRTGHLVTCFHCARRLKKAGASCPICKKEIQLVIKVFIA
```

8.3 Competitive binding of two different ligands to a protein

molecule

The solution given by Wang (Wang, 1995) rewritten using symbols used in the dissertation (see section 2.1.1) is:

$$[P] = -\frac{a}{3} + \frac{2}{3}\sqrt{a^2 - 3b} \cos\left(\frac{\theta}{3}\right)$$

$$[PI] = \frac{I_T\left(2\sqrt{a^2 - 3b}\cos\left(\frac{\theta}{3}\right) - a\right)}{\left(3K_i + 2\sqrt{a^2 - 3b}\cos\left(\frac{\theta}{3}\right) - a\right)}$$

$$[PL] = \frac{P_T\left(2\sqrt{a^2 - 3b}\cos\left(\frac{\theta}{3}\right) - a\right)}{\left(3K_D + 2\sqrt{a^2 - 3b}\cos\left(\frac{\theta}{3}\right) - a\right)}$$

$$a = K_D + K_i + I_T + L_T - P_T$$

$$b = K_D(I_T - P_T) + K_i(L_T - P_T) + K_iK_D$$

$$c = -K_DK_iP_T$$

$$\theta = \cos^{-1}\left(\frac{-2a^3 + 9ab - 27c}{2\sqrt{(a^2 - 3b)^3}}\right)$$

8.4 Ernst angle and relaxation in a multiple scan NMR experiment

Derivation after (Schanda 2009).
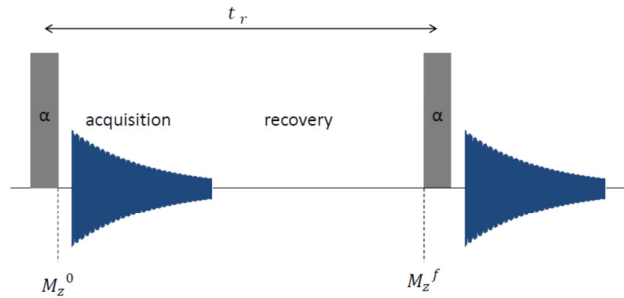
Figure 57 Scheme of a multiple scan NMR experiment

A simple NMR experiment shown in Figure 57 consists of pulses of a flip angle α and negligible duration and acquisition and recovery periods denoted as . The Bloch equation for this example would be:

When we note that:

And we see that:

The signal detected in the NMR experiment (S) is proportional to the transverse magnetization, so:

And the signal to noise ratio is proportional to square root from number of scans *n*:

Combining all the dependencies we obtain:

8.5 Solomon equations for selective excitation

Assume a simple spin system consisting of two cross-relaxing hydrogen spins denoted as I and S with auto-relaxation rates $\rho_I = \rho_S = \rho$ and cross-relaxation rates $\sigma_{IS} = \sigma_{SI} = \sigma$.

The general Solomon equation for this system would be:

$$\frac{d}{dt}\begin{bmatrix} I_z^0 - I_{z\,eq} \\ S_z^0 - S_{z\,eq} \end{bmatrix} = -\begin{bmatrix} \rho & \sigma \\ \sigma & \rho \end{bmatrix}\begin{bmatrix} I_z - I_{z\,eq} \\ S_z - S_{z\,eq} \end{bmatrix}$$

$$\frac{d\left(I_z^0 - I_{z\,eq}\right)}{dt} = -\rho\left(I_z - I_{z\,eq}\right) - \sigma\left(S_z - S_{z\,eq}\right)$$

$$\frac{d\left(S_z^0 - S_{z\,eq}\right)}{dt} = -\rho\left(S_z - S_{z\,eq}\right) - \sigma\left(I_z - I_{z\,eq}\right)$$

And if we consider the sum and difference of magnetizations:

$$\frac{d\left(I_z^0 - I_{z\,eq} + S_z^0 - S_{z\,eq}\right)}{dt}$$

$$= -\rho\left(I_z - I_{z\,eq}\right) - \sigma\left(S_z - S_{z\,eq}\right) - \rho\left(S_z - S_{z\,eq}\right) - \sigma\left(I_z - I_{z\,eq}\right)$$

$$= -(\rho + \sigma)\left(I_z - I_{z\,eq} + S_z - S_{z\,eq}\right)$$

$$\frac{d\left(I_z - I_{z\,eq} - S_z + S_{z\,eq}\right)}{dt}$$

$$= -\rho\left(I_z - I_{z\,eq}\right) - \sigma\left(S_z - S_{z\,eq}\right) + \rho\left(S_z - S_{z\,eq}\right) + \sigma\left(I_z - I_{z\,eq}\right)$$

$$= -(\rho - \sigma)\left(I_z - I_{z\,eq} - S_z + S_{z\,eq}\right)$$

In the case of selective excitation of spin S, the initial conditions are:

$$I_z = I_{z\,eq}$$

$$S_z = 0$$

And the equations become:

$$\frac{d\left(I_z - I_{z\,eq} + S_z - S_{z\,eq}\right)}{dt} = -(\rho + \sigma) \cdot -S_{z\,eq}$$

$$\frac{d\left(I_z - I_{z\,eq} - S_z + S_{z\,eq}\right)}{dt} = -(\rho - \sigma) \cdot S_{z\,eq}$$

And after solving them, we obtain:

$$I_z(t) - I_{z\,eq} + S_z(t) - S_{z\,eq} = -S_{z\,eq} \cdot e^{-(\rho+\sigma)\cdot t}$$

$$I_z(t) - I_{z\,eq} - S_z(t) + S_{z\,eq} = S_{z\,eq} \cdot e^{-(\rho-\sigma)\cdot t}$$

Addition of the equations above gives:

$$2I_z(t) - 2I_{z\,eq} = S_{z\,eq} \cdot \left(e^{-(\rho-\sigma)\cdot t} - e^{-(\rho+\sigma)\cdot t}\right)$$

Whereas their subtraction gives:

$$2S_z(t) - 2S_{z\,eq} = -S_{z\,eq} \cdot \left(e^{-(\rho-\sigma)\cdot t} + e^{-(\rho+\sigma)\cdot t}\right)$$

Ordering the sides we obtain equations describing the longitudinal magnetization as function of time:

$$I_z(t) = I_{z\,eq} + \frac{1}{2}S_{z\,eq} \cdot \left(e^{-(\rho-\sigma)\cdot t} - e^{-(\rho+\sigma)\cdot t}\right)$$

$$S_z(t) = S_{z\,eq} - \frac{1}{2}S_{z\,eq} \cdot \left(e^{-(\rho-\sigma)\cdot t} + e^{-(\rho+\sigma)\cdot t}\right)$$

8.6 Calculation of auto-relaxation and cross-relaxation rates

The calculation is based on Chapter 5 of (Cavanagh 2007).

The cross-relaxation and auto-relaxation rates expressed in terms of spectral density are:

$$\rho = d^2 \cdot \left(J(0) + 3J(\omega) + 6J(2\omega) \right)$$

$$\sigma = \frac{1}{10} \cdot d^2 \cdot \left(6J(2\omega) - J(0) \right)$$

$$d = \frac{\mu_0 \cdot \hbar \cdot \gamma^2}{4\pi \cdot r^3}$$

Where μ_0 is the magnetic permeability of free space, γ - the gyromagnetic ratio of the proton, r – intranuclear distance.

Assuming isotropic molecular tumbling with correlation time τ_c, the spectral density function may be expressed as:

$$J(\omega) = \frac{2}{5} \frac{\tau_c}{1 + \omega^2 \tau_c^2}$$

9. Index of Equations, Figures and Tables

10. Bibliography

Allen, J. G., M. P. Bourbeau, G. E. Wohlhieter, M. D. Bartberger, K. Michelsen, R. Hungate, R. C. Gadwood, R. D. Gaston, B. Evans, L. W. Mann, M. E. Matison, S. Schneider, X. Huang, D. Yu, P. S. Andrews, A. Reichelt, A. M. Long, P. Yakowec, E. Y. Yang, T. A. Lee and J. D. Oliner (2009). "Discovery and optimization of chromenotriazolopyrimidines as potent inhibitors of the mouse double minute 2-tumor protein 53 protein-protein interaction." Journal of Medicinal Chemistry **52**(22): 7044-7053.

Argentini, M., N. Barboule and B. Wasylyk (2001). "The contribution of the acidic domain of MDM2 to p53 and MDM2 stability." Oncogene **20**(11): 1267-1275.

Aso, M., Y. Yui and M. Kakishita (1988). "Effects of Thermal-Denaturation on the Longitudinal Relaxation-Time (T1) of Water Protons in Protein Solutions - Study of the Factors Determining the T1 of Water Protons." Magnetic Resonance Imaging **6**(1): 17-25.

Ayed, A., F. A. Mulder, G. S. Yi, Y. Lu, L. E. Kay and C. H. Arrowsmith (2001). "Latent and active p53 are identical in conformation." Nat Struct Biol **8**(9): 756-760.

Azmi, A. S., P. A. Philip, F. W. Beck, Z. Wang, S. Banerjee, S. Wang, D. Yang, F. H. Sarkar and R. M. Mohammad (2011). "MI-219-zinc combination: a new paradigm in MDM2 inhibitor-based therapy." Oncogene **30**(1): 117-126.

Baell, J. B. and G. A. Holloway (2010). "New substructure filters for removal of pan assay interference compounds (PAINS) from screening libraries and for their exclusion in bioassays." Journal of Medicinal Chemistry **53**(7): 2719-2740.

Barak, Y., T. Juven, R. Haffner and M. Oren (1993). "mdm2 expression is induced by wild type p53 activity." EMBO J **12**(2): 461-468.

Bennett-Lovsey, R., S. E. Hart, H. Shirai and K. Mizuguchi (2002). "The SWIB and the MDM2 domains are homologous and share a common fold." Bioinformatics **18**(4): 626-630.

Bernal, F., A. F. Tyler, S. J. Korsmeyer, L. D. Walensky and G. L. Verdine (2007). "Reactivation of the p53 tumor suppressor pathway by a stapled p53 peptide." J Am Chem Soc **129**(9): 2456-2457.

Bernal, F., M. Wade, M. Godes, T. N. Davis, D. G. Whitehead, A. L. Kung, G. M. Wahl and L. D. Walensky (2010). "A stapled p53 helix overcomes HDMX-mediated suppression of p53." Cancer Cell **18**(5): 411-422.

Bista, M., K. Kowalska, W. Janczyk, A. Domling and T. A. Holak (2009). "Robust NMR screening for lead compounds using tryptophan-containing proteins." Journal of the American Chemical Society **131**(22): 7500-7501.

Bloembergen, N. and R. V. Pound (1954). "Radiation Damping in Magnetic Resonance Experiments." Physical Review **95**(1): 8-12.

Bodenhausen, G. and D. J. Ruben (1980). "Natural Abundance N-15 Nmr by Enhanced Heteronuclear Spectroscopy." Chemical Physics Letters **69**(1): 185-189.

Boeckler, F. M., A. C. Joerger, G. Jaggi, T. J. Rutherford, D. B. Veprintsev and A. R. Fersht (2008). "Targeted rescue of a destabilized mutant of p53 by an in silico screened drug." Proc Natl Acad Sci U S A **105**(30): 10360-10365.

Boetther, A. (2008). WO 2008119741.

Bon, R. S., C. Hong, M. J. Bouma, R. F. Schmitz, F. J. de Kanter, M. Lutz, A. L. Spek and R. V. Orru (2003). "Novel multicomponent reaction for the combinatorial synthesis of 2-imidazolines." Org Lett **5**(20): 3759-3762.

Bond, G. L., W. Hu, E. E. Bond, H. Robins, S. G. Lutzker, N. C. Arva, J. Bargonetti, F. Bartel, H. Taubert, P. Wuerl, K. Onel, L. Yip, S. J. Hwang, L. C. Strong, G. Lozano and A. J. Levine (2004). "A single nucleotide polymorphism in the MDM2 promoter attenuates the p53 tumor suppressor pathway and accelerates tumor formation in humans." Cell **119**(5): 591-602.

Bottger, A., V. Bottger, C. Garcia-Echeverria, P. Chene, H. K. Hochkeppel, W. Sampson, K. Ang, S. F. Howard, S. M. Picksley and D. P. Lane (1997). "Molecular characterization of the hdm2-p53 interaction." J Mol Biol **269**(5): 744-756.

Bottger, V., A. Bottger, C. Garcia-Echeverria, Y. F. Ramos, A. J. van der Eb, A. G. Jochemsen and D. P. Lane (1999). "Comparative study of the p53-mdm2 and p53-MDMX interfaces." Oncogene **18**(1): 189-199.

Brutscher, B., E. Lescop and P. Schanda (2007). "A set of BEST triple-resonance experiments for time-optimized protein resonance assignment." Journal of Magnetic Resonance **187**(1): 163-169.

Bullock, A. N., J. Henckel, B. S. DeDecker, C. M. Johnson, P. V. Nikolova, M. R. Proctor, D. P. Lane and A. R. Fersht (1997). "Thermodynamic stability of wild-type and mutant p53 core domain." Proc Natl Acad Sci U S A **94**(26): 14338-14342.

Cavanagh, J., W. J. Fairbrother, A. G. Palmer, M. Rance and N. J. Skleton (2007). "Protein NMR spectroscopy: Principles and Practice." Elsevier Academic Press.

Cheng, Q., L. Chen, Z. Li, W. S. Lane and J. Chen (2009). "ATM activates p53 by regulating MDM2 oligomerization and E3 processivity." EMBO J **28**(24): 3857-3867.

Chipuk, J. E., U. Maurer, D. R. Green and M. Schuler (2003). "Pharmacologic activation of p53 elicits Bax-dependent apoptosis in the absence of transcription." Cancer Cell **4**(5): 371-381.

Cho, Y., S. Gorina, P. D. Jeffrey and N. P. Pavletich (1994). "Crystal structure of a p53 tumor suppressor-DNA complex: understanding tumorigenic mutations." Science **265**(5170): 346-355.

Ciulli, A., G. Williams, A. G. Smith, T. L. Blundell and C. Abell (2006). "Probing hot spots at protein-ligand binding sites: a fragment-based approach using biophysical methods." Journal of Medicinal Chemistry **49**(16): 4992-5000.

Clore, G. M., J. Ernst, R. Clubb, J. G. Omichinski, W. M. Kennedy, K. Sakaguchi, E. Appella and A. M. Gronenborn (1995). "Refined solution structure of the oligomerization domain of the tumour suppressor p53." Nat Struct Biol **2**(4): 321-333.

Colaluca, I. N., D. Tosoni, P. Nuciforo, F. Senic-Matuglia, V. Galimberti, G. Viale, S. Pece and P. P. Di Fiore (2008). "NUMB controls p53 tumour suppressor activity." Nature **451**(7174): 76-80.

Crunkhorn, S. (2011). "Anticancer drugs: stapled peptide rescues p53." Nat Rev Drug Discov **10**(1): 21.

Czarna, A., B. Beck, S. Srivastava, G. M. Popowicz, S. Wolf, Y. Huang, M. Bista, T. A. Holak and A. Domling (2010). "Robust generation of lead compounds for protein-protein interactions by computational and MCR chemistry: p53/Hdm2 antagonists." Angew Chem Int Ed Engl **49**(31): 5352-5356.

Czarna, A., G. M. Popowicz, A. Pecak, S. Wolf, G. Dubin and T. A. Holak (2009). "High affinity interaction of the p53 peptide-analogue with human Mdm2 and Mdmx." Cell Cycle **8**(8): 1176-1184.

D'Silva, L., P. Ozdowy, M. Krajewski, U. Rothweiler, M. Singh and T. A. Holak (2005). "Monitoring the effects of antagonists on protein-protein interactions with NMR spectroscopy." J Am Chem Soc **127**(38): 13220-13226.

Dalvit, C., P. Floersheim, M. Zurini and A. Widmer (1999). "Use of organic solvents and small molecules for locating binding sites on proteins in solution." Journal of Biomolecular Nmr **14**(1): 23-32.

Dastidar, S. G., D. P. Lane and C. S. Verma (2008). "Multiple peptide conformations give rise to similar binding affinities: molecular simulations of p53-MDM2." J Am Chem Soc **130**(41): 13514-13515.

Dastidar, S. G., D. P. Lane and C. S. Verma (2009). "Modulation of p53 binding to MDM2: computational studies reveal important roles of Tyr100." BMC Bioinformatics **10 Suppl 15**: S6.

Dastidar, S. G., D. Raghunathan, J. Nicholson, T. R. Hupp, D. P. Lane and C. S. Verma (2011). "Chemical states of the N-terminal "lid" of MDM2 regulate p53 binding: simulations reveal complexities of modulation." Cell Cycle **10**(1): 82-89.

Dawson, R., L. Muller, A. Dehner, C. Klein, H. Kessler and J. Buchner (2003). "The N-terminal domain of p53 is natively unfolded." J Mol Biol **332**(5): 1131-1141.

Ding, K., Y. Lu, Z. Nikolovska-Coleska, S. Qiu, Y. Ding, W. Gao, J. Stuckey, K. Krajewski, P. P. Roller, Y. Tomita, D. A. Parrish, J. R. Deschamps and S. Wang (2005). "Structure-based design of potent non-peptide MDM2 inhibitors." J Am Chem Soc **127**(29): 10130-10131.

Ding, K., Y. Lu, Z. Nikolovska-Coleska, G. Wang, S. Qiu, S. Shangary, W. Gao, D. Qin, J. Stuckey, K. Krajewski, P. P. Roller and S. Wang (2006). "Structure-based design of spiro-oxindoles as potent, specific small-molecule inhibitors of the MDM2-p53 interaction." Journal of Medicinal Chemistry **49**(12): 3432-3435.

Dominguez, C., R. Boelens and A. M. J. J. Bonvin (2003). "HADDOCK: A protein-protein docking approach based on biochemical or biophysical information." Journal of the American Chemical Society **125**(7): 1731-1737.

Domling, A. (2006). "Recent developments in isocyanide based multicomponent reactions in applied chemistry." Chemical Reviews **106**(1): 17-89.

Domling, A. (2008). "Small molecular weight protein-protein interaction antagonists: an insurmountable challenge?" Curr Opin Chem Biol **12**(3): 281-291.

Domling, A. and I. Ugi (2000). "Multicomponent reactions with isocyanides." Angewandte Chemie-International Edition **39**(18): 3169-3210.

Dornan, D. and T. R. Hupp (2001). "Inhibition of p53-dependent transcription by BOX-I phospho-peptide mimetics that bind to p300." EMBO Rep **2**(2): 139-144.

el-Deiry, W. S. (1998). "p21/p53, cellular growth control and genomic integrity." Curr Top Microbiol Immunol **227**: 121-137.

el-Deiry, W. S., S. E. Kern, J. A. Pietenpol, K. W. Kinzler and B. Vogelstein (1992). "Definition of a consensus binding site for p53." Nat Genet **1**(1): 45-49.

el-Deiry, W. S., T. Tokino, V. E. Velculescu, D. B. Levy, R. Parsons, J. M. Trent, D. Lin, W. E. Mercer, K. W. Kinzler and B. Vogelstein (1993). "WAF1, a potential mediator of p53 tumor suppression." Cell **75**(4): 817-825.

Ernst, R. R., G. Bodehausen and A. Wokaun (1990). "Principles of Nuclear Magnetic Resonance in One and Two Dimensions." Oxford Science Publications.

Fasan, R., R. L. Dias, K. Moehle, O. Zerbe, D. Obrecht, P. R. Mittl, M. G. Grutter and J. A. Robinson (2006). "Structure-activity studies in a family of beta-hairpin protein epitope mimetic inhibitors of the p53-HDM2 protein-protein interaction." Chembiochem 7(3): 515-526.

Fersht, A. R. (1998). "Structure and Mechanism in Protein Science: A Guide to Enzyme Catalysis and Protein Folding." W. H. Freeman.

Fielding, L. (2007). "NMR methods for the determination of protein-ligand dissociation constants." Progress in Nuclear Magnetic Resonance Spectroscopy 51(4): 219-242.

Finch, R. A., D. B. Donoviel, D. Potter, M. Shi, A. Fan, D. D. Freed, C. Y. Wang, B. P. Zambrowicz, R. Ramirez-Solis, A. T. Sands and N. Zhang (2002). "mdmx is a negative regulator of p53 activity in vivo." Cancer Research 62(11): 3221-3225.

Gardino, A. K., J. Villali, A. Kivenson, M. Lei, C. F. Liu, P. Steindel, E. Z. Eisenmesser, W. Labeikovsky, M. Wolf-Watz, M. W. Clarkson and D. Kern (2009). "Transient non-native hydrogen bonds promote activation of a signaling protein." Cell 139(6): 1109-1118.

Geen, H. and R. Freeman (1991). "Band-Selective Radiofrequency Pulses." Journal of Magnetic Resonance 93(1): 93-141.

Grasberger, B. L., T. Lu, C. Schubert, D. J. Parks, T. E. Carver, H. K. Koblish, M. D. Cummings, L. V. LaFrance, K. L. Milkiewicz, R. R. Calvo, D. Maguire, J. Lattanze, C. F. Franks, S. Zhao, K. Ramachandren, G. R. Bylebyl, M. Zhang, C. L. Manthey, E. C. Petrella, M. W. Pantoliano, I. C. Deckman, J. C. Spurlino, A. C. Maroney, B. E. Tomczuk, C. J. Molloy and R. F. Bone (2005). "Discovery and cocrystal structure of benzodiazepinedione HDM2 antagonists that activate p53 in cells." Journal of Medicinal Chemistry 48(4): 909-912.

Gu, J., H. Kawai, L. Nie, H. Kitao, D. Wiederschain, A. G. Jochemsen, J. Parant, G. Lozano and Z. M. Yuan (2002). "Mutual dependence of MDM2 and MDMX in their functional inactivation of p53." J Biol Chem 277(22): 19251-19254.

Gu, W., X. L. Shi and R. G. Roeder (1997). "Synergistic activation of transcription by CBP and p53." Nature 387(6635): 819-823.

Gueron, M., P. Plateau and M. Decorps (1991). "Solvent Signal Suppression in Nmr." Progress in Nuclear Magnetic Resonance Spectroscopy 23: 135-209.

Guo, Z., U. Mohanty, J. Noehre, T. K. Sawyer, W. Sherman and G. Krilov (2010). "Probing the alpha-helical structural stability of stapled p53 peptides: molecular dynamics simulations and analysis." Chem Biol Drug Des 75(4): 348-359.

Ha, J. H., E. Y. Won, J. S. Shin, M. Jang, K. S. Ryu, K. H. Bae, S. G. Park, B. C. Park, H. S. Yoon and S. W. Chi (2011). "Molecular mimicry-based repositioning of nutlin-3 to anti-apoptotic Bcl-2 family proteins." J Am Chem Soc 133(5): 1244-1247.

Hansen, D. F., P. Vallurupalli and L. E. Kay (2008). "Using relaxation dispersion NMR spectroscopy to determine structures of excited, invisible protein states." Journal of Biomolecular Nmr 41(3): 113-120.

Helton, E. S. and X. Chen (2007). "p53 modulation of the DNA damage response." J Cell Biochem 100(4): 883-896.

Henzler-Wildman, K. and D. Kern (2007). "Dynamic personalities of proteins." Nature 450(7172): 964-972.

Hu, B., D. M. Gilkes and J. Chen (2007). "Efficient p53 activation and apoptosis by simultaneous disruption of binding to MDM2 and MDMX." Cancer Research **67**(18): 8810-8817.

Huang, X. (2003). "Fluorescence polarization competition assay: the range of resolvable inhibitor potency is limited by the affinity of the fluorescent ligand." Journal of Biomolecular Screening **8**(1): 34-38.

Huang, Y., S. Wolf, M. Bista, L. Meireles, C. Camacho, T. A. Holak and A. Domling (2010). "1,4-Thienodiazepine-2,5-diones via MCR (I): synthesis, virtual space and p53-Mdm2 activity." Chem Biol Drug Des **76**(2): 116-129.

Hubbard, S. (1996). "NACCESS - accesibility calculations." http://www.bioinf.manchester.ac.uk/naccess/.

Huth, J. R., R. Mendoza, E. T. Olejniczak, R. W. Johnson, D. A. Cothron, Y. Liu, C. G. Lerner, J. Chen and P. J. Hajduk (2005). "ALARM NMR: a rapid and robust experimental method to detect reactive false positives in biochemical screens." J Am Chem Soc **127**(1): 217-224.

Irwin, J. J. and B. K. Shoichet (2005). "ZINC--a free database of commercially available compounds for virtual screening." J Chem Inf Model **45**(1): 177-182.

Iyappan, S., H. P. Wollscheid, A. Rojas-Fernandez, A. Marquardt, H. C. Tang, R. K. Singh and M. Scheffner (2010). "Turning the RING domain protein MdmX into an active ubiquitin-protein ligase." J Biol Chem **285**(43): 33065-33072.

Jamieson, E. R. and S. J. Lippard (1999). "Structure, Recognition, and Processing of Cisplatin-DNA Adducts." Chem Rev **99**(9): 2467-2498.

Jeffrey, P. D., S. Gorina and N. P. Pavletich (1995). "Crystal structure of the tetramerization domain of the p53 tumor suppressor at 1.7 angstroms." Science **267**(5203): 1498-1502.

Joerger, A. C. and A. R. Fersht (2008). "Structural biology of the tumor suppressor p53." Annu Rev Biochem **77**: 557-582.

Jones, S. N., A. R. Hancock, H. Vogel, L. A. Donehower and A. Bradley (1998). "Overexpression of Mdm2 in mice reveals a p53-independent role for Mdm2 in tumorigenesis." Proc Natl Acad Sci U S A **95**(26): 15608-15612.

Jorgensen, W. L. and E. M. Duffy (2000). "Prediction of drug solubility from Monte Carlo simulations." Bioorg Med Chem Lett **10**(11): 1155-1158.

Joseph, T. L., D. Lane and C. S. Verma (2010). "Stapled peptides in the p53 pathway: computer simulations reveal novel interactions of the staples with the target protein." Cell Cycle **9**(22): 4560-4568.

Joseph, T. L., A. Madhumalar, C. J. Brown, D. P. Lane and C. S. Verma (2010). "Differential binding of p53 and nutlin to MDM2 and MDMX: Computational studies." Cell Cycle **9**(6): 1167-1181.

Ju, C. and J. P. Uetrecht (2002). "Mechanism of idiosyncratic drug reactions: reactive metabolite formation, protein binding and the regulation of the immune system." Curr Drug Metab **3**(4): 367-377.

Juven-Gershon, T., O. Shifman, T. Unger, A. Elkeles, Y. Haupt and M. Oren (1998). "The Mdm2 oncoprotein interacts with the cell fate regulator Numb." Mol Cell Biol **18**(7): 3974-3982.

Kabsch, W. (1993). "Automatic processing of rotation diffraction data from crystals of initially unknown symmetry and cell constants." Journal of Applied Crystallography **26**(6): 795-800.

Kaplan, A. P. and P. A. Bartlett (1991). "Synthesis and evaluation of an inhibitor of carboxypeptidase A with a Ki value in the femtomolar range." Biochemistry **30**(33): 8165-8170.

Kay, L. E., P. Keifer and T. Saarinen (1992). "Pure Absorption Gradient Enhanced Heteronuclear Single Quantum Correlation Spectroscopy with Improved Sensitivity." Journal of the American Chemical Society **114**(26): 10663-10665.

Kazimierczuk, K., J. Stanek, A. Zawadzka-Kazimierczuk and W. Kozminski (2010). "Random sampling in multidimensional NMR spectroscopy." Prog Nucl Magn Reson Spectrosc **57**(4): 420-434.

Kessler, H., S. Mronga and G. Gemmecker (1991). "Multidimensional Nmr Experiments Using Selective Pulses." Magnetic Resonance in Chemistry **29**(6): 527-557.

Kitayner, M., H. Rozenberg, N. Kessler, D. Rabinovich, L. Shaulov, T. E. Haran and Z. Shakked (2006). "Structural basis of DNA recognition by p53 tetramers." Mol Cell **22**(6): 741-753.

Knockaert, M., P. Greengard and L. Meijer (2002). "Pharmacological inhibitors of cyclin-dependent kinases." Trends Pharmacol Sci **23**(9): 417-425.

Kortemme, T. and D. Baker (2002). "A simple physical model for binding energy hot spots in protein-protein complexes." Proc Natl Acad Sci U S A **99**(22): 14116-14121.

Kostic, M., T. Matt, M. A. Martinez-Yamout, H. J. Dyson and P. E. Wright (2006). "Solution structure of the Hdm2 C2H2C4 RING, a domain critical for ubiquitination of p53." J Mol Biol **363**(2): 433-450.

Krajewski, M., U. Rothweiler, L. D'Silva, S. Majumdar, C. Klein and T. A. Holak (2007). "An NMR-based antagonist induced dissociation assay for targeting the ligand-protein and protein-protein interactions in competition binding experiments." J Med Chem **50**(18): 4382-4387.

Krajewski, M., U. Rothweiler, L. D'Silva, S. Majumdar, C. Klein and T. A. Holak (2007). "An NMR-Based antagonist induced dissociation assay for targeting the ligand-protein and protein-protein interactions in competition binding experiments." Journal of Medicinal Chemistry **50**(18): 4382-4387.

Kuntz, I. D., K. Chen, K. A. Sharp and P. A. Kollman (1999). "The maximal affinity of ligands." Proc Natl Acad Sci U S A **96**(18): 9997-10002.

Kupce, E., J. Boyd and I. D. Campbell (1995). "Short Selective Pulses for Biochemical Applications." Journal of Magnetic Resonance Series B **106**(3): 300-303.

Kussie, P. H., S. Gorina, V. Marechal, B. Elenbaas, J. Moreau, A. J. Levine and N. P. Pavletich (1996). "Structure of the MDM2 oncoprotein bound to the p53 tumor suppressor transactivation domain." Science **274**(5289): 948-953.

Lamzin, V. S. and K. S. Wilson (1993). "Automated refinement of protein models." Acta Crystallographica Section D **49**(1): 129-147.

Lange, O. F., N. A. Lakomek, C. Fares, G. F. Schroder, K. F. Walter, S. Becker, J. Meiler, H. Grubmuller, C. Griesinger and B. L. de Groot (2008). "Recognition dynamics up to microseconds revealed from an RDC-derived ubiquitin ensemble in solution." Science **320**(5882): 1471-1475.

Leach, A. R., V. J. Gillet, R. A. Lewis and R. Taylor (2010). "Three-dimensional pharmacophore methods in drug discovery." Journal of Medicinal Chemistry **53**(2): 539-558.

Lee, H., K. H. Mok, R. Muhandiram, K. H. Park, J. E. Suk, D. H. Kim, J. Chang, Y. C. Sung, K. Y. Choi and K. H. Han (2000). "Local structural elements in the mostly unstructured transcriptional activation domain of human p53." J Biol Chem **275**(38): 29426-29432.

Li, C., M. Pazgier, M. Liu, W. Y. Lu and W. Lu (2009). "Apamin as a template for structure-based rational design of potent peptide activators of p53." Angew Chem Int Ed Engl **48**(46): 8712-8715.

Li, C., M. Pazgier, W. Yuan, M. Liu, G. Wei, W. Y. Lu and W. Lu (2010). "Systematic mutational analysis of peptide inhibition of the p53-MDM2/MDMX interactions." J Mol Biol **398**(2): 200-213.

Li, S. C., Z. Songyang, S. J. Vincent, C. Zwahlen, S. Wiley, L. Cantley, L. E. Kay, J. Forman-Kay and T. Pawson (1997). "High-affinity binding of the Drosophila Numb phosphotyrosine-binding domain to peptides containing a Gly-Pro-(p)Tyr motif." Proc Natl Acad Sci U S A **94**(14): 7204-7209.

Lian, L. Y., I. L. Barsukov, M. J. Sutcliffe, K. H. Sze and G. C. Roberts (1994). "Protein-ligand interactions: exchange processes and determination of ligand conformation and protein-ligand contacts." Methods Enzymol **239**: 657-700.

Liao, J. C., R. Lam, V. Brazda, S. Duan, M. Ravichandran, J. Ma, T. Xiao, W. Tempel, X. Zuo, Y. X. Wang, N. Y. Chirgadze and C. H. Arrowsmith (2011). "Interferon-inducible protein 16: insight into the interaction with tumor suppressor p53." Structure **19**(3): 418-429.

Linares, L. K., A. Hengstermann, A. Ciechanover, S. Muller and M. Scheffner (2003). "HdmX stimulates Hdm2-mediated ubiquitination and degradation of p53." Proc Natl Acad Sci U S A **100**(21): 12009-12014.

Linke, K., P. D. Mace, C. A. Smith, D. L. Vaux, J. Silke and C. L. Day (2008). "Structure of the MDM2/MDMX RING domain heterodimer reveals dimerization is required for their ubiquitylation in trans." Cell Death Differ **15**(5): 841-848.

Lipinski, C. A., F. Lombardo, B. W. Dominy and P. J. Feeney (2001). "Experimental and computational approaches to estimate solubility and permeability in drug discovery and development settings." Adv Drug Deliv Rev **46**(1-3): 3-26.

Liu, M., C. Li, M. Pazgier, Y. Mao, Y. Lv, B. Gu, G. Wei, W. Yuan, C. Zhan, W. Y. Lu and W. Lu (2010). "D-peptide inhibitors of the p53-MDM2 interaction for targeted molecular therapy of malignant neoplasms." Proc Natl Acad Sci U S A **107**(32): 14321-14326.

Lohrum, M. A., R. L. Ludwig, M. H. Kubbutat, M. Hanlon and K. H. Vousden (2003). "Regulation of HDM2 activity by the ribosomal protein L11." Cancer Cell **3**(6): 577-587.

Lopez-Borges, S. and P. A. Lazo (2000). "The human vaccinia-related kinase 1 (VRK1) phosphorylates threonine-18 within the mdm-2 binding site of the p53 tumour suppressor protein." Oncogene **19**(32): 3656-3664.

Lor, L. A., J. Schneck, D. E. McNulty, E. Diaz, M. Brandt, S. H. Thrall and B. Schwartz (2007). "A simple assay for detection of small-molecule redox activity." J Biomol Screen **12**(6): 881-890.

Luna, R. M. D., D. S. Wagner and G. Lozano (1995). "Rescue of Early Embryonic Lethality in Mdm2-Deficient Mice by Deletion of P53." Nature **378**(6553): 203-206.

Marine, J. C. and A. G. Jochemsen (2004). "Mdmx and Mdm2: brothers in arms?" Cell Cycle **3**(7): 900-904.

Marine, J. C. and A. G. Jochemsen (2005). "Mdmx as an essential regulator of p53 activity." Biochem Biophys Res Commun **331**(3): 750-760.

Markus, M. A., K. T. Dayie, P. Matsudaira and G. Wagner (1994). "Effect of Deuteration on the Amide Proton Relaxation Rates in Proteins -

Heteronuclear Nmr Experiments on Villin 14t." Journal of Magnetic Resonance Series B **105**(2): 192-195.

Marx, J. (2007). "Oncology. Recruiting the cell's own guardian for cancer therapy." Science **315**(5816): 1211-1213.

Massova, I. and P. A. Kollman (1999). "Computational Alanine Scanning To Probe Protein–Protein Interactions: A Novel Approach To Evaluate Binding Free Energies." J Am Chem Soc **121**(36): 8133-8143.

Mattos, C. and D. Ringe (1996). "Locating and characterizing binding sites on proteins." Nature Biotechnology **14**(5): 595-599.

Mcconnell, H. M. (1958). "Reaction Rates by Nuclear Magnetic Resonance." Journal of Chemical Physics **28**(3): 430-431.

McCoy, M. A., J. J. Gesell, M. M. Senior and D. F. Wyss (2003). "Flexible lid to the p53-binding domain of human Mdm2: implications for p53 regulation." Proc Natl Acad Sci U S A **100**(4): 1645-1648.

McGaughey, G. B., M. Gagne and A. K. Rappe (1998). "pi-Stacking interactions. Alive and well in proteins." J Biol Chem **273**(25): 15458-15463.

Meireles, L. M., A. S. Domling and C. J. Camacho (2010). "ANCHOR: a web server and database for analysis of protein-protein interaction binding pockets for drug discovery." Nucleic Acids Res **38**(Web Server issue): W407-411.

Miliani de Marval, P. L. and Y. Zhang (2011). "The RP-Mdm2-p53 pathway and tumorigenesis." Oncotarget **2**(3): 234-238.

Miller, J. H. (1972). "Experiments in molecular genetics." Cold Spring Harbor Laboratory Press.

Mittag, T., L. E. Kay and J. D. Forman-Kay (2010). "Protein dynamics and conformational disorder in molecular recognition." J Mol Recognit **23**(2): 105-116.

Miyashita, T. and J. C. Reed (1995). "Tumor suppressor p53 is a direct transcriptional activator of the human bax gene." Cell **80**(2): 293-299.

Mohammad, R. M., J. Wu, A. S. Azmi, A. Aboukameel, A. Sosin, S. Wu, D. Yang, S. Wang and A. M. Al-Katib (2009). "An MDM2 antagonist (MI-319) restores p53 functions and increases the life span of orally treated follicular lymphoma bearing animals." Mol Cancer **8**: 115.

Mori, S., C. Abeygunawardana, M. O. Johnson and P. C. van Zijl (1995). "Improved sensitivity of HSQC spectra of exchanging protons at short interscan delays using a new fast HSQC (FHSQC) detection scheme that avoids water saturation." J Magn Reson B **108**(1): 94-98.

Murshudov, G. N., A. A. Vagin and E. J. Dodson (1997). "Refinement of Macromolecular Structures by the Maximum-Likelihood Method." Acta Crystallographica Section D **53**(3): 240-255.

Nucci, N. V., M. S. Pometun and A. J. Wand (2011). "Site-resolved measurement of water-protein interactions by solution NMR." Nature Structural & Molecular Biology **18**(2): 245-249.

Okorokov, A. L., M. B. Sherman, C. Plisson, V. Grinkevich, K. Sigmundsson, G. Selivanova, J. Milner and E. V. Orlova (2006). "The structure of p53 tumour suppressor protein reveals the basis for its functional plasticity." EMBO J **25**(21): 5191-5200.

Olejniczak, E. T. and M. A. Weiss (1990). "Are Methyl-Groups Relaxation Sinks in Small Proteins." Journal of Magnetic Resonance **86**(1): 148-155.

Olivier, M., R. Eeles, M. Hollstein, M. A. Khan, C. C. Harris and P. Hainaut (2002). "The IARC TP53 database: new online mutation analysis and recommendations to users." Hum Mutat **19**(6): 607-614.

Orekhov, V. Y., I. Ibraghimov and M. Billeter (2003). "Optimizing resolution in multidimensional NMR by three-way decomposition." Journal of Biomolecular Nmr **27**(2): 165-173.

Otting, G., E. Liepinsh and K. Wuthrich (1991). "Protein Hydration in Aqueous-Solution." Science **254**(5034): 974-980.

Pazgier, M., M. Liu, G. Zou, W. Yuan, C. Li, J. Li, J. Monbo, D. Zella, S. G. Tarasov and W. Lu (2009). "Structural basis for high-affinity peptide inhibition of p53 interactions with MDM2 and MDMX." Proc Natl Acad Sci U S A **106**(12): 4665-4670.

Pellecchia, M., I. Bertini, D. Cowburn, C. Dalvit, E. Giralt, W. Jahnke, T. L. James, S. W. Homans, H. Kessler, C. Luchinat, B. Meyer, H. Oschkinat, J. Peng, H. Schwalbe and G. Siegal (2008). "Perspectives on NMR in drug discovery: a technique comes of age." Nat Rev Drug Discov **7**(9): 738-745.

Pellecchia, M., D. S. Sem and K. Wuthrich (2002). "NMR in drug discovery." Nat Rev Drug Discov **1**(3): 211-219.

Pervushin, K., B. Vogeli and A. Eletsky (2002). "Longitudinal (1)H relaxation optimization in TROSY NMR spectroscopy." J Am Chem Soc **124**(43): 12898-12902.

Phan, J., Z. Li, A. Kasprzak, B. Li, S. Sebti, W. Guida, E. Schonbrunn and J. Chen (2010). "Structure-based design of high affinity peptides inhibiting the interaction of p53 with MDM2 and MDMX." J Biol Chem **285**(3): 2174-2183.

Piotto, M., V. Saudek and V. Sklenar (1992). "Gradient-tailored excitation for single-quantum NMR spectroscopy of aqueous solutions." J Biomol NMR **2**(6): 661-665.

Popowicz, G. M., A. Czarna and T. A. Holak (2008). "Structure of the human Mdmx protein bound to the p53 tumor suppressor transactivation domain." Cell Cycle **7**(15): 2441-2443.

Popowicz, G. M., A. Czarna, U. Rothweiler, A. Szwagierczak, M. Krajewski, L. Weber and T. A. Holak (2007). "Molecular basis for the inhibition of p53 by Mdmx." Cell Cycle **6**(19): 2386-2392.

Popowicz, G. M., A. Czarna, S. Wolf, K. Wang, W. Wang, A. Domling and T. A. Holak (2010). "Structures of low molecular weight inhibitors bound to MDMX and MDM2 reveal new approaches for p53-MDMX/MDM2 antagonist drug discovery." Cell Cycle **9**(6): 1104-1111.

Popowicz, G. M., A. Domling and T. A. Holak (2011). "The structure-based design of Mdm2/Mdmx-p53 inhibitors gets serious." Angew Chem Int Ed Engl **50**(12): 2680-2688.

Prives, C., M. V. Poyurovsky, C. Katz, O. Laptenko, R. Beckerman, M. Lokshin, J. Ahn, I. J. L. Byeon, R. Gabizon, M. Mattia, A. Zupnick, L. M. Brown and A. Friedler (2010). "The C terminus of p53 binds the N-terminal domain of MDM2." Nature Structural & Molecular Biology **17**(8): 982-U995.

Rajamani, D., S. Thiel, S. Vajda and C. J. Camacho (2004). "Anchor residues in protein-protein interactions." Proc Natl Acad Sci U S A **101**(31): 11287-11292.

Reed, D., Y. Shen, A. A. Shelat, L. A. Arnold, A. M. Ferreira, F. Zhu, N. Mills, D. C. Smithson, C. A. Regni, D. Bashford, S. A. Cicero, B. A. Schulman, A. G. Jochemsen, R. K. Guy and M. A. Dyer (2010). "Identification and

characterization of the first small molecule inhibitor of MDMX." J Biol Chem **285**(14): 10786-10796.

Rehm, T., R. Huber and T. A. Holak (2002). "Application of NMR in structural proteomics: screening for proteins amenable to structural analysis." Structure **10**(12): 1613-1618.

Reich, H. J. (1995). "WinDNMR: Dynamic NMR Spectra for Windows." J Chem Educ **72**(12): 1086.

Rice, P., I. Longden and A. Bleasby (2000). "EMBOSS: the European Molecular Biology Open Software Suite." Trends Genet **16**(6): 276-277.

Roth, G. J., N. Stanford and P. W. Majerus (1975). "Acetylation of prostaglandin synthase by aspirin." Proc Natl Acad Sci U S A **72**(8): 3073-3076.

Rothweiler, U., A. Czarna, L. Weber, G. M. Popowicz, K. Brongel, K. Kowalska, M. Orth, O. Stemmann and T. A. Holak (2008). "NMR screening for lead compounds using tryptophan-mutated proteins." J Med Chem **51**(16): 5035-5042.

Rustandi, R. R., D. M. Baldisseri and D. J. Weber (2000). "Structure of the negative regulatory domain of p53 bound to S100B(betabeta)." Nat Struct Biol **7**(7): 570-574.

Sakaguchi, K., S. Saito, Y. Higashimoto, S. Roy, C. W. Anderson and E. Appella (2000). "Damage-mediated phosphorylation of human p53 threonine 18 through a cascade mediated by a casein 1-like kinase - Effect on Mdm2 binding." Journal of Biological Chemistry **275**(13): 9278-9283.

Sakurai, K., C. Schubert and D. Kahne (2006). "Crystallographic analysis of an 8-mer p53 peptide analogue complexed with MDM2." J Am Chem Soc **128**(34): 11000-11001.

Sanchez, M. C., J. G. Renshaw, G. Davies, P. N. Barlow and M. Vogtherr (2010). "MDM4 binds ligands via a mechanism in which disordered regions become structured." FEBS Lett **584**(14): 3035-3041.

Sayan, B. S., A. E. Sayan, R. A. Knight, G. Melino and G. M. Cohen (2006). "p53 is cleaved by caspases generating fragments localizing to mitochondria." J Biol Chem **281**(19): 13566-13573.

Schafmeister, C. E., J. Po and G. L. Verdine (2000). "An all-hydrocarbon cross-linking system for enhancing the helicity and metabolic stability of peptides." Journal of the American Chemical Society **122**(24): 5891-5892.

Schanda, P. (2009). "Fast-pulsing longitudinal relaxation optimized techniques: Enriching the toolbox of fast biomolecular NMR spectroscopy." Progress in Nuclear Magnetic Resonance Spectroscopy **55**: 238-265.

Schanda, P., E. Kupce and B. Brutscher (2005). "SOFAST-HMQC experiments for recording two-dimensional heteronuclear correlation spectra of proteins within a few seconds." Journal of Biomolecular Nmr **33**(4): 199-211.

Schon, O., A. Friedler, M. Bycroft, S. M. Freund and A. R. Fersht (2002). "Molecular mechanism of the interaction between MDM2 and p53." J Mol Biol **323**(3): 491-501.

Shangary, S., D. Qin, D. McEachern, M. Liu, R. S. Miller, S. Qiu, Z. Nikolovska-Coleska, K. Ding, G. Wang, J. Chen, D. Bernard, J. Zhang, Y. Lu, Q. Gu, R. B. Shah, K. J. Pienta, X. Ling, S. Kang, M. Guo, Y. Sun, D. Yang and S. Wang (2008). "Temporal activation of p53 by a specific MDM2 inhibitor is selectively toxic to tumors and leads to complete tumor growth inhibition." Proc Natl Acad Sci U S A **105**(10): 3933-3938.

Sherr, C. J. (2006). "Divorcing ARF and p53: an unsettled case." Nat Rev Cancer **6**(9): 663-673.

Showalter, S. A., L. Bruschweiler-Li, E. Johnson, F. Zhang and R. Bruschweiler (2008). "Quantitative lid dynamics of MDM2 reveals differential ligand binding modes of the p53-binding cleft." J Am Chem Soc **130**(20): 6472-6478.

Shuker, S. B., P. J. Hajduk, R. P. Meadows and S. W. Fesik (1996). "Discovering high-affinity ligands for proteins: SAR by NMR." Science **274**(5292): 1531-1534.

Siegel, M. M. (2002). "Early discovery drug screening using mass spectrometry." Curr Top Med Chem **2**(1): 13-33.

Singh, J., R. C. Petter, T. A. Baillie and A. Whitty (2011). "The resurgence of covalent drugs." Nat Rev Drug Discov **10**(4): 307-317.

Sivakolundu, S. G., A. Nourse, S. Moshiach, B. Bothner, C. Ashley, J. Satumba, J. Lahti and R. W. Kriwacki (2008). "Intrinsically unstructured domains of Arf and Hdm2 form bimolecular oligomeric structures in vitro and in vivo." J Mol Biol **384**(1): 240-254.

Sot, B., S. M. Freund and A. R. Fersht (2007). "Comparative biophysical characterization of p53 with the pro-apoptotic BAK and the anti-apoptotic BCL-xL." J Biol Chem **282**(40): 29193-29200.

Sperandio, O., C. H. Reynes, A. C. Camproux and B. O. Villoutreix (2010). "Rationalizing the chemical space of protein-protein interaction inhibitors." Drug Discov Today **15**(5-6): 220-229.

Sternbach, L. H. (1983). "The Benzodiazepine Story." Journal of Psychoactive Drugs **15**(1-2): 15-17.

Stoll, R., C. Renner, S. Hansen, S. Palme, C. Klein, A. Belling, W. Zeslawski, M. Kamionka, T. Rehm, P. Muhlhahn, R. Schumacher, F. Hesse, B. Kaluza, W. Voelter, R. A. Engh and T. A. Holak (2001). "Chalcone derivatives antagonize interactions between the human oncoprotein MDM2 and p53." Biochemistry **40**(2): 336-344.

Stoll, R., C. Renner, P. Muhlhahn, S. Hansen, R. Schumacher, F. Hesse, B. Kaluza, R. A. Engh, W. Voelter and T. A. Holak (2000). "Sequence-specific 1H, 15N, and 13C assignment of the N-terminal domain of the human oncoprotein MDM2 that binds to p53." Journal of Biomolecular Nmr **17**(1): 91-92.

Stommel, J. M., N. D. Marchenko, G. S. Jimenez, U. M. Moll, T. J. Hope and G. M. Wahl (1999). "A leucine-rich nuclear export signal in the p53 tetramerization domain: regulation of subcellular localization and p53 activity by NES masking." EMBO J **18**(6): 1660-1672.

Suzuki, H. I., K. Yamagata, K. Sugimoto, T. Iwamoto, S. Kato and K. Miyazono (2009). "Modulation of microRNA processing by p53." Nature **460**(7254): 529-533.

Takahashi, K., C. Uchida, R. W. Shin, K. Shimazaki and T. Uchida (2008). "Prolyl isomerase, Pin1: new findings of post-translational modifications and physiological substrates in cancer, asthma and Alzheimer's disease." Cell Mol Life Sci **65**(3): 359-375.

Tang, C., J. Iwahara and G. M. Clore (2006). "Visualization of transient encounter complexes in protein-protein association." Nature **444**(7117): 383-386.

Tang, L., E. Nogales and C. Ciferri (2010). "Structure and function of SWI/SNF chromatin remodeling complexes and mechanistic implications for transcription." Prog Biophys Mol Biol **102**(2-3): 122-128.

Thut, C. J., J. L. Chen, R. Klemm and R. Tjian (1995). "p53 transcriptional activation mediated by coactivators TAFII40 and TAFII60." Science **267**(5194): 100-104.

Tidow, H., R. Melero, E. Mylonas, S. M. Freund, J. G. Grossmann, J. M. Carazo, D. I. Svergun, M. Valle and A. R. Fersht (2007). "Quaternary structures of tumor suppressor p53 and a specific p53 DNA complex." Proc Natl Acad Sci U S A **104**(30): 12324-12329.

Toledo, F. and B. Bardot (2009). "Cancer: Three birds with one stone." Nature **460**(7254): 466-467.

Toledo, F. and G. M. Wahl (2006). "Regulating the p53 pathway: in vitro hypotheses, in vivo veritas." Nat Rev Cancer **6**(12): 909-923.

Ugi, I., A. Demharter, W. Horl and T. Schmid (1996). "Ugi reactions with trifunctional alpha-amino acids, aldehydes, isocyanides and alcohols." Tetrahedron **52**(35): 11657-11664.

Ugi, I., A. Domling and W. Horl (1994). "Multicomponent reactions in organic chemistry." Endeavour **18**(3): 115-122.

Uhrinova, S., D. Uhrin, H. Powers, K. Watt, D. Zheleva, P. Fischer, C. McInnes and P. N. Barlow (2005). "Structure of free MDM2 N-terminal domain reveals conformational adjustments that accompany p53-binding." J Mol Biol **350**(3): 587-598.

Vagin, A. and A. Teplyakov (1997). "MOLREP: an automated program for molecular replacement." Journal of Applied Crystallography **30**(6): 1022-1025.

Vassilev, L. T. (2007). "MDM2 inhibitors for cancer therapy." Trends Mol Med **13**(1): 23-31.

Vassilev, L. T., B. T. Vu, B. Graves, D. Carvajal, F. Podlaski, Z. Filipovic, N. Kong, U. Kammlott, C. Lukacs, C. Klein, N. Fotouhi and E. A. Liu (2004). "In vivo activation of the p53 pathway by small-molecule antagonists of MDM2." Science **303**(5659): 844-848.

Veprintsev, D. B., S. M. Freund, A. Andreeva, S. E. Rutledge, H. Tidow, J. M. Canadillas, C. M. Blair and A. R. Fersht (2006). "Core domain interactions in full-length p53 in solution." Proc Natl Acad Sci U S A **103**(7): 2115-2119.

Vousden, K. H. and D. P. Lane (2007). "p53 in health and disease." Nat Rev Mol Cell Biol **8**(4): 275-283.

Wade, M. and G. M. Wahl (2009). "Targeting Mdm2 and Mdmx in cancer therapy: better living through medicinal chemistry?" Mol Cancer Res **7**(1): 1-11.

Wade, M., Y. V. Wang and G. M. Wahl (2010). "The p53 orchestra: Mdm2 and Mdmx set the tone." Trends Cell Biol **20**(5): 299-309.

Wade, M., E. T. Wong, M. Tang, J. M. Stommel and G. M. Wahl (2006). "Hdmx modulates the outcome of p53 activation in human tumor cells." J Biol Chem **281**(44): 33036-33044.

Walker, K. K. and A. J. Levine (1996). "Identification of a novel p53 functional domain that is necessary for efficient growth suppression." Proc Natl Acad Sci U S A **93**(26): 15335-15340.

Wallace, A. C., R. A. Laskowski and J. M. Thornton (1995). "LIGPLOT: a program to generate schematic diagrams of protein-ligand interactions." Protein Eng **8**(2): 127-134.

Wang, Y., A. Rosengarth and H. Luecke (2007). "Structure of the human p53 core domain in the absence of DNA." Acta Crystallogr D Biol Crystallogr **63**(Pt 3): 276-281.

Wang, Z. X. (1995). "An exact mathematical expression for describing competitive binding of two different ligands to a protein molecule." <u>FEBS Lett</u> **360**(2): 111-114.

Weber, J. D., L. J. Taylor, M. F. Roussel, C. J. Sherr and D. Bar-Sagi (1999). "Nucleolar Arf sequesters Mdm2 and activates p53." <u>Nat Cell Biol</u> **1**(1): 20-26.

Wells, J. A. and C. L. McClendon (2007). "Reaching for high-hanging fruit in drug discovery at protein-protein interfaces." <u>Nature</u> **450**(7172): 1001-1009.

Wells, M., H. Tidow, T. J. Rutherford, P. Markwick, M. R. Jensen, E. Mylonas, D. I. Svergun, M. Blackledge and A. R. Fersht (2008). "Structure of tumor suppressor p53 and its intrinsically disordered N-terminal transactivation domain." <u>Proc Natl Acad Sci U S A</u> **105**(15): 5762-5767.

Wermuth, C. G., C. R. Ganellin, P. Lindberg and L. A. Mitscher (1998). "Glossary of terms used in medicinal chemistry." <u>Pure Appl. Chem.</u> **70**: 1129-1143.

Wilkins, M. R., E. Gasteiger, A. Bairoch, J. C. Sanchez, K. L. Williams, R. D. Appel and D. F. Hochstrasser (1999). "Protein identification and analysis tools in the ExPASy server." <u>Methods Mol Biol</u> **112**: 531-552.

Worrall, E. G., L. Worrall, E. Blackburn, M. Walkinshaw and T. R. Hupp (2010). "The effects of phosphomimetic lid mutation on the thermostability of the N-terminal domain of MDM2." <u>J Mol Biol</u> **398**(3): 414-428.

Wuthrich, K. (1986). "NMR of Proteins and Nucleic Acids." <u>Wiley-Interscience, New York</u>.

Wüthrich, K. (1986). "NMR of Proteins and Nucleic Acids."

Xu, J. and G. F. Morris (1999). "p53-mediated regulation of proliferating cell nuclear antigen expression in cells exposed to ionizing radiation." <u>Mol Cell Biol</u> **19**(1): 12-20.

Yu, G. W., M. D. Allen, A. Andreeva, A. R. Fersht and M. Bycroft (2006). "Solution structure of the C4 zinc finger domain of HDM2." <u>Protein Sci</u> **15**(2): 384-389.

Yu, G. W., S. Rudiger, D. Veprintsev, S. Freund, M. R. Fernandez-Fernandez and A. R. Fersht (2006). "The central region of HDM2 provides a second binding site for p53." <u>Proceedings of the National Academy of Sciences of the United States of America</u> **103**(5): 1227-1232.

Zdzalik, M., K. Pustelny, S. Kedracka-Krok, K. Huben, A. Pecak, B. Wladyka, S. Jankowski, A. Dubin, J. Potempa and G. Dubin (2010). "Interaction of regulators Mdm2 and Mdmx with transcription factors p53, p63 and p73." <u>Cell Cycle</u> **9**(22): 4584-4591.

Zondlo, S. C., A. E. Lee and N. J. Zondlo (2006). "Determinants of specificity of MDM2 for the activation domains of p53 and p65: proline27 disrupts the MDM2-binding motif of p53." <u>Biochemistry</u> **45**(39): 11945-11957.